SSC-154

The Superconducting Super Collider

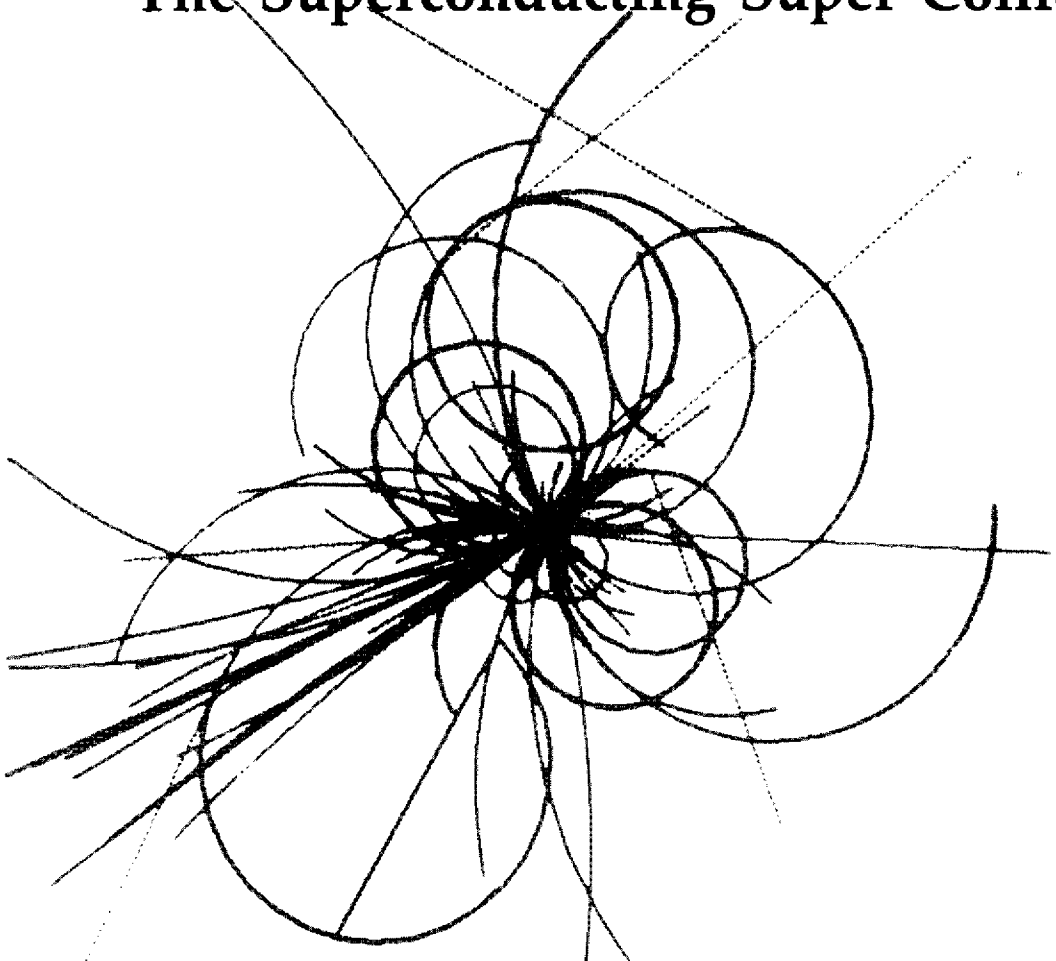

Hadron Colliders Beyond the Z^0

Chris Quigg
SSC Central Design Group

January 1988

SSC-154

HADRON COLLIDERS BEYOND THE Z^0*

Chris Quigg
SSC Central Design Group†
c/o Lawrence Berkeley Laboratory, 1 Cyclotron Road, Berkeley, CA 94720

January 1988

*Lectures delivered at the SLAC Summer Institute, August 10–21, 1987
†Operated by Universities Research Association for the U. S. Department of Energy

HADRON COLLIDERS BEYOND THE Z^0

CHRIS QUIGG
SSC Central Design Group
Lawrence Berkeley Laboratory
Berkeley, California 94720

Abstract

I summarize the case for new physics at the TeV scale, and review the physics possibilities of multi-TeV hadron colliders. Characteristics of the experimental environment are surveyed.

1 INTRODUCTION

The picture[1] of the fundamental constituents of matter and the interactions among them that has emerged in recent years is one of great beauty and simplicity. All matter appears to be composed of *quarks* and *leptons*, which are pointlike, structureless, spin-$\frac{1}{2}$ particles. If we leave aside gravitation, which is a negligible perturbation at the energy scales usually considered, the interactions among these particles are of three types: weak, electromagnetic, and strong. All three of these interactions are described by gauge theories and are mediated by spin-1 gauge bosons. The quarks experience all three interactions; the leptons participate only in the weak and electromagnetic interactions. By the Standard Model we will understand two elements:

- The $SU(3)_c \otimes SU(2)_L \otimes U(1)_Y$ gauge theory of the strong, weak, and electromagnetic interactions; and
- Three generations of color-triplet quarks: u, d, s, c, b, $[t]$, and color-singlet leptons: e, ν_e, μ, ν_μ, τ, ν_τ.

The Standard Model has an appealing simplicity and an impressive generality. The picture at which we have arrived has a pleasing degree of coherence, and holds the promise of deeper understanding — in the form of a further unification of the interactions — still to come.

This is an accomplishment worthy of the pleasure we take in it, but if we have come impressively far in the past two decades, we still have quite far to go. The very success of the standard $SU(3)_c \otimes SU(2)_L \otimes U(1)_Y$ model prompts new questions: Why does it work? Can it be complete? Where will it fail? As we shall see, the Standard Model itself hints that the frontier of our ignorance

lies at $\sim$ 1 TeV for collisions among the fundamental constituents. In more general terms, the success of the Standard Model suggests that a significant step beyond present-day energies is needed, to see breakdowns of our current understanding. A high-luminosity, multi-TeV proton-proton collider is the most technically assured and cost-effective instrument to take such a step, and to make possible a timely and thorough exploration of the 1 TeV scale.

My aim in these lectures is to review the scientific motivation for exploring the 1-TeV scale and beyond, with special attention to the capabilities of hadron colliders. The essential elements of supercollider physics are covered at greater length in *EHLQ*.[2] Many details are investigated in the proceedings of various workshops,[3–8] and in lecture notes from other schools.[9–11] To set the stage for the main topics, we begin by characterizing the proton beam itself.

2 What is a proton?

For the construction of large accelerators, we are limited to beams of charged, stable particles, which means to electrons and protons. With current methods, it is feasible to produce intense proton beams of tens of TeV, but electron beams of only about a tenth of a TeV. So far as we know, the electron is an elementary point particle ($r_e \lesssim 10^{-16}$ cm), but the proton is a composite system. Our ability to exploit the energy advantage of proton beams therefore depends on our knowledge of what a proton is, and how it behaves in high energy collisions. The purpose of this section is to summarize the state of our knowledge.

The static properties of a proton are well characterized by a description of a proton as a three-quark (uud) bound state, with a radius $r_p \sim 1$ fm. This picture accounts for the essential features of magnetic moments, axial charges, electromagnetic form factors, and such.[12]

In collision, especially for the purpose of hard scattering,

> a proton is a broad-band, unselected beam of quarks, antiquarks, and gluons,

and possibly other constituents as well. The composition of this mixed beam depends on how you inspect it: the more virtual the probe, the more sensitive it will be to short time-scale fluctuations.

It is fruitful to analyze the proton in the framework of the *parton model* with QCD refinements. The fundamental quantity in this picture is $f_i^{(a)}(x_a, Q^2)$, the number density of partons of species i with momentum fraction x_a of hadron a seen by a probe with resolving power characterized by Q^2.

Up to now, the best information on parton distributions (or hadron structure functions) comes from measurements of deeply inelastic lepton scattering, the reactions

$$eN \rightarrow e + \text{anything}, \tag{2.1}$$

$$\mu N \rightarrow \mu + \text{anything}, \tag{2.2}$$

$$\nu_\mu N \rightarrow \mu + \text{anything}, \tag{2.3}$$

and

$$\nu_\mu N \rightarrow \nu_\mu + \text{anything}. \tag{2.4}$$

For the scattering of charged leptons at present energies, the probe is a virtual photon (with usually negligible corrections for the exchange of a virtual Z^0). In the charged-current reaction (2.3), the nucleon is probed by $W^\pm$; in the neutral-current reaction (2.4), the probe is the Z^0.

The kinematic notation for deeply inelastic scattering is indicated in Fig. 1. From the four-momenta indicated there we may form the useful invariants

$$s = (\ell + P)^2, \tag{2.5}$$

$$Q^2 \equiv -q^2 = -(\ell - \ell')^2, \tag{2.6}$$

$$\nu = q \cdot P/M, \tag{2.7}$$

where M is the target mass, and

$$W^2 = 2M\nu + M^2 - Q^2 \tag{2.8}$$

is the square of the invariant mass of the produced hadronic system "anything." It is convenient to work in terms of Bjorken's dimensionless variables

$$x = Q^2/2M\nu, \tag{2.9}$$

the momentum fraction of the struck parton, and

$$y = \nu/E_{\text{lab}}, \tag{2.10}$$

the fractional energy loss of the leptons in the laboratory frame.

For electromagnetic scattering, we may write the differential cross section as

$$\frac{d\sigma}{dxdy} = \frac{4\pi\alpha^2 s}{Q^4}\left[F_2(x)(1-y) + F_1(x)xy^2\right]. \tag{2.11}$$

In the parton model, $2xF_1(x) = F_2(x)$, and the structure function F_2 of the proton may be written as

$$F_2^{ep}(x)/x = \frac{4}{9}\left(u(x) + \overline{u}(x)\right) + \frac{1}{9}\left(d(x) + \overline{d}(x)\right) + \frac{1}{9}\left(s(x) + \overline{s}(x)\right) + \ldots \tag{2.12}$$

The structure function of the neutron is obtained by an isospin rotation, which is to say, by the replacement $u \leftrightarrow d$. The parton distributions satisfy the momentum sum rule,

$$\sum_{i=\substack{\text{parton}\\\text{species}}} \int_0^1 dx x f_i(x) = 1. \tag{2.13}$$

An important early result was the recognition that charged partons do not carry all the momentum of the nucleon. We may see this by approximating

$$F_2^{ep}(x) + F_2^{en}(x) = \frac{5x}{9}\left(u(x) + \overline{u}(x) + d(x) + \overline{d}(x)\right). \tag{2.14}$$

A measurement of F_2 then leads to an estimate of the momentum carried by charged partons through the connection

$$\begin{aligned} \frac{9}{5}\int_0^1 dx\left(F_2^{ep}(x) + F_2^{en}(x)\right) &= \sum_{i=\substack{\text{quarks+}\\\text{antiquarks}}} \int_0^1 dx x f_i(x) \\ &= 0.45 \text{ experimental.} \end{aligned} \tag{2.15}$$

Unless most of the momentum of the nucleon is carried by strange (and heavier) quarks, this implies that about half the momentum of a proton is carried by neutrals.

Charged-current scattering of neutrinos from nucleons has also been studied extensively. We define an "isoscalar nucleon" $N \equiv \frac{1}{2}(p+n)$. The differential cross sections for scattering of neutrinos and antineutrinos are then

$$\frac{d\sigma(\nu N \to \mu^- + X)}{dxdy} = \frac{G_F^2 ME}{\pi}\left[(u(x) + d(x)) + \left(\overline{u}(x) + \overline{d}(x)\right)(1-y)^2\right], \tag{2.16}$$

$$\frac{d\sigma(\overline{\nu} N \to \mu^+ + X)}{dxdy} = \frac{G_F^2 ME}{\pi}\left[(u(x) + d(x))(1-y)^2 + \left(\overline{u}(x) + \overline{d}(x)\right)\right]. \tag{2.17}$$

The difference $\sigma(\nu N) - \sigma(\overline{\nu} N)$ allows a determination of the excess of quarks over antiquarks, i.e., the distribution of "valence" quarks that determine the nucleon quantum numbers:

$$u(x) - \overline{u}(x) + d(x) - \overline{d}(x) \equiv u_{valence} + d_{valence}. \tag{2.18}$$

Viewed at very long wavelengths, the proton appears structureless, but as Q^2 increases and the resolution becomes finer, the proton is revealed as a composite object characterized, for example, by rapidly falling elastic form factors that decrease as $1/Q^4$. According to the parton model, which ignores interactions

among the constituents of the proton, the picture for deeply inelastic scattering is then exceedingly simple, as sketched in Fig. 2. Once Q^2 has become large enough for the quark constituents to be resolved, no finer structure is seen. The quarks are structureless, have no size, and thus introduce no length scale. When Q^2 exceeds a few GeV^2, all fixed mass scales become irrelevant and the structure functions and parton distributions do not depend upon Q^2. That this is approximately so in Nature may be seen from the measurements of $F_2^{\mu p}(x)$ shown in Fig. 3.

In an interacting field theory, however, a more complex picture of hadron structure emerges. As Q^2 increases beyond the magnitude required to resolve quarks, the quarks themselves are found to have an apparent structure, which arises from the interactions mediated by the gluon fields. This is indicated in Fig. 4. The parton distributions *evolve* with Q^2 as a result of quantum fluctuations shown there. The virtual dissociation of a quark into a quark and gluon, shown in Fig. 5, degrades the valence quark distribution. The virtual dissociation of a gluon into a $q\overline{q}$ pair, shown in Fig. 6, enhances the population of quarks and antiquarks.

It is therefore plausible to expect, in any interacting field theory, that as Q^2 increases the structure function will fall at large values of x and rise at small values of x, as sketched in Fig. 7. In most field theories, there is a power-law dependence on Q^2, but in asymptotically free gauge theories such as QCD, the dependence on Q^2 is only logarithmic.

The evolution of neutrino structure functions is indicated in Fig. 8, which shows the Q^2-dependence of

$$\mathcal{F}_2^{\nu N} = x\left[u(x) + \overline{u}(x) + d(x) + \overline{d}(x)\right], \tag{2.19}$$

and in Fig. 9, which displays that of the flavor "nonsinglet" structure function

$$x\mathcal{F}_3^{\nu N} = x\left[u(x) - \overline{u}(x) + d(x) - \overline{d}(x)\right]. \tag{2.20}$$

The latter, which measures the valence quark distribution, is of special interest because it receives no contribution from the dissociation of gluons into quark-antiquark pairs; it is simply degraded, with increasing Q^2, by gluon radiation from the valence quarks. It therefore offers, in principle, a means for studying the evolution of the quark distributions uncomplicated by the need to know anything about the gluon distribution.

Once parton distributions have been measured in detail at some value of $Q^2 = Q_0^2$, and the running coupling constant $\alpha_s(Q^2)$ of the strong interactions has been determined, QCD permits us to compute the parton distributions at higher values of Q^2. A convenient formalism is provided by the Altarelli-Parisi equations,[15] integro-differential equations for the parton distributions.[16] It is worth recalling a few of the essentials here.

It is conventional to parameterize the strong coupling constant as

$$1/\alpha_s(Q^2) = \frac{33 - 2N_f}{12\pi} \ln(Q^2/\Lambda^2), \tag{2.21}$$

where N_f is the number of "active" quark flavors, and to determine Λ from the evolution of structure functions. For example, if we define the second moment

$$\Delta_2(Q^2) = \int_0^1 dx x \left[u_v(x) + d_v(x)\right] \tag{2.22}$$

of the valence quark distribution, then the Altarelli-Parisi equations give

$$\frac{\Delta_2(Q^2)}{\Delta_2(Q_0^2)} = \left[\frac{\alpha_s(Q_0^2)}{\alpha_s(Q^2)}\right]^{6A_2/(33-2N_f)}, \tag{2.23}$$

where $A_2 \simeq 1.78$. Knowing $\int_0^1 dx x \mathcal{F}_3(x, Q^2)$ at different values of Q^2 thus allows, in principle, a direct determination of the QCD scale parameter Λ. In practice, the limited statistics of neutrino experiments, the small available range in $\ln(Q^2)$, and other factors limit the precision of such determinations.

If the evolution of $F_2^{\mu N}$ or $\mathcal{F}_2^{\nu N}$, either of which is measured with higher statistics than $x\mathcal{F}_3^{\nu N}$, is to be used for a determination of Λ, we are faced with the problem that the gluon distribution is not measured directly in lepton scattering. Its character must be inferred from the rate of evolution of the antiquark distribution, and so is coupled with the value of Λ.

Finally, let us note from the representative data displayed in Figs. 3, 8, and 9 that no detailed measurements have been carried out for values of $x \lesssim 10^{-2}$.

The discovery reach of a hadron supercollider is determined by hard scattering processes in which the constituents interact at high energies, as depicted in Fig. 10. Cross sections may be calculated in the renormalization group improved parton model, provided we know the behavior of the quark and gluon distributions within the proton as functions of x and Q^2. For the parton subprocesses of interest, the range over which the structure functions must be known is

$$(10 \text{ GeV})^2 \lesssim Q^2 \lesssim (10^4 \text{ GeV})^2, \tag{2.24}$$

which may correspond to $\langle x \rangle$ as small as 10^{-4}. With the parton distributions written as $f_i^{(a)}(x, Q^2)$ for the number density of partons of species i in hadron a, hadronic cross sections are given schematically by

$$\begin{aligned} d\sigma(a + b \to c + X) &= \sum_{ij} \int dx_a dx_b \cdot \\ &\quad f_i^{(a)}(x_a, Q^2) f_j^{(b)}(x_b, Q^2) d\hat{\sigma}(i + j \to c + X), \end{aligned} \tag{2.25}$$

where $d\hat{\sigma}$ represents the elementary cross section. The parton-level cross sections are known for a great many reactions of potential interest.

In *EHLQ* we produced two sets of distribution functions that behave sensibly over the kinematic range of interest. This was done by constructing initial distributions at $Q_0^2 = 5$ GeV^2 using the CDHS structure functions,[17] subject to the constraints of momentum and flavor sum rules, and under the assumption that there are no "intrinsic" heavy flavor components. We then evolved the distributions to $Q^2 > Q_0^2$ using the (first-order) Altarelli-Parisi equations. We studied in detail two distributions, characterized by the QCD scale parameters $\Lambda = 200$ MeV and 290 MeV, and gave a detailed discussion of the uncertainties. The two sets of input distributions are extracted assuming that

$$\sigma_L/\sigma_T \equiv 0.1 \quad \text{(Set 1)}, \tag{2.26}$$

or that the ratio σ_L/σ_T is as given by QCD (Set 2). At $Q_0^2 = 5$ GeV^2, these are characterized by

$$\begin{aligned} xu_v(x,Q_0^2) &= 1.78x^{0.5}(1-x^{1.51})^{3.5}, \\ xd_v(x,Q_0^2) &= 0.67x^{0.4}(1-x^{1.51})^{4.5}, \\ xu_s(x,Q_0^2) &= 0.182(1-x)^{8.54}, \\ xs_s(x,Q_0^2) &= 0.081(1-x)^{8.54}, \\ xG(x,Q_0^2) &= (2.62+9.17x)(1-x)^{5.90}, \\ \Lambda &= 200 \text{ MeV}, \end{aligned} \tag{2.27}$$

for Set 1, and

$$\begin{aligned} xu_s(x,Q_0^2) &= 0.185(1-x)^{7.12}, \\ xs_s(x,Q_0^2) &= 0.0795(1-x)^{7.12}, \\ xG(x,Q_0^2) &= (1.75+15.575x)(1-x)^{6.03}, \\ \Lambda &= 290 \text{ MeV}, \end{aligned} \tag{2.28}$$

with the same valence distributions for Set 2. The input distributions of Set 1 are summarized in Fig. 11.

A rather complete discussion of the properties of the resulting distributions is given in *EHLQ*. It is worth looking at one example of the Q^2-evolution of the structure functions to see that they behave in a reasonable fashion and fulfill our qualitative expectations for the effects of QCD on parton distributions. Figure 12 shows the behavior of the gluon structure function $xG(x,Q^2)$ of Set 1 as a function of Q^2 for four values of x: 10^{-1}, 10^{-2}, 10^{-3}, and 10^{-4}. At large

x, the distribution decreases with increasing Q^2, but at small values of x, the distribution grows as Q^2 increases.

As a final partial answer to our question, "What is a proton?" let us look at the flavor content of the proton, as measured by the momentum fraction

$$\int_0^1 dx x f_i(x, Q^2) \tag{2.29}$$

carried by each parton species. This is shown in Fig. 13 for the *EHLQ* 1986 Set 2. As Q^2 increases, momentum is shared more and more equally among the quark and antiquark flavors, reflecting the trend toward the asymptotic values

$$\begin{aligned} \int_0^1 dx x G(x, Q^2 \to \infty) &= \frac{8}{17}, \\ \int_0^1 dx x q_s(x, Q^2 \to \infty) &= \frac{3}{68} \text{ (each flavor)}, \\ \int_0^1 dx x q_v(x, Q^2 \to \infty) &= 0, \end{aligned} \tag{2.30}$$

expected in QCD with six quark flavors and no light colored superpartners. It is easy to verify that the momentum sum rule (2.13) is satisfied:

$$\frac{8}{17} + 6 \text{ flavors} \cdot 2 \text{ (quarks+antiquarks)} \cdot \frac{3}{68} = 1. \tag{2.31}$$

3 What Landmarks Do We Expect?

We have already remarked in the Introduction on the importance of the 1-TeV scale. In this section, we wish to review for the first time some of the arguments that lead to an identification of the 1-TeV scale as a key landmark. As we shall see again and again in different ways, our understanding of the spontaneous breaking of the electroweak gauge symmetry is incomplete. A more complete understanding can be obtained only with the aid of a thorough knowledge of what takes place on the 1-TeV scale.

Let us review the essential elements of the Weinberg-Salam $SU(2)_L \otimes U(1)_Y$ model of weak and electromagnetic interactions. To save writing, we shall speak of the model as it applies to a single generation of leptons. In this form, the model is neither complete nor consistent: anomaly cancellation requires that a doublet of color-triplet quarks accompany each doublet of color-singlet leptons. However, the needed generalizations are simple enough to make that we need not write them out.

We begin by specifying the fermions: a left-handed weak isospin doublet

$$\mathsf{L} = \begin{pmatrix} \nu_e \\ e \end{pmatrix}_L \tag{3.1}$$

with weak hypercharge $Y_L = -1$, and a right-handed weak isospin singlet

$$\mathsf{R} \equiv e_R \tag{3.2}$$

with weak hypercharge $Y_R = -2$.

The electroweak gauge group, $SU(2)_L \otimes U(1)_Y$, implies two sets of gauge fields: a weak isovector $\vec{b}_\mu$, with coupling constant g, and a weak isoscalar $\mathcal{A}_\mu$, with coupling constant g'. Corresponding to these gauge fields are the field-strength tensors $\vec{F}_{\mu\nu}$ for the weak-isospin symmetry and $f_{\mu\nu}$ for the weak-hypercharge symmetry.

We may summarize the interactions by the Lagrangian

$$\mathcal{L} = \mathcal{L}_{\text{gauge}} + \mathcal{L}_{\text{leptons}} \ , \tag{3.3}$$

with

$$\mathcal{L}_{\text{gauge}} = -\frac{1}{4} F^{\ell}_{\mu\nu} F^{\ell\mu\nu} - \frac{1}{4} f_{\mu\nu} f^{\mu\nu}, \tag{3.4}$$

and

$$\begin{aligned} \mathcal{L}_{\text{leptons}} &= \overline{\mathsf{R}}\, i\gamma^\mu \left(\partial_\mu + i\frac{g'}{2}\mathcal{A}_\mu Y \right) \mathsf{R} \\ &+ \overline{\mathsf{L}}\, i\gamma^\mu \left(\partial_\mu + i\frac{g'}{2}\mathcal{A}_\mu Y + i\frac{g}{2}\vec{\tau}\cdot\vec{b}_\mu \right) \mathsf{L}. \end{aligned} \tag{3.5}$$

To hide the electroweak symmetry, we introduce a complex doublet of scalar fields

$$\phi \equiv \begin{pmatrix} \phi^+ \\ \phi^0 \end{pmatrix} \tag{3.6}$$

with weak hypercharge $Y_\phi = +1$. Add to the Lagrangian new terms for the interaction and propagation of the scalars,

$$\mathcal{L}_{\text{scalar}} = (\mathcal{D}^\mu \phi)^\dagger (\mathcal{D}_\mu \phi) - V(\phi^\dagger \phi), \tag{3.7}$$

where the gauge-covariant derivative is

$$\mathcal{D}_\mu = \partial_\mu + i\frac{g'}{2}\mathcal{A}_\mu Y + i\frac{g}{2}\vec{\tau}\cdot\vec{b}_\mu \ , \tag{3.8}$$

and the potential interaction has the form

$$V(\phi^\dagger\phi) = \mu^2(\phi^\dagger\phi) + |\lambda|\,(\phi^\dagger\phi)^2. \tag{3.9}$$

We are also free to add a Yukawa interaction between the scalar fields and the leptons:

$$\mathcal{L}_{\text{Yukawa}} = -G_e \left[\overline{\mathsf{R}}(\phi^\dagger \mathsf{L}) + (\overline{\mathsf{L}}\phi)\mathsf{R} \right]. \tag{3.10}$$

The electroweak symmetry is spontaneously broken if the parameter $\mu^2 < 0$. The minimum energy, or vacuum state, may then be chosen to correspond to the vacuum expectation value

$$\langle\phi\rangle_0 = \begin{pmatrix} 0 \\ v/\sqrt{2} \end{pmatrix}, \tag{3.11}$$

where

$$\begin{aligned} v = \sqrt{-\mu^2/|\lambda|} &= \left(G_F\sqrt{2}\right)^{-\frac{1}{2}} \\ &\approx 246 \text{ GeV} \end{aligned} \tag{3.12}$$

is fixed by the low-energy phenomenology of charged current interactions.

The spontaneous symmetry breaking has several important consequences:

- Electromagnetism is mediated by a massless photon, coupled to the electric charge;
- The mediator of the charged current weak interaction acquires a mass characterized by $M_W^2 = \pi\alpha/G_F\sqrt{2}\sin^2\theta_W$, where θ_W is the weak mixing angle;
- The mediator of the neutral current weak interaction acquires a mass characterized by $M_Z^2 = M_W^2/\cos^2\theta_W$;
- A massive neutral scalar particle, the Higgs boson, appears, but its mass is not predicted;
- Fermions (the electron in our abbreviated treatment) can acquire mass.

Before reviewing the significance of the 1-TeV scale, it will be useful to recall why a Higgs boson, or its Doppelgänger, must exist. One path to the (theoretical!) discovery of the Higgs boson involves the role of the Higgs boson in the cancellation of high-energy divergences. An illuminating example is provided by the reaction

$$e^+e^- \to W^+W^-, \tag{3.13}$$

which is described in lowest order in the Weinberg-Salam theory by the four Feynman graphs in Fig. 14. The leading divergence in the $J = 1$ amplitude of the neutrino-exchange diagram in Fig. 14(a) is cancelled by the contributions of the direct-channel γ- and Z^0-exchange diagrams of Figs. 14(b) and (c). However, the $J = 0$ scattering amplitude, which exists in this case because the electrons are massive and may therefore be found in the "wrong" helicity state, grows as $s^{1/2}$ for the production of longitudinally polarized gauge bosons. The resulting

divergence is precisely cancelled by the Higgs boson graph of Fig. 14(d). If the Higgs boson did not exist, we should have to invent something very much like it. From the point of view of S-matrix theory, the Higgs-electron-electron coupling must be proportional to the electron mass, because "wrong helicity" amplitudes are always proportional to the fermion mass.

Let us summarize: Without spontaneous symmetry breaking in the Standard Model, there would be no Higgs boson, no longitudinal gauge bosons, and no extreme divergence difficulties. (Nor would there be a viable low-energy phenomenology of the weak interactions.) The most severe divergences are eliminated by the gauge structure of the couplings among gauge bosons and leptons. A lesser, but still potentially fatal, divergence arises because the electron has acquired mass — because of the Higgs mechanism. Spontaneous symmetry breaking provides its own cure by supplying a Higgs boson to remove the last divergence. A similar interplay and compensation must exist in any satisfactory theory.

It is well known that the Standard Model does not give a precise prediction for the mass of the Higgs boson. We can, however, use arguments of self-consistency to place plausible lower and upper bounds on the mass of the Higgs particle in the minimal model. A lower bound is obtained by computing[18] the first quantum corrections to the classical potential (3.9). Requiring that $\langle\phi\rangle_0 \neq 0$ be an absolute minimum of the one-loop potential yields the condition

$$\begin{aligned} M_H^2 &> 3G_F\sqrt{2}(2M_W^4 + M_Z^4)/16\pi^2 \\ &\gtrsim 7\ \mathrm{GeV}/c^2\,. \end{aligned} \tag{3.14}$$

Unitarity arguments[19] lead to a conditional upper bound on the Higgs boson mass. It is straightforward to compute the amplitudes $\mathcal{M}$ for gauge boson scattering at high energies, and to make a partial-wave decomposition, according to

$$\mathcal{M}(s,t) = 16\pi \sum_J (2J+1) a_J(s) P_J(\cos\theta)\,. \tag{3.15}$$

Most channels "decouple," in the sense that partial-wave amplitudes are small at all energies (except very near the particle poles, or at exponentially large energies), for any value of the Higgs boson mass M_H. Four channels are interesting:

$$W_L^+W_L^- \quad Z_L^0Z_L^0/\sqrt{2} \quad HH/\sqrt{2} \quad HZ_L^0\,, \tag{3.16}$$

where the subscript L denotes the longitudinal polarization states, and the factors of $\sqrt{2}$ account for identical particle statistics. For these, the s-wave amplitudes are all asymptotically constant (i.e., well-behaved) and proportional to

$G_F M_H^2$. In the high-energy limit,

$$\lim_{s \gg M_H^2} (a_0) \to \frac{-G_F M_H^2}{4\pi\sqrt{2}} \cdot \begin{bmatrix} 1 & 1/\sqrt{8} & 1/\sqrt{8} & 0 \\ 1/\sqrt{8} & 3/4 & 1/4 & 0 \\ 1/\sqrt{8} & 1/4 & 3/4 & 0 \\ 0 & 0 & 0 & 1/2 \end{bmatrix} . \tag{3.17}$$

Requiring that the largest eigenvalue respect the partial-wave unitarity condition $|a_0| \leq 1$ yields

$$M_H < \left(\frac{8\pi\sqrt{2}}{3G_F}\right)^{1/2} = 1 \text{ TeV}/c^2 \tag{3.18}$$

as a condition for perturbative unitarity.

If the bound is respected, weak interactions remain weak at all energies, and perturbation theory is everywhere reliable. If the bound is violated, perturbation theory breaks down, and weak interactions among $W^\pm$, Z, and H become strong on the 1-TeV scale. This means that the features of strong interactions at GeV energies will come to characterize electroweak gauge boson interactions at TeV energies. We interpret this to mean that new phenomena are to be found in the electroweak interactions at energies not much larger than 1 TeV.

Does this analysis mean that the observation of a light Higgs boson would remove the motivation for exploring the 1-TeV scale? Decidedly not! The Standard Model is unnatural and gives us no means of understanding why a light Higgs boson should emerge. The problem is nicely illustrated by an analysis due to 't Hooft.[20]

Consider the Lagrangian $\mathcal{L}(\Lambda)$ as an effective field theory that describes physics at the shortest distances probed (characterized by an energy scale Λ) and at all longer distances, in terms of the fields or degrees of freedom appropriate to that scale. At a higher energy scale Λ', the appropriate Lagrangian $\mathcal{L}(\Lambda')$ may involve different degrees of freedom. In this sense, any Lagrangian we encounter should be thought of as an effective Lagrangian describing physics in terms of the degrees of freedom characteristic of the highest energy scale probed by experiment. In spite of the occasional assertions by some of our visionary colleagues, we can never be certain that we have encountered all the fundamental fields that are to be discovered, up to the highest energies.

What properties must an effective Lagrangian display in order that it can consistently represent the low-energy effective interactions of some unknown dynamics acting at a higher energy scale? We say that the Lagrangian $\mathcal{L}(\Lambda)$ is *natural* if every small parameter ξ (in units of the requisite power of Λ) is associated with an approximate symmetry of $\mathcal{L}(\Lambda)$ that becomes an exact symmetry in the limit $\xi \to 0$. This is to say that dynamical accidents are unnatural and unsatisfying.

This definition has two important virtues:

- To determine whether a theory is natural at a scale Λ requires no knowledge of physics at scales above Λ.
- A Lagrangian unnatural on a scale Λ is unnatural on all higher scales $\Lambda' > \Lambda$.

For the Weinberg-Salam Lagrangian, the only possible additional symmetry that could allow for a naturally small scalar mass is invariance under a shift in the scalar field ϕ, which would call for $|\lambda|$, $\mu \to 0$. Such a symmetry is broken by gauge interactions and scalar self-interactions. The theory is natural only if

$$\frac{M_H^2}{\Lambda^2} \gtrsim O(|\lambda|),\ O(\alpha)\ . \tag{3.19}$$

Therefore, since $M_H^2 \approx \lambda v^2$, the theory is natural only for scales

$$\Lambda \lesssim O(v) \approx 246 \text{ GeV} \sim M_W\ . \tag{3.20}$$

Consequently we conclude that values $M_H \ll M_W$ are unnatural.

We shall give a more operational discussion of the naturalness problem at the beginning of the next Lecture (Section 4). For now, let us note that two strategies for resolving the unnaturalness of the electroweak theory suggest themselves:

- Eliminate the scalars as fundamental degrees of freedom in $\mathcal{L}$ for $\Lambda \gg G_F^{-\frac{1}{2}}$.
- Associate an approximate symmetry with light scalars.

These two strategies correspond to the ideas of technicolor and compositeness, and of supersymmetry. Both alternatives require new physics at or below the 1-TeV scale.

4 Why there must be new physics on the 1-TeV scale

The Standard Model is incomplete[21]; it does not explain how the scale of electroweak symmetry breaking is maintained in the presence of quantum corrections. The problem of the scalar sector can be summarized neatly as follows.[22] The Higgs potential of the $SU(2)_L \otimes U(1)_Y$ electroweak theory is

$$V(\phi^\dagger\phi) = \mu^2(\phi^\dagger\phi) + |\lambda|\,(\phi^\dagger\phi)^2\ . \tag{4.1}$$

With μ_0^2 chosen to be less than zero, the electroweak symmetry is spontaneously broken down to the $U(1)$ of electromagnetism, as the scalar field acquires a vacuum expectation value fixed by the low energy phenomenology,

$$\langle\phi\rangle_0 = \sqrt{-\mu^2/2|\lambda|} \equiv (G_F\sqrt{8})^{-1/2} \approx 175 \text{ GeV} . \tag{4.2}$$

Beyond the classical approximation, scalar mass parameters receive quantum corrections involving loops containing particles of spins $J = 1, 1/2$, and 0:

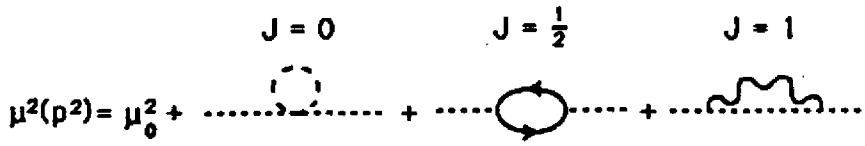

(4.3)

The loop integrals are potentially divergent. Symbolically, we may summarize the content of Eq. (4.3) as

$$m^2(p^2) = m^2(\Lambda^2) + Cg^2 \int_{p^2}^{\Lambda^2} dk^2 + \cdots , \tag{4.4}$$

where Λ defines a reference scale at which the value of m^2 is known, g is the coupling constant of the theory, and C is a constant of proportionality, calculable in any particular theory. Instead of dealing with the relationship between observables and parameters of the Lagrangian, we choose to describe the variation of an observable with the momentum scale. In order for the mass shifts induced by radiative corrections to remain under control (i.e., not to greatly exceed the value measured on the laboratory scale), either

- Λ must be small, so the range of integration is not enormous, or
- new physics must intervene to cut off the integral.

In the standard $SU(3)_c \otimes SU(2)_L \otimes U(1)_Y$ model, the natural reference scale is the Planck mass,

$$\Lambda \sim M_{\text{Planck}} \approx 10^{19} \text{ GeV} . \tag{4.5}$$

In a unified theory of the strong, weak, and electromagnetic interactions, the natural scale is the unification scale,

$$\Lambda \sim M_U \approx 10^{15} \text{ GeV} . \tag{4.6}$$

Both estimates are very large compared to the scale of electroweak symmetry breaking (4.2). We are therefore assured that new physics must intervene at an energy of approximately 1 TeV, in order that the shifts in m^2 not be much larger than (4.2).

Only a few distinct classes of scenarios for controlling the contribution of the integral in (4.4) can be envisaged. The supersymmetric solution[23] is especially elegant. Exploiting the fact that fermion loops contribute with an overall minus sign (because of Fermi statistics), supersymmetry balances the contributions of fermion and boson loops. In the limit of unbroken supersymmetry, in which the masses of bosons are degenerate with those of their fermion counterparts, the cancellation is exact:

$$\sum_{i=\substack{\text{fermions}\\+\text{bosons}}} C_i \int dk^2 = 0 \,. \tag{4.7}$$

If the supersymmetry is broken (as it must be in our world), the contribution of the integrals may still be acceptably small if the fermion-boson mass splittings ΔM are not too large. The condition that $g^2 \Delta M^2$ be "small enough" leads to the requirement that superpartner masses be less than about 1 TeV/c^2.

A second solution to the problem of the enormous range of integration in (4.4) is offered by theories of dynamical symmetry breaking such as Technicolor.[24] In the technicolor scenario, the Higgs boson is composite, and new physics arises on the scale of its binding, $\Lambda_{TC} \simeq O(1 \text{ TeV})$. Thus the effective range of integration is cut off, and mass shifts are under control.

A third possibility, which is appealingly economical but entails the sacrifice of perturbation theory for the electroweak interactions, is that of a strongly interacting gauge sector.[25] This would give rise to WW resonances, multiple production of gauge bosons, and other new phenomena.

Nature may choose any (or none) of these human inventions, but we are driven unavoidably to the conclusion that some new physics must occur on the 1-TeV scale.

5 Some discovery possibilities of a hadron collider

We have seen that the Standard Model hints that the frontier of our ignorance lies at about 1 TeV for collisions among the fundamental constituents. This conclusion is specific to the issue of electroweak symmetry breaking. More generally, the success of our theoretical framework suggests that a significant step is needed to see breakdowns of the Standard Model. Hadron colliders offer a broad range of discovery possibilities when we take a large step into unexplored territory. Let us consider a few examples.

5.1 New gauge bosons

There are many reasons to be open to the possibility of new gauge bosons:

- High energy parity restoration in an $SU(2)_L \otimes SU(2)_R \otimes U(1)_Y$ electroweak gauge theory;
- The occurrence of extra $U(1)$ gauge symmetries, implying additional Z^0s, for example in unification groups larger than $SU(5)$;
- The low-energy gauge groups emerging from superstring models.

In a specific theory, the calculation of $W^\pm$ and Z^0 production rates is easily modified to yield an estimate of the cross section for the production of new gauge bosons. As an example, I show in Fig. 15 the cross section for production of a new W-boson with standard gauge couplings to the light quarks. For the 40 TeV energy projected for the SSC, we may anticipate sensitive searches out to a mass of about 6 TeV/c^2.

The exceptional group E_6 has a long history as a candidate group for the unification of the strong, weak, and electromagnetic interactions. Historically, the motivation for considering E_6 derived mainly from the observation that E_6 is the group beyond $SO(10)$, which is in turn the group beyond $SU(5)$:

$$E_6 \supset SO(10) \supset SU(5). \tag{5.1}$$

The current revival is owed to the possibility that E_6 may be the surviving symmetry of the $E_8 \otimes E_8'$ internal symmetry group of the heterotic string.[26] Like all applications of superstring ideas to phenomenology, the "derivation" of E_6 is very vague and tentative. However, in the spirit of these lectures, it provides us with an excuse to look again at some possible consequences of an E_6 gauge symmetry.

The spectrum of quarks and leptons can be read off from the fundamental **27** representation of the group:

$$\begin{array}{llcccccccccc}
E_6: & \mathbf{27} & = & \multicolumn{5}{c}{\underbrace{\qquad\qquad\mathbf{16}\qquad\qquad}} & \oplus & \multicolumn{3}{c}{\underbrace{\qquad\mathbf{10}\qquad}} & \oplus & \underbrace{\mathbf{1}} \;: SO(10) \\
 & & SU(5): & \mathbf{10} & \oplus & \mathbf{5^*} & \oplus & \mathbf{1} & & \mathbf{5} & \oplus & \mathbf{5^*} & & \mathbf{1} \\
 & & & u & & d^c & & N_e^c & & h & & h^c & & n \\
 & & & d & & e & & & & E^+ & & E^- & & \\
 & & & u^c & & \nu_e & & & & N_E^c & & \nu_E & & \\
 & & & e^c & & & & & & & & & & \\
\text{charge } Q^{(\eta)} & & & -\frac{2}{3} & & \frac{1}{3} & & -\frac{5}{3} & & \frac{4}{3} & & \frac{1}{3} & & -\frac{5}{3}
\end{array} . \tag{5.2}$$

The $\mathbf{10} \oplus \mathbf{5}^*$ of $SU(5)$ constitute the standard generation. The remaining member of the $SO(10)$ $\mathbf{16}$ is a right-handed neutrino. Among the novel particles characteristic of E_6, the new charge$-\frac{1}{3}$ weak isoscalar quark is of especial interest.

With respect to interactions, we are interested in a spontaneous symmetry breaking scheme that will lead eventually to $SU(3)_c \otimes SU(2)_L \otimes U(1)_Y$. Thus we wish to break

$$E_6 \to \cdots \to SU(3)_c \otimes SU(2)_L \otimes U(1)_Y [\otimes \mathcal{G}], \tag{5.3}$$

where $\mathcal{G}$ denotes possible additional symmetries that survive to low energies. There are examples in superstring theories of symmetry breaking induced by an E_6 adjoint $\mathbf{78}$ of Higgs bosons. This leads naturally to one or more extra $U(1)$'s at low energies, which in turn implies an extra gauge boson Z', coupled to a new conserved current corresponding to the charge $Q^{(\eta)}$.

To identify the gauge bosons (which lie in the adjoint $\mathbf{78}$ representation), we decompose

$$E_6 \supset SU(3)_c \otimes SU(3)_L \otimes SU(3)_R, \tag{5.4}$$

where the subscripts L and R denote left and right. The adjoint representation contains

$$\mathbf{78} = (\mathbf{8},\mathbf{1},\mathbf{1}) \oplus (\mathbf{1},\mathbf{8},\mathbf{1}) \oplus (\mathbf{1},\mathbf{1},\mathbf{8}) \oplus (\mathbf{3}^*,\mathbf{3},\mathbf{3}) \oplus (\mathbf{3},\mathbf{3}^*,\mathbf{3}^*). \tag{5.5}$$

The color octets are of course the familiar gluons. Among the $SU(3)_L$ octets, the particles transforming under $SU(2)_L$ as triplets or singlet are the $W^\pm$, Z^0, and γ. The color triplets are leptoquark gauge bosons. Finally, among the $SU(3)_R$ octets, the particle transforming as a singlet under $SU(2)_R$ corresponds to the new neutral gauge boson Z'.

An additional neutral gauge boson is of interest because it may have observable consequences in the near future. Already, interesting limits can be set on the mass of the Z' by considering the effect it would have on neutral current processes. Consider, for illustration, a heavy Z', unmixed with the Standard Model Z^0, and with a (suitably defined) gauge coupling equal to that of the normal Z^0. Neutrino-quark neutral current processes would then be mediated by the two diagrams shown in Fig. 16. The contribution of the Z'-exchange diagram modifies the chiral couplings $L_\nu L_q$ and $L_\nu R_q$, which become

$$\begin{aligned} \tilde{L}_\nu \tilde{L}_q &= \tau_{3L} - 2e_q x_W \boxed{+Q_\nu^{(\eta)} Q_q^{(\eta)} x_W \cdot \left(\frac{M_Z}{M_{Z'}}\right)^2} \,, \\ \tilde{L}_\nu \tilde{R}_q &= \qquad - 2e_q x_W \boxed{-Q_\nu^{(\eta)} Q_{q^c}^{(\eta)} x_W \cdot \left(\frac{M_Z}{M_{Z'}}\right)^2} \,, \end{aligned} \tag{5.6}$$

where $x_W = \sin^2\theta_W$. The quantities $\mathcal{Q}_\nu$ and $\mathcal{Q}_q$ are the charges of the neutrino and quark under the new $U(1)$ symmetry. The extra neutral gauge boson suggested by many superstring theories couples to a charge $\mathcal{Q}_\eta$, as listed in (5.2). From the agreement of the measured u and d chiral couplings with the Standard Model, one may conclude[27] that

$$M_{Z'} \gtrsim 150 \text{ GeV}/c^2. \tag{5.7}$$

The Z' is somewhat harder to produce in $p^\pm p$ collisions than a standard Z^0 of the same mass, because the couplings to light quarks are inhibited. In terms of the quark-antiquark luminosities defined in Ref. 2, for example, we may express the cross sections as

$$\begin{aligned}\sigma\begin{pmatrix} Z \\ Z' \end{pmatrix} &= \frac{G_F\pi}{3\sqrt{2}}\sum_q \begin{pmatrix} L_q^2 + R_q^2 \\ (\mathcal{Q}_q^2 + \mathcal{Q}_{q^c}^2)x_W \end{pmatrix} \frac{\tau}{M^2}\frac{d\mathcal{L}_{q\bar{q}}}{d\tau} \\ &\simeq 0.07\cdot\left[\begin{pmatrix} 0.57 \\ 0.20 \end{pmatrix}\tau\frac{d\mathcal{L}_{u\bar{u}}}{d\tau} + \begin{pmatrix} 0.74 \\ 0.13 \end{pmatrix}\tau\frac{d\mathcal{L}_{d\bar{d}}}{d\tau}\right],\end{aligned} \tag{5.8}$$

where $M = M_Z$ or $M_{Z'}$ and $\tau = M^2/s$. The branching fractions of Z' into various decay modes are collected in Table 1. The branching ratio for the decay into charged leptons is thus, for example,

$$\Gamma(Z' \to e^+e^-) \simeq 3\%/n_g, \tag{5.9}$$

where n_g is the number of generations, which is somewhat smaller (by about $1/n_g$) than that of the conventional Z^0. The production cross section for the new $Z^{0\prime}$ is shown in Fig. 17. We expect to be sensitive to this new object in the lepton pair channel for masses as large as about $3-4$ TeV/c^2 in the SSC environment.

5.2 Sources of heavy quarks

The sources of heavy quarks are strong-interaction production in the reactions $gg \to Q\overline{Q}$ and $q\overline{q} \to Q\overline{Q}$, and electroweak production through the decays of $W^\pm$ and Z^0. The latter have the advantage of known cross sections, which is to say cross sections that can be measured from the leptonic decays of the gauge bosons, and calculable branching ratios. Howevever, they lead to very large rates only for the decays of real (not virtual) gauge bosons. This makes them an attractive option for the top-quark search at the $S\overline{p}pS$ and at the Tevatron.

The cross sections for the strong interaction processes are known in QCD perturbation theory:[28]

$$\frac{d\hat{\sigma}(gg \to Q\overline{Q})}{d\hat{t}} = \frac{\pi\alpha_s^2}{8\hat{s}^2} \cdot \left\{ \frac{6(\hat{t}-m^2)(\hat{u}-m^2)}{\hat{s}^2} + \right. \tag{5.10}$$

$$\left[\left(\frac{4}{3} \cdot \frac{(\hat{t}-m^2)(\hat{u}-m^2) - 2m^2(\hat{t}+m^2)}{(\hat{t}-m^2)^2} \right.\right.$$

$$\left. + \frac{3(\hat{t}-m^2)(\hat{u}-m^2) + m^2(\hat{u}-\hat{t})}{\hat{s}(\hat{t}-m^2)} \right)$$

$$\left. \left. + (t \leftrightarrow u) \right] - \frac{m^2(\hat{s}-4m^2)}{3(\hat{t}-m^2)(\hat{u}-m^2)} \right\},$$

which is generally dominant, and

$$\frac{d\hat{\sigma}(q\overline{q} \to Q\overline{Q})}{d\hat{t}} = \frac{4\pi\alpha_s^2}{9\hat{s}^2} \left[\frac{(\hat{t}-m^2)^2 + (\hat{u}-m^2)^2 + 2m^2\hat{s}}{\hat{s}^2} \right], \tag{5.11}$$

which is generally negligible.

I show in Fig. 18 the yield of heavy quarks from these sources for the $\overline{p}p$ colliders. Similar results are given for supercollider energies in *EHLQ*. A word of caution is in order for these estimates. When the "heavy" quark is light on the scale set by the elementary collisions, the next-order production process $gg \to gQ\overline{Q}$ may dominate.[29] A simple estimate will show why this is so. For $s_{Q\overline{Q}}/\hat{s} \ll 1$ and $\hat{s} \gg 4M_Q^2$, we may approximate the cross section by considering the process

$$\begin{array}{lll} gg & \to & g\,g \\ & & \quad \hookrightarrow Q\overline{Q}, \end{array} \tag{5.12}$$

the branching of a produced gluon into a $Q\overline{Q}$ pair. The ratio of three-body and two-body cross sections will be

$$\frac{\sigma(gg \to gQ\overline{Q})}{\sigma(gg \to Q\overline{Q})} \simeq \underbrace{\frac{\sigma(gg \to gg)}{\sigma(gg \to Q\overline{Q})}}_{O(100)} \cdot \underbrace{\frac{\alpha_s}{3\pi}}_{0.02} \cdot \underbrace{\log\left(\frac{\hat{s}}{4M_Q^2}\right)}_{2-4} \tag{5.13}$$

$$\simeq O(5-10),$$

where we have taken the ratio of the two-body cross sections at 90° (compare Table 2 below). The three-body reaction mechanism is undoubtedly already preëminent for b-quark production at the $S\overline{p}pS$. The two mechanisms may in some measure be distinguished topologically. The $Q\overline{Q}$ final state leads to heavy quarks on opposite sides of the beam axis, whereas the $gQ\overline{Q}$ final state places both heavy quarks on the same side of the beam axis. A full $O(\alpha_s^3)$ calculation of the elementary cross section has been given recently.[30]

At the SSC, we expect an event rate sufficient for the discovery of heavy quarks with masses up to about 2 TeV/c^2.

5.3 Two-jet Events

If partons i and j with incident momenta p_1 and p_2 initiate a two-body collision with outgoing momenta p_3 and p_4, it is useful to employ the parton-level Mandelstam invariants

$$\left.\begin{aligned} \hat{s} &= (p_1+p_2)^2 \\ \hat{t} &= (p_1-p_3)^2 \to -(\hat{s}/2)(1-\cos\theta^*) \\ \hat{u} &= (p_1-p_4)^2 \to -(\hat{s}/2)(1+\cos\theta^*) \end{aligned}\right\}. \tag{5.14}$$

The elementary cross section $\hat{\sigma}(\hat{s},\hat{t},\hat{u}) \sim O(\alpha_s^2)$ will lead to two-jet final states when $\hat{s}$ and $\hat{t}$ are "large."

In the hadronic collision itself, useful kinematic variables are $p_\perp$, the transverse momentum of either jet, and the jet rapidities

$$y_i = \frac{1}{2}\log\frac{E+p_\parallel}{E-p_\parallel}\,, \tag{5.15}$$

where $p_\parallel$ is the component of jet momentum along the beam direction. The cross section for the production of two jets in the collision of hadrons a and b is then represented as

$$\frac{d^3\sigma}{dy_1 dy_2 dp_\perp} = \frac{2\pi\tau p_\perp}{\hat{s}}\sum_{ij}\frac{1}{1+\delta_{ij}} f_i^{(a)}(x_a,M^2) f_j^{(b)}(x_b,M^2)\hat{\sigma}_{ij}(\hat{s},\hat{t},\hat{u}). \tag{5.16}$$

An immediate ambiguity arises in the lowest-order calculation: what value is to be taken for the scale M^2? Although a full evaluation[31] of the $O(\alpha_s^3)$ corrections shows that there is no simple answer, the choice $M^2 = p_\perp^2/4$ has sometimes been suggested as minimizing higher-order effects.

The Born diagrams for two-body scattering in QCD are shown in Fig. 19. If we idealize the partons as massless, we may write the $2 \to 2$ parton cross sections as

$$\frac{d\hat{\sigma}}{d\hat{t}} = \frac{\pi\alpha_s(Q^2)^2}{\hat{s}^2}\,|\mathcal{M}|^2\,, \tag{5.17}$$

where $|\mathcal{M}|^2$, the dimensionless square of the matrix element, is averaged over initial colors and spins and summed over final colors and spins. Expressions for the matrix elements[32] are collected in Table 2. The angular distributions corresponding to these elementary processes are sketched in Fig. 20. The dominant characteristic of many of these reactions is an angular dependence

$$\frac{d\sigma}{d\cos\theta^*} \sim \frac{1}{(1-\cos\theta^*)^2}, \tag{5.18}$$

arising from the t-channel gluon exchange, analogous to the t-channel photon exchange that drives the Rutherford formula. In terms of the variable $\chi \equiv \cot^2(\theta^*/2)$, the angular distribution may be reëxpressed as

$$\frac{d\sigma}{d\chi} \sim \text{constant}. \tag{5.19}$$

I show in Fig. 21 the angular distribution of two-jet events in the dijet c.m. frame, for dijets with effective masses in the interval

$$150 \text{ GeV}/c^2 < M(\text{jet-jet}) < 250 \text{ GeV}/c^2, \tag{5.20}$$

as observed by the UA1 Collaboration.[34] To first approximation, the distribution is flat in χ, as our simple analogy with Rutherford scattering would suggest. In more detail, it agrees very precisely with the prediction of the parton model, shown as the solid curve.

A further indication that the parton-model procedure is sound, and that knowledge of the structure functions derived from experiments on deeply inelastic lepton scattering is adequate, is provided by other $S\bar{p}pS$ data on hadron jets. Figure 22 shows representative data from the UA1 Collaboration[35] on the inclusive jet cross section $d\sigma/dp_\perp dy\,|_{y=0}$, compared with the predictions of the QCD Born term. The agreement is quite satisfactory.[36]

Thus satisfied with the reasonableness of our procedure, we may make the extrapolation to supercollider energies. We first show in Fig. 23 the one-jet differential cross section $d\sigma/dp_\perp dy|_{y=0}$ for pp collisions at 40 TeV. The figure shows separately the contributions of gluon-gluon final states ($gg \to gg$ or $q\bar{q} \to gg$, dot-dashed curves), gluon-quark final states ($gq \to gq$ or $g\bar{q} \to g\bar{q}$, dotted curves), and quark-quark final states ($qq \to qq$, $q\bar{q} \to q\bar{q}$, $\bar{q}\bar{q} \to \bar{q}\bar{q}$, or $gg \to q\bar{q}$, dashed curves).

Another interesting observable is the distribution of two-jet invariant masses $\mathcal{M}$. Figure 24 shows the mass spectrum $d\sigma/d\mathcal{M}$ for pairs of jets produced with $|y_i| < 1.5$ in 40 TeV pp collisions. Again the contributions of gluon-gluon, gluon-quark, and quark-quark final states are displayed separately. These jet-jet mass spectra represent a background for any new particles, such as new gauge bosons or Higgs bosons, that decay into jet pairs.

Figure 25 shows the transverse energy (E_T) range that can be explored at the level of at least one event per GeV of E_T per unit rapidity at 90° in the c.m. The results are presented in terms of the transverse energy per event, which corresponds to twice the transverse momentum $p_\perp$ of a jet. At 40 TeV we can expect to study jet pairs with E_T up to about 10 TeV.

We can show in perturbative QCD that jets should exist, and become increasingly collimated with increasing jet energies. The fraction f of all fragmentations

of quark jets in which a fraction $1-\epsilon$ of the jet energy is contained within a cone of half-angle $\delta(E)$ about the jet axis is[37]

$$f = 1 - \frac{4\alpha_s}{3\pi}\left(3\log\delta + 4\log\delta\log 2\epsilon + \pi^2/3 - 7/4\right) . \tag{5.21}$$

Gluon jets should be broader than quark jets.[38] For the same fractional energy contained in a cone,

$$\delta_{gluon} = [\delta_{quark}]^{4/9} . \tag{5.22}$$

5.4 Pairs of gauge bosons

Incisive tests of the structure of the electroweak interactions may be achieved in detailed measurements of the cross sections for the production of W^+W^-, $W^\pm Z^0$, Z^0Z^0, $W^\pm\gamma$, and $Z^0\gamma$ pairs. The rate for $W^\pm\gamma$ production is sensitive to the magnetic moment of the intermediate boson. In the Standard Model there are important cancellations in the amplitudes for W^+W^- and $W^\pm Z^0$ production that rely on the gauge structure of the WWZ trilinear coupling. The Z^0Z^0 and $Z^0\gamma$ reactions do not probe trilinear gauge couplings in the Standard Model, but are sensitive to nonstandard interactions such as those that might arise if the gauge bosons were composite. In addition, the W^+W^- and Z^0Z^0 final states may be significant backgrounds to the detection of heavy Higgs bosons and possible new degrees of freedom.

The intrinsic interest in the process $q_i\bar{q}_i \to W^+W^-$, which accounts in part for plans to study e^+e^- annihilations at c.m. energies around 180 GeV at LEP, is owed to the sensitivity of the cross section to the interplay among the γ-, Z^0-, and quark-exchange contributions. As we have seen in connection with Fig. 14, in the absence of the Z^0-exchange term, the cross section for production of a pair of longitudinally polarized intermediate bosons is proportional to $\hat{s}$, in gross violation of unitarity. It is important to verify that the amplitude is damped as expected. The mass spectrum of W^+W^- pairs is of interest both for the verification of gauge cancellations and for the assessment of backgrounds to heavy Higgs boson decays. This is shown for intermediate bosons satisfying $|y| < 2.5$ in Fig. 26. The number of pairs produced at high energies seems adequate for a test of the gauge cancellations, provided that the intermediate bosons can be detected with high efficiency.

Table 3 shows the expected yields of pairs of electroweak gauge bosons at the $Sp\bar{p}S$, the Tevatron, and the SSC. At 630 GeV and an integrated luminosity of 10^{37} cm^{-2} = 10 pb^{-1}, prospects for the study of W^+W^- pairs are remote. It may be barely possible to initiate studies at 1.8 TeV and 10^{38} cm^{-2} = 100 pb^{-1}. At 40 TeV and 10^{40} cm^{-2} = 10^4 pb^{-1}, we can look forward to 2×10^6 W^+W^- pairs per year. Efficient detection is the key to incisive studies.

6 TECHNICOLOR

There is at the present time no direct experimental evidence that compels the modification or extension of the Standard Model. The motivations for going beyond the Standard Model, or for attempting to "complete" it, are based upon aesthetic principles of theoretical simplicity and elegance, or demands for internal consistency. Having reviewed some of the arguments for elaborating upon the Standard Model, we now consider the first of several possible extensions: the technicolor scheme of dynamical symmetry breaking. We are not looking for a replacement of the Standard Model, for we expect that the Standard Model will remain as the low-energy limit of a more complete theory, much as the four-fermion description of the charged current weak interaction emerges as the low-energy limit of the Weinberg-Salam model.

6.1 THE IDEA OF TECHNICOLOR

The dynamical symmetry breaking approach, of which technicolor theories are exemplars, is modeled upon our understanding of another manifestation of spontaneous symmetry breaking in Nature, the superconducting phase transition. The macroscopic order parameter of the Ginzburg-Landau phenomenology[39] corresponds to the wave function of superconducting charge carriers. It acquires a nonzero vacuum expectation value in the superconducting state. The microscopic Bardeen-Cooper-Schrieffer theory[40] identifies the dynamical origin of the order parameter with the formation of bound states of elementary fermions, the Cooper pairs of electrons. The basic idea of the technicolor mechanism is to replace the elementary Higgs boson of the Standard Model by a fermion-antifermion bound state. By analogy with the superconducting phase transition, the dynamics of the fundamental technicolor gauge interactions among technifermions generate scalar bound states, and these play the role of the Higgs fields.

In the case of superconductivity, the elementary fermions (electrons) and the gauge interactions (QED) needed to generate the scalar bound states are already present in the theory. Could we achieve a scheme of similar economy for the electroweak symmetry breaking transition?

Consider an $SU(3)_c \otimes SU(2)_L \otimes U(1)_Y$ theory of massless up and down quarks. Because the strong interaction is strong, and the electroweak interaction is feeble, we may consider the $SU(2)_L \otimes U(1)_Y$ interaction as a perturbation. For vanishing quark masses, QCD has an exact $SU(2)_L \otimes SU(2)_R$ chiral symmetry. At an energy scale $\sim \Lambda_{QCD}$, the strong interactions become strong, fermion condensates appear, and the chiral symmetry is spontaneously broken

$$SU(2)_L \otimes SU(2)_R \rightarrow SU(2)_V \tag{6.1}$$

to the familiar flavor symmetry. Three Goldstone bosons appear, one for each broken generator of the original chiral invariance. These were identified by Nambu[41] as three massless pions.

The broken generators are three axial currents whose couplings to pions are measured by the pion decay constant f_π. When we turn on the $SU(2)_L \otimes U(1)_Y$ electroweak interaction, the electroweak gauge bosons couple to the axial currents, and acquire masses of order $\sim g f_\pi$. The massless pions thus disappear from the physical spectrum, having become the longitudinal components of the weak gauge bosons. This achieves much of what we desire. Unfortunately, the mass acquired by the intermediate bosons is far smaller than required for a successful low-energy phenomenology; it is only

$$M_W \sim 30 \text{ MeV}/c^2 \,. \tag{6.2}$$

6.2 A MINIMAL MODEL

The simplest transcription of these ideas to the electroweak sector is the minimal technicolor model of Weinberg[42] and Susskind.[43] The technicolor gauge group is taken to be $SU(N)_{TC}$ (usually $SU(4)_{TC}$), so the gauge interactions of the theory are generated by

$$SU(4)_{TC} \otimes SU(3)_c \otimes SU(2)_L \otimes U(1)_Y \,. \tag{6.3}$$

The technifermions are a chiral doublet of massless color singlets

$$\begin{pmatrix} U \\ D \end{pmatrix}_L \quad U_R,\ D_R \,. \tag{6.4}$$

With the electric charge assignments $Q(U) = \frac{1}{2}$ and $Q(D) = -\frac{1}{2}$, the theory is free of electroweak anomalies. The ordinary fermions are all technicolor singlets.

In analogy with our discussion of chiral symmetry breaking in QCD, we assume that the chiral TC symmetry is broken,

$$SU(2)_L \otimes SU(2)_R \otimes U(1)_V \to SU(2)_V \otimes U(1)_V \,. \tag{6.5}$$

Three would-be Goldstone bosons emerge. These are the technipions

$$\pi_T^+,\quad \pi_T^0,\quad \pi_T^-, \tag{6.6}$$

for which we are free to *choose* the technipion decay constant as

$$F_\pi = \left(G_F\sqrt{2}\right)^{-1/2} = 247 \text{ GeV} \,. \tag{6.7}$$

When the electroweak interactions are turned on, the technipions become the longitudinal components of the intermediate bosons, which acquire masses

$$\begin{aligned} M_W^2 &= g^2 F_\pi^2/4 &&= \frac{\pi\alpha}{G_F\sqrt{2}\sin^2\theta_W} \\ M_Z^2 &= (g^2+g'^2)\,F_\pi^2/4 &&= M_W^2/\cos^2\theta_W \end{aligned} \tag{6.8}$$

that have the canonical Standard Model values, thanks to our choice (6.7) of the technipion decay constant.

Working by analogy with QCD, we may guess the spectrum of other $F\overline{F}$ bound states as follows:

$$\left.\begin{array}{rl} 1^{--}\text{ technirhos} & \rho_T^+,\ \rho_T^0,\ \rho_T^- \\ 1^{--}\text{ techniomega} & \omega_T \\ 0^{-+}\text{ technieta} & \eta_T \\ 0^{++}\text{ technisigma} & \sigma_T \end{array}\right\}, \tag{6.9}$$

all with masses on the order of the technicolor scale $\Lambda_{TC} \sim O(1\ \mathrm{TeV}/c^2)$, since they do not originate as Goldstone bosons. The dominant decay of the technirho will be

$$\rho_T \to \pi_T \pi_T\ , \tag{6.10}$$

i.e. into pairs of longitudinally polarized gauge bosons. Standard estimates lead to

$$\begin{aligned} M(\rho_T) &\approx 1.77\ \mathrm{TeV}/c^2 \\ \Gamma(\rho_T) &\approx 325\ \mathrm{GeV}\ . \end{aligned} \tag{6.11}$$

Minimal technicolor leads to an enhancement of the cross section for the production of pairs of gauge bosons, which we may estimate by applying "technivector meson dominance" to the Standard Model expressions. I show in Fig. 27 the mass spectrum of $Z^0W^+ + Z^0W^-$ pairs produced in pp collisions at 20, 40, and 100 TeV, with and without the technirho enhancement. Both intermediate bosons are required to satisfy $|y| < 1.5$. The technirho enhancement amounts to nearly a doubling of the cross section in the resonance region. However, because the absolute rates are small, the convincing observation of this enhancement is perhaps the most challenging for both collider and experiment that we have encountered. In a standard *SSC* run with integrated luminosity of 10^{40} cm^{-2}, the number of excess events will be 420 on a background of 130 at 40 TeV.

6.3 Extended Technicolor

Technicolor shows how the generation of intermediate boson masses could arise without fundamental scalars or unnatural adjustments of parameters. It

thus provides an elegant solution to the naturalness problem of the Standard Model. However, it has one major deficiency: it offers no explanation for the origin of quark and lepton masses, because no Yukawa couplings are generated between Higgs fields and quarks or leptons.

A possible approach to the problem of quark and lepton masses is suggested by "extended technicolor" models. We imagine that the technicolor gauge group is embedded in a larger extended technicolor gauge group,

$$G_{TC} \subset G_{ETC} \ , \tag{6.12}$$

which couples quarks and leptons to the technifermions. If the ETC symmetry is spontaneously broken down to the TC symmetry

$$G_{ETC} \to G_{TC} \ , \tag{6.13}$$

at a scale

$$\Lambda_{ETC} \sim 30 \ - \ 300 \text{ TeV} \ , \tag{6.14}$$

then the quarks and leptons may acquire masses

$$m \sim \Lambda_{TC}^3 / \Lambda_{ETC}^2 \ . \tag{6.15}$$

The outlines of this strategy are given in Refs. 44 and 45, but no "standard" ETC model has been constructed.

As a representative of the ETC strategy we may consider a model due to Farhi and Susskind.[46] Their model is built on new fundamental constituents, which are analogs of the ordinary quarks (the techniquarks)

$$\begin{pmatrix} U \\ D \end{pmatrix}_L \quad U_R, \ D_R \tag{6.16}$$

and of the ordinary leptons (the technileptons)

$$\begin{pmatrix} N \\ E \end{pmatrix}_L \quad N_R, \ E_R \ . \tag{6.17}$$

These technifermions are bound by the $SU(N)_{TC}$ gauge interaction, which is assumed to become strong at $\Lambda_{TC} \sim 1$ TeV. Among the $F\overline{F}$ bound states are

eight color singlet, technicolor singlet pseudoscalar states [labeled by (I, I_3)]

$$\left.\begin{array}{ll} \pi_T^+ & (1,1) \\ \pi_T^0 & (1,0) \\ \pi_T^- & (1,-1) \end{array}\right\} \text{become longitudinal } W^\pm,\ Z^0$$

$$\left.\begin{array}{ll} P^+ & (1,1) \\ P^0 & (1,0) \\ P^- & (1,-1) \\ P^{0\prime} & (0,0) \end{array}\right\} \text{pseudo} - \text{Goldstone bosons} \quad , \tag{6.18}$$

$$\eta_T' \quad (0,0) \qquad \text{techniflavor singlet}$$

plus the corresponding technivector mesons. Like the η' of QCD, the η_T' couples to an anomalous current, so it is expected to acquire a mass on the order of several hundred GeV/c^2. The pseudo-Goldstone bosons are massless in the absence of electroweak and ETC interactions.

The possibilities for study of the light particles implied in such a model have been examined recently by Eichten, Hinchliffe, Lane, and myself.[47] Some consequences of the extended technicolor interaction are examined in detail. In the absence of extended technicolor interactions the neutral technipions P^0 and $P^{0\prime}$ remain massless, while the charged technipions P^+ and P^- acquire electroweak masses of a few GeV/c^2. When ETC interactions are included, the technipion masses have been estimated as[45,48]

$$\begin{aligned} 8\ \text{GeV}/c^2 < \quad & M(P^\pm) \quad < 40\ \text{GeV}/c^2\,, \\ 2\ \text{GeV}/c^2 < \quad & M(P^0, P^{0\prime}) \quad < 40\ \text{GeV}/c^2\,. \end{aligned} \tag{6.19}$$

If, as expected in the simplest models of Higgs bosons, the couplings of pseudoscalars into fermion pairs are proportional to fermion mass, the dominant decay modes will be

$$\begin{aligned} P^+ &\rightarrow t\bar{b}, c\bar{b}, c\bar{s}, \tau^+\nu \\ P^0 &\rightarrow b\bar{b}, c\bar{c}, \tau^+\tau^- \\ P^{0\prime} &\rightarrow b\bar{b}, c\bar{c}, \tau^+\tau^-;\ gg\,. \end{aligned} \tag{6.20}$$

Despite the possible similarities between Higgs bosons and technipions, there are important distinguishing characteristics. First, in the Standard Model, there is a direct HZZ coupling in the Lagrangian, whereas in the Farhi-Susskind model the P^0ZZ coupling is induced. As a consequence, we would expect the decay of a virtual $Z^* \rightarrow ZH$ to be about four orders of magnitude stronger than that of

$Z^* \to ZP^0$. If a Higgs-like entity is seen in the reaction

$$e^+e^- \to Z^0 \;\to\; Z^*H \quad \hookrightarrow \ell^+\ell^- \,, \tag{6.21}$$

then it is the Higgs, and technicolor is ruled out. Second, in a multi-Higgs model, the decay $Z^0 \to H^0H^{0\prime}$ is allowed (although the rate depends on details, such as mixing angles). In contrast, the decay $Z^0 \to P^0P^{0\prime}$ is inhibited; we therefore expect

$$\Gamma(Z^0 \to P^0P^{0\prime}) \ll \Gamma(Z^0 \to H^0H^{0\prime}) \,. \tag{6.22}$$

A clear presentation of the differences between Higgs bosons and technipions is given in Ref. 49.

A number of searches for charged scalars have been carried out in electron-positron annihilations into hadrons.[50] The most complete to date was reported recently by the CELLO Collaboration working at PETRA.[51] Their results, summarized in Fig. 28, rule out charged Higgs bosons or technipions with masses up to about 19 GeV/c^2.

It is interesting to ask why the top quark has not been seen[52] in the UA1 Experiment. At the current level of integrated luminosity, one may still be skeptical of nondiscovery claims, but let us take those seriously and ask for possible physics reasons behind the nonobservation. The least interesting possibility is that the top quark is so heavy that it lies outside the explored range. More amusing is the possibility that the expected signal in the weak semileptonic decay

$$t \to b\ell^+\nu \,, \tag{6.23}$$

which occurs in order G_F^2, might be swamped by the semiweak decay

$$t \to P^+ + (b \text{ or } s \text{ or } d) \,, \tag{6.24}$$

which occurs in order G_F. The technipion decay mode would dramatically shorten the t-quark lifetime, and reduce the semileptonic branching ratio. Perhaps the nonobservation of the top quark signals the discovery of technicolor?

The next good place to look for light technipions is in experiments at SLC and LEP, where the study of rare decays of the Z^0 will become possible. Figure 29 shows that the branching ratio expected for the decay $Z^0 \to P^+P^-$ can be expected at the level of 10^{-3} or more, for technipion masses up to about 40 GeV/c^2. The technipion pairs are to be reconstructed in final states such as $(c\bar{b})(\bar{c}b)$, etc.

Our principal interest here is in pure technicolor aspects, specifically the search for heavy particles, which awaits supercollider experimentation. In the

Farhi-Susskind model, the mass and width of the technirho may be scaled from the known properties of the ρ-meson in QCD. We expect

$$\begin{aligned} M(\rho_T) &\approx 885 \text{ GeV}/c^2 \\ \Gamma(\rho_T) &\approx 500 \text{ GeV} , \end{aligned} \tag{6.25}$$

if the technicolor gauge group is $SU(4)_{TC}$. Among technirho enhancements, the most prominent is expected to be in the $W^{\pm}Z^0$ channel, which will be somewhat easier to observe than the corresponding effect in the minimal model. The resulting mass spectrum is shown in Fig. 30.

6.4 Colored Technipions

From the color-triplet $(U\ D)$ and color-singlet $(N\ E)$ technifermions, we may build ${}^1S_0\ (F\overline{F})$ states:

- an isospin triplet $P_3^1,\ P_3^0,\ P_3^{-1}$ of color triplets;
- an isospin singlet color triplet state P_3';
- the corresponding antitriplet states;
- an isospin triplet $P_8^+,\ P_8^0,\ P_8^-$ of color octets;
- an isoscalar color-octet state $P_8^{0\prime}$

with masses (acquired from the color interaction) of

$$\begin{aligned} M(P_3) &\approx 160 \text{ GeV}/c^2 \\ M(P_8) &\approx 240 \text{ GeV}/c^2 . \end{aligned} \tag{6.26}$$

With the standard charge assignments, the P_3 and P_3' charges are

$$(5/3, 2/3, -1/3; 2/3) . \tag{6.27}$$

The isoscalar $P^{0\prime}$ may be produced copiously by gluon-gluon fusion, which leads to equal cross sections in $p^{\pm}p$ collisions. The differential cross section (summed over the eight colors of the produced particle) is

$$\left.\frac{d\sigma(ab \to P_8^{0\prime} + \text{ anything})}{dy}\right|_{y=0} = \frac{5\alpha_s^2}{24\pi F_\pi^2} \cdot \tau f_g^{(a)}(\sqrt{\tau}, M_{P_8}^2) f_g^{(b)}(\sqrt{\tau}, M_{P_8}^2) , \tag{6.28}$$

where $\tau = M_P^2/s$ This is shown as a function of the technipion mass in Fig. 31. The dominant decay modes will be

$$P_8^{0\prime} \to \begin{cases} gg \\ t\bar{t} \end{cases} . \tag{6.29}$$

The expected branching ratios depend upon the top quark mass, but 50% into each channel is a guess that will not be misleading. In the $t\bar{t}$ channel, the expected signal and background are approximately equal, and the number of events is quite large at supercollider energies. The signal-to-background improves somewhat with increasing technipion mass. The main issues for detection are the identification of t-quarks and the resolution in invariant mass of the reconstructed pairs. This is an appropriate topic for detector studies.

Pairs of colored technipions also will be produced with substantial cross sections at supercollider energies, principally by gluon fusion. As a first example, I show in Fig. 32 the integrated cross section for the reaction

$$pp \to P_3\overline{P}_3 + \text{ anything} \tag{6.30}$$

with and without the technirho ($\rho_8^{0\prime}$) enhancement. The expected decays of the color triplet technipions are

$$P_3 \to q\bar{\ell} \text{ or } \bar{q}\bar{q} , \tag{6.31}$$

i.e., final states such as $t\tau^+$, $t\nu_\tau$, $b\tau^+$, $\bar{t}\bar{b}$, etc. As a second example, I show in Fig. 33 the integrated cross section for the reaction

$$pp \to P_8\overline{P}_8 + \text{ anything} \tag{6.32}$$

with and without the technirho ($\rho_8^{0\prime}$) enhancement. These cross sections are typically $\sim$ 15 times the cross sections for color triplet technipion production, and comparable to the cross sections for single $P_8^{0\prime}$ production.

The expected decays of octet technipions, in addition to those given in (6.29), are

$$\begin{aligned} P_8^+ &\to t\bar{b} , \\ P_8^0 &\to t\bar{t} . \end{aligned} \tag{6.33}$$

The signature for the $P_8^+P_8^-$ channel is therefore $t\bar{b}$ on one side of the beam and $\bar{t}b$ on the other. If the heavy flavors can be tagged with high efficiency, we know of no significant conventional backgrounds.

6.5 Appraisal

If the technicolor hypothesis correctly describes the breakdown of the electroweak gauge symmetry, there will be a number of spinless technipions with masses below the technicolor scale of about 1 TeV. Some of these, the color singlet, technicolor singlet particles, should be quite light (masses $\lesssim 40$ GeV/c^2) and can be studied using the current generation of e^+e^- and $\overline{p}p$ colliders. The colored particles are probably inacessible to experiment before a supercollider comes into operation, as are technivector mesons. In *EHLQ* we have made a rough appraisal of the minimum effective luminosities required for the observation of various technicolor signals. Full exploitation of the scientific opportunities requires the efficient identification and measurement of heavy quark flavors, and the ability to identify intermediate bosons in complex events. Our expectation is that if the appropriate effort is made in detector development, a 40 TeV collider that supports experimentation at an integrated luminosity of 10^{39} cm^{-2} will be sufficient to either confirm or rule out the technicolor hypothesis.

7 Experimental environment of the SSC

What will experimentation be like at the SSC? Specific analysis of signals and backgrounds is quite fruitful, and has been the object of many of the studies carried out over the past four years.[2–8] However, we must also be aware of the general environment in which detectors must function and events must be selected and recorded.

The basic parameters of the SSC are set out in the Conceptual Design Report,[53] a non–site-specific conception of a $20 \oplus 20$ TeV proton-proton collider 83 km in circumference. The design calls for two clusters of interaction regions incorporating both physics experimental areas and major supporting equipment, a configuration that seems advantageous from the point of view of operating efficiency, economics, sociology, and accelerator physics. At the design luminosity of 10^{33} cm^{-2}sec^{-1}, interactions will occur at the rate of

$$0.016 \cdot (\sigma_t/1 \text{ mb}) \text{ interactions/crossing} . \tag{7.1}$$

The length of each bunch of protons is 6.0–7.3 cm, and adjacent bunches are separated by 5.1 m. A sketch of the layout proposed for the SSC is shown in Fig. 34.

We expect the total cross section at 40 TeV to lie in the range

$$100 \text{ mb} \lesssim \sigma_t \lesssim 200 \text{ mb} \ , \tag{7.2}$$

so that the event rate at the design luminosity may range up to 2×10^8 per

second. The current best guess for the total cross section, based on the fits[54] shown in Fig. 35, is $\sigma_t = 138$ mb .

A good way to gain respect for the conditions that will prevail at the SSC is to examine the trigger rate for events with transverse energy E_T greater than some threshold E_T^{min}. This is shown in Fig. 36 for the nominal operating conditions of the SSC: $\sqrt{s} = 40$ TeV and $\mathcal{L} = 10^{33}$ cm^{-2}sec^{-1}, as well as at 10 and 100 TeV. At 40 TeV, a "high-E_T" trigger with threshold set at 2 TeV will count at 1 Hz from two-jet QCD events. This is of interest in planning triggers that will efficiently select interesting events from the $2 \cdot 10^8$ interactions that will take place each second in an SSC interaction region.

Particle multiplicities will also be large. In QCD, we can estimate[55] the multiplicity of partons in a gluon jet as

$$\langle n(Q) \rangle_g \propto (\log Q/\Lambda)^{-c} \exp\left(\sqrt{\frac{12 \log Q/\Lambda}{\pi b_0}}\right) , \tag{7.3}$$

where $Q \sim p_\perp$ measures the virtualness of the jet, and

$$b_0 = (33 - 2N_f)/12\pi \; ; \quad \text{and } c = (11 + 22N_f/27)/8\pi b_0 \; , \tag{7.4}$$

where N_f is the number of active quark flavors. This result depends critically on taking account of quantum mechanical interference; in a purely probabilistic ("branching") approach, the exponent is larger by a factor of $\sqrt{2}$.

The multiplicity difference between quark jets and gluon jets is also calculable in perturbative QCD. The result[56] is

$$\frac{\langle n(Q) \rangle_g}{\langle n(Q) \rangle_q} = \frac{9}{4} \cdot (1 - 0.27\sqrt{\alpha_s} - 0.07\alpha_s) \; . \tag{7.5}$$

The multiplicity growth expected in quark jets, normalized to the observed multiplicity of hadrons produced in e^+e^- annihilations, is shown in Fig. 37. There we see graphically the importance of including coherence effects. The multiplicities expected in a 1-TeV jet are impressively large.

Finally, the fragmentation of gluon jets into heavy quark pairs is expected to be reliably calculated in perturbation theory.[57] We expect about 0.1 ($c\bar{c}$) pair per gluon jet at the $Sp\bar{p}S$, and this is about what is seen.[58] For heavier flavors and higher energies, we may take some guidance from the evolution of a gluon jet into heavy flavors as given by perturbation theory, in Fig. 38. Roughly speaking, a 1-TeV gluon will yield 0.5 pair of c-quarks, 0.25 pair of b-quarks, and 0.05 t-quarks.

8 SUPERSYMMETRY[59]

In relativistic quantum field theory, continuous symmetries of the S-matrix normally are based on Lie algebras. A familiar example is the $SU(2)$ symmetry of isospin, generated by the algebra

$$[T^j, T^k] = i\varepsilon^{jkl} T_l \,, \tag{8.1}$$

where ε^{jkl} is the antisymmetric three-index symbol. The most general form[60] of symmetries of the S-matrix is the combination of Poincaré invariance plus internal symmetries. The space-time symmetries are generated by the momentum operator P^μ, the generator of translations, and by $M^{\mu\nu}$, the generator of Lorentz boosts and rotations. This leads to the familiar classification of particles by mass and spin. Internal symmetries are generated by the generators of the symmetry group G, which we denote generically as X_a. These objects commute with the generators of space-time symmetries,

$$\left.\begin{aligned} [X_a, P^\mu] &= 0 \\ [X_a, M^{\mu\nu}] &= 0 \end{aligned}\right\} \,, \tag{8.2}$$

and with the Hamiltonian $\mathcal{H}$ of the world,

$$[X_a, \mathcal{H}] = 0 \,, \tag{8.3}$$

so we may simultaneously specify internal quantum numbers along with masses and spins. This leads to the useful classification of particles by representations of the symmetry group G. Examples of internal symmetries are global symmetries such as the flavor symmetries and the $U(1)$ symmetry associated with baryon number conservation, and the local (gauged) symmetries such as $SU(3)_c \otimes SU(2)_L \otimes U(1)_Y$.

The notion of Lie algebras may be generalized to the *graded Lie algebras* defined by both commutators and anticommutators:

$$\left.\begin{aligned} [X, X'] &\sim X'' \\ \{Q, Q'\} &\sim X \\ [Q, X] &\sim Q'' \end{aligned}\right\} \,. \tag{8.4}$$

The generators of the graded Lie algebras are of two kinds. The scalar charges X_a make up the odd part of the algebra, while the spinorial charges Q_a make up the even part. Among the graded Lie algebras, the only ones consistent with relativistic quantum field theory are the supersymmetry algebras,[61] in simplest form

$$\left.\begin{aligned} \{Q_a, \bar{Q}^b\} &\sim \delta_a^b \gamma \cdot P \\ \{Q, Q\} &= 0 = \{\bar{Q}, \bar{Q}\} \\ [P, Q] &= 0 = [P, \bar{Q}] \end{aligned}\right\} \,, \tag{8.5}$$

where $\bar{Q}$ is the Hermitian conjugate of Q, a and b are internal symmetry labels, and P is a momentum 4-vector.

A particle is transformed by a scalar charge into a partner with the same mass and spin. An example is the action of T_i, which generates isospin rotations about the i–axis. A particle is transformed by a spinorial charge into a superpartner whose spin differs by 1/2 unit, but which otherwise has identical quantum numbers. Thus arises a connection between fermions and bosons.

8.1 The Spectrum of Superpartners

In a supersymmetric theory, particles fall into multiplets that are representations of the supersymmetry algebra. Superpartners share all quantum numbers except spin; if the supersymmetry is unbroken, they are degenerate in mass. The number of fermion states (counted as degrees of freedom) is identical with the number of boson states. In nearly all supersymmetric theories, the superpartners carry a new fermionic quantum number R, which is exactly conserved. This means that the lightest superpartner will be absolutely stable. In Table 4 we list the fundamental fields of the Standard Model and their superpartners. By examining the quantum numbers of known particles, we readily see that there are no candidates for supersymmetric pairs among them. Supersymmetry therefore means doubling the particle spectrum, compared with the Standard Model. In fact, we must expand the spectrum slightly further, because the minimal supersymmetric extension of the Standard Model requires at least two doublets of Higgs bosons. In a supersymmetric theory, the supermultiplets are labelled by the chirality of the fermions they contain, and only supermultiplets of the same chirality can have Yukawa couplings to one another. This means that, in contrast to the situation in the Standard Model, the Higgs doublet that gives mass to the charge 2/3 quarks cannot be the charge conjugate of the Higgs doublet that gives mass to the charge -1/3 quarks, because the charge conjugate of a right-handed (super)field is left-handed.[62]

The interactions among old and new particles are prescribed by the supersymmetric extension of the usual interaction Lagrangian, which we shall take to be the $SU(3)_c \otimes SU(2)_L \otimes U(1)_Y$ theory. If supersymmetry is an invariance of the Lagrangian, it is evidently a broken symmetry, because observationally boson masses are not equal to the masses of their fermion counterparts. For supersymmetry to resolve the hierarchy problem, we have seen that it must be effectively unbroken above the electroweak scale of $O(1\ \text{TeV})$. This suggests that superpartner masses will themselves be $\lesssim 1\ \text{TeV}/c^2$.

There is no convincing theory for masses of the superpartners. (This is not worse than the situation for the masses of the usual fermions or scalars.) As for the ordinary particles, however, we can derive relations among superparticle

masses, and infer restrictions on the masses. Three kinds of indirect methods yield interesting relations:

- The role of virtual superpartners in rare processes. An example within the Standard Model is the limit on the $m_c - m_u$ mass splitting inferred from the magnitude of the $K^0 - \overline{K}^0$ transition amplitude.
- Cosmological constraints. A Standard Model example is the bound on the sum of light neutrino masses inferred from the limits on the mass density of the Universe.
- The distortion of Standard Model predictions. A conventional example is the bound on the number of light neutrino species inferred from the total width of the Z^0.

Not only is there no convincing theory for the masses of superpartners, even the *ordering* of superpartner masses is quite model dependent. What this means for direct searches is that one must consider all reasonable possibilities. In practice, this entails

- Searching for all superpartners,
- Considering all plausible decay modes of each one, and
- Making use of existing experimental constraints.

In spite of its wide-open nature, the search for supersymmetry is an urgent matter, because supersymmetry is one possible solution to the naturalness problem of scalar masses. Moreover, finding supersymmetry on the 1-TeV scale would provide powerful encouragement for superstring theories.

It is generally expected that the photino $\tilde{\gamma}$ is the lightest superpartner and hence stable. If global supersymmetry is spontaneously broken, the theory acquires a massless Goldstone *fermion*, the Goldstino $\tilde{\mathcal{G}}$. Decays of the form

$$\tilde{\gamma} \to \gamma \tilde{\mathcal{G}} \tag{8.6}$$

are then allowed. In supergravity theories, based upon spontaneously broken *local* supersymmetry, the Goldstino becomes the helicity $\pm 1/2$ components of the massive, spin-3/2 gravitino, and may not be available as a decay product of a light photino. The other popular candidates for the lightest superpartner arethe *sneutrino*, $\tilde{\nu}$, and the Higgsino, $\tilde{H}$. Any of these candidates is a weakly interacting neutral particle, which will result in undetected energy. Although it is important to consider all possibilities systematically, we shall assume for most of today's discussion that the lightest superpartner is the photino.

The strongly interacting superparticles are of particular interest because they are produced at substantial rates in hadron-hadron collisions. Possible decay chains and signatures for squarks and gluinos are indicated in Fig. 39. For each unstable strongly interacting superpartner produced, we expect one, two, or three jets, accompanied by missing energy.

Before we turn to our main subject, the search for supersymmetry at high energies, it will be useful to have in mind a rough summary of the limits on masses of superpartners as they stand before the analysis of data from the $S\bar{p}pS$ collider. I caution that every entry hangs on assumptions about decay chains, etc., and that few categorical statements are reliable. For thorough discussions of the considerations that underlie the limits, see the papers by Haber and Kane, and by Dawson, et al., in Ref. 23. An abbreviated statement of existing limits is given in Table 5.[63]

8.2 Superparticle Searches in $p^{\pm}p$ Collisions

Over the past few years, a great deal of effort has gone into estimating production rates for superpartners. For example, Sally Dawson, Estia Eichten, and I[23] have evaluated all the lowest-order (Born diagram) cross sections $d\hat{\sigma}/d\hat{t}$ and $\hat{\sigma}$ for the production of

$$(\tilde{q}, \tilde{\ell}^{\pm}, \tilde{\nu}, \tilde{g}, \tilde{\gamma}, \tilde{Z}^0, \tilde{H}^0, \tilde{H}^{0\prime}, \tilde{W}^{\pm}, \tilde{H}^{\pm})^2 \tag{8.7}$$

final states in parton–parton collisions, including the possibility of mixing among $(\tilde{\gamma}, \tilde{Z}, \tilde{H}^0, \tilde{H}^{0\prime})$ or $(\tilde{W}^{\pm}, \tilde{H}^{\pm})$. We have also calculated the processes initiated by e^+e^- collisions. Many of these reactions have been studied by others as well; complete references are given in our paper. The approximate magnitudes of the cross sections are indicated in Table 6.

The outlines of the search for supersymmetry at the SSC are given in *EHLQ*.[2] Considerable progress in the areas of simulation, search strategies, and the implications of unfavorable decay channels can be traced in Refs. 4–8 and 59. Cross sections for the production of superpartners should be quite ample for a luminosity of 10^{32} cm^{-2}sec^{-1} or more, and a c.m. energy of 40 TeV. As examples, I show in Figs. 40–42 the integrated cross sections for the production of superpartners with rapidities $|y_i| < 1.5$, for the reactions

$$pp \to \tilde{g}\tilde{g} + \text{anything}, \tag{8.8}$$

$$pp \to \tilde{g}\tilde{q} + \text{anything}, \tag{8.9}$$

and

$$pp \to \tilde{g}\tilde{\gamma} + \text{anything}, \tag{8.10}$$

respectively.

On the basis of these and other cross section calculations and a rudimentary assessment of the requirements for detection, we have estimated the discovery limits for various energies and luminosities. These estimates are shown in Table 7 for gluinos, squarks, photinos, zinos, winos, and sleptons. We infer from these estimates that a 40-TeV $p^{\pm}p$ collider with integrated luminosity exceeding 10^{39} cm^{-2} should be adequate to establish the presence or absence of the superpartners predicted by models of low-energy supersymmetry.

8.3 Conclusions

We have examined a general class of supersymmetric theories in which the effective low-energy theory relevant at 1 TeV or below is the supersymmetric extension of $SU(3)_c \otimes SU(2)_L \otimes U(1)_Y$. The search for supersymmetry is complicated by the absence of reliable predictions for the masses of superpartners. Low-energy supersymmetry is surprisingly unconstrained by experiment, in spite of increasing efforts over the past four years. For example, photinos as light as a few GeV$/c^2$ are allowed for some ranges of parameters, in all scenarios. Interesting limits can be placed on *stable* squarks and sleptons. For *unstable* scalar quarks, stringent limits exist only if the photino is massless.

A complete catalogue of total and differential cross sections exists for the production of superpartners in $p^{\pm}p$ and e^+e^- collisions. Detailed simulations, including detector characteristics, are required; important work along these lines is in progress, but continued iteration with experimental reality will be needed. At the $S\overline{p}pS$ and Tevatron colliders, rates are ample for superpartner masses up to about 100 GeV$/c^2$, but good signatures beyond the traditional "missing E_T" tag must be devised. The SSC will permit the study of squarks and gluinos up to masses of 1 Tev$/c^2$ and beyond.

9 Concluding remarks

In this brief survey, it has been possible only to scratch the surface of the physics opportunities presented by a high-energy, high-luminosity hadron collider. The examples we have considered here do begin to indicate the scope of physics issues to be addressed, ranging from detailed study of known particles, such as the intermediate bosons, to the search for high-mass exotica. The comprehensive studies of physics possibilities carried out over the past four years have shown convincingly that

> A 40 TeV collider which permits experimentation at integrated luminosities of at least 10^{39} cm^{-2} will make possible detailed exploration of the 1-TeV scale.

This conclusion is based on detailed consideration of the canonical inventions intended to improve the Standard Model, technicolor and supersymmetry, and of the Standard Model itself. In addition, there are many opportunities for exploring constituent interactions at subenergies up to about 10 TeV in the study of jets, the search for additional gauge bosons, etc. "Fixed-target style" colliding beams experiments may be well suited to address rare W decays and heavy flavor physics, for example. The SSC is not by any means a one-issue laboratory, and it is important that we mount a diversity of experimental initiatives, to realize its full scientific potential.

With respect to experimentation at the SSC, there are a few detector issues that I like to raise at every opportunity.

- The utility of high-efficiency W and Z detectors. The discovery physics we have considered in assessing the physics prospects of the SSC can all be done by relying upon the leptonic decays of the gauge bosons, but we can move to a deeper level of experimentation by learning to use the nonleptonic decays as well.

- The UA1 experiment has already indicated the value of "hermetic" detectors, which can capture and measure all the visible energy emitted in the central region. For a general-purpose SSC detector, it is of interest to require hermeticity for rapidities $|y| < 3$.

- Examples from technicolor and the Higgs sector of the Standard Model indicate that good-efficiency $\tau, b, \ldots$ tags will be of considerable value in enhancing signals over background. Full utilization of the heavy-flavor tag requires measuring the four-momenta of the short-lived particles as well.

- How to reduce the interaction rate of $\sim 10^8$ Hz to the $O(1\text{ Hz})$ rate at which complex events can be written on storage media (magnetic tapes, optical discs)? There are many opportunities for creativity here!

- Bringing remote local intelligence into the detector components themselves requires the implementation of radiation-hardened electronics, especially near the beam directions.

We are faced with great opportunities!

****

It is a pleasure to thank the organizers, staff, and students of the 1987 SLAC Summer Institute for warm hospitality, efficient organization, and interesting and provocative discussions. I am grateful to Bob Cahn, Sally Dawson, Estia Eichten, Keith Ellis, Ian Hinchliffe, Ken Lane, Hallsie Reno, and other colleagues for discussion of the subjects treated in these lectures. I thank Kate Metropolis for comments on the manuscript.

Footnotes and References

[1] For thorough introductions to the current paradigm, see L. B. Okun, *Leptons and Quarks* (North-Holland, Amsterdam, 1981); D. H. Perkins, *Introduction to High Energy Physics,* third edition (Addison-Wesley, Reading, Mass., 1987); C. Quigg, *Gauge Theories of the Strong, Weak, and Electromagnetic Interactions* (Benjamin / Cummings, Reading, Mass., 1983).

[2] E. Eichten, I. Hinchliffe, K. Lane, and C. Quigg, *Rev. Mod. Phys.* **56**, 579 (1984); *ibid.* **58**, 1065E (1986).

[3] *Large Hadron Collider in the LEP Tunnel,* edited by G. Brianti, et al., CERN 84-10.

[4] *Proceedings of the 1984 Summer Study on Design and Utilization of the Superconducting Super Collider,* edited by R. Donaldson and J. G. Morfín (Fermilab, Batavia, Illinois, 1984); *Proceedings of the Workshop on Electroweak Symmetry Breaking,* edited by T. Appelquist, M. K. Gaillard, and I. Hinchliffe, LBL-18571; *$\bar{p}p$ Options for the Supercollider,* edited by J. E. Pilcher and A. R. White (University of Chicago, 1984); *Physics at the Superconducting Super Collider Summary Report,* edited by P. Hale and B. Winstein (Fermilab, 1984).

[5] *Supercollider Physics,* edited by D. E. Soper (World Scientific, Singapore, 1986).

[6] *Proceedings of the Summer Study on the Physics of the Superconducting Supercollider, Snowmass, 1986,* edited by Rene Donaldson and Jay Marx (Division of Particles and Fields of the American Physical Society, New York, 1987).

[7] *Les Rencontres de Physique de la Vallée d'Aoste, Results and Perspectives in Particle Physics,* edited by M. Greco (Editions Frontières, Gif-sur-Yvette, France, 1987).

[8] *Proceedings of the Workshop on Experiments, Detectors, and Experimental Areas for the Supercollider,* Berkeley, 1987, edited by Rene Donaldson and M. D. Gilchriese (World Scientific, Singapore, to be published).

[9] E. Eichten, in *High Energy Physics 1985: Proceedings of the Yale Theoretical Advanced Study Institute,* edited by M. J. Bowick and F. Gürsey (World Scientific, Singapore, 1985), p. 609.

[10] I. Hinchliffe, in *From the Planck Scale to the Weak Scale: Towards a Theory of the Universe,* Proceedings of the Theoretical Advanced Study Institute in Particle Physics, Santa Cruz, 1986, edited by H. Haber (World Scientific, Singapore, 1987).

[11] C. Quigg, "Supercollider Physics: a Prospectus," in *Strings, Lattice Gauge Theory, High Energy Phenomenology,* Proceedings of the Winter School, Panchgani, India, 25 January – 5 February 1986, edited by V. Singh and S. R. Wadia (World Scientific, Singapore, 1987), p. 361.

[12] F. E. Close, *An Introduction to Quarks and Partons* (Academic, New York, 1979); J. L. Rosner, "Quark Models," in *Techniques and Concepts of High Energy Physics,* St. Croix, 1980, edited by T. Ferbel (Plenum, New York, 1981), p. 1.; C. Quigg, "Models for Hadrons," lectures given at l'Ecole d'Eté de Physique Théorique, Les Houches, in *Gauge Theories in High Energy Physics,* edited by M. K. Gaillard and R. Stora (North-Holland, Amsterdam, 1983), p. 645.

[13] J. J. Aubert, et al. (EMC Collaboration), *Nucl. Phys.* **B259**, 189 (1985) (hydrogen); *ibid.* **B272**, 158 (1986) (iron); *ibid.* **B293**, 740 (1987) (deuterium).

[14] D. B. MacFarlane, et al. (CCFRR Collaboration), *Z. Phys. C***26**, 1 (1984).

[15] G. Altarelli and G. Parisi, *Nucl. Phys.* **B126**, 298 (1977).

[16] The standard form of the Altarelli-Parisi equations and the Mellin transform method of solution in terms of moments of the parton distributions are treated in Quigg, Ref. 1. A technique with better convergence properties follows from applying the Altarelli-Parisi strategy to $x\times$ the parton distributions; this is used and explained in *EHLQ*, Ref. 2.

[17] H. Abramowicz, et al., *Z. Phys. C***13**, 199 (1982); *C***17**, 283 (1983).

[18] A. D. Linde, *Zh. Eksp. Teor. Fiz. Pis'ma Red.* **23**, 73 (1976) [*JETP Lett.* **23**, 64 (1976)]; S. Weinberg, *Phys. Rev. Lett.* **36**, 294 (1976).

[19] B. W. Lee, C. Quigg, and H. B. Thacker, *Phys. Rev. D***16**, 1519 (1977). For a somewhat different approach that leads to similar constraints on the mass of the Higgs boson, see M. Veltman, *Acta Phys. Polon. B***8**, 475 (1977).

[20] G. 't Hooft, in *Recent Developments in Gauge Theories,* edited by G. 't Hooft, et al. (Plenum, New York, 1980), p. 135.

[21] For a summary of the standard shortcomings, see *EHLQ*, Ref. 2.

[22] M. Veltman, *Acta Phys. Polon. B*12, 437 (1981); C. H. Llewellyn Smith, *Phys. Rep.* **105**, 53 (1984).

[23] Reviews of the experimental implications of supersymmetry on the scale of electroweak symmetry breaking appear in D. V. Nanopoulos and A. Savoy-Navarro (Editors), *Phys. Rep.* **105**, 1 (1984); H. E. Haber and G. L. Kane, *ibid.* **117**, 75 (1985); S. Dawson, E. Eichten, and C. Quigg, *Phys. Rev. D*31, 1581 (1985); R. M. Barnett, H. E. Haber, and G. L. Kane, *Nucl. Phys.* **B267**, 625 (1986). See also the papers cited in §8.

[24] For reviews of the technicolor idea, see E. Farhi and L. Susskind, *Phys. Rep.* **74**, 277 (1981); R. Kaul, *Rev. Mod. Phys.* **55**, 449 (1983). A recent study for the current generation of accelerators appears in E. Eichten, I. Hinchliffe, K. D. Lane, and C. Quigg, *Phys. Rev. D*34, 1547 (1986).

[25] The idea of a strongly interacting gauge sector is an evergreen in particle theory. In the context of the Standard Model, early discussions appear in the papers of Ref. 19. Recent investigations appropriate to the super-collider scale are reported in M. Chanowitz and M. K. Gaillard, *Nucl. Phys.* **B261**, 379 (1985); *Phys. Lett.* **142B**, 85 (1984); M. Chanowitz, M. Golden, and H. Georgi, *Phys. Rev. D*36, 1490 (1987).

[26] M. Green and J. Schwarz, *Phys. Lett.* **149B**, 117 (1984), *ibid.* **151B**, 21 (1985); D. J. Gross, J. A. Harvey, E. Martinec, and R. Rolm, *Phys. Rev. Lett.* **54**, 502 (1985), *Nucl. Phys.* **B256**, 253 (1985); E. Witten, *Nucl. Phys.* **B258**, 75 (1985); M. Dine, V. Kaplunovsky, M. Mangano, C. Nappi, and N. Seiberg, *Nucl. Phys.* **B259**, 519 (1985).

[27] L. S. Durkin and P. Langacker, *Phys. Lett.* **166B**, 436 (1986); P. Binétruy, S. Dawson, I. Hinchliffe, and M. Sher, *Nucl. Phys.* **B273**, 501 (1986); J. L. Rosner, in *Proceedings of the International Symposium on Particle and Nuclear Physics,* Beijing, 1985, edited by Ning Hu and Chong-shi Wu (World Scientific, Singapore, 1986), p. 196; E. Cohen, J. Ellis, K. Enqvist, and D. V. Nanopoulos, *Phys. Lett.* **161B**, 85 (1985), *ibid.* **165**, 76 (1985); D. London and J. L. Rosner, *Phys. Rev. D*34, 1530 (1986); V. Barger, N. G. Deshpande, and K. Whisnant, *Phys. Rev. Lett.* **56**, 30 (1986), *Phys. Rev. D*33, 1912 (1986). Somewhat sharper bounds arise from a comparison of $\overline{x}_W \equiv 1 - M_W^2/M_Z^2$ with x_W measured in deeply inelastic neutrino scattering. See J. Ellis, K. Enqvist, D. V. Nanopoulos,

and F. Zwirner, *Mod. Phys. Lett. A* **1**, 57 (1986); U. Amaldi, et al., *Phys. Rev. D*36, 1385 (1987).

[28] B. L. Combridge, *Nucl. Phys.* **B151**, 429 (1979).

[29] Z. Kunszt and E. Pietarinen, *Z. Phys. C*2, 355 (1979); Z. Kunszt, E. Pietarinen, and E. Reya, *Phys. Rev. D*21, 73 (1980); F. Halzen and P. Hoyer, *Phys. Lett.* **154B**, 324 (1985).

[30] P. Nason, S. Dawson, and R. K. Ellis, FNAL-Pub-87/222-T.

[31] R. K. Ellis, M. A. Furman, H. E. Haber and I. Hinchliffe, *Nucl. Phys.* **B173**, 397 (1980); W. Slominski and W. Furmanski, Krakow preprint TPJU-11/81 (1981); R. K. Ellis and J. C. Sexton, *Nucl. Phys.* **B269**, 445 (1986).

[32] The elementary cross sections have been calculated by many authors. Convenient summaries are given in *EHLQ* and in J. F. Owens, E. Reya, and M. Glück, *Phys. Rev. D*18, 1501 (1978).

[33] R. N. Cahn, in *Proceedings of the 10th SLAC Summer Institute,* edited by Anne Mosher, SLAC Report No. 259, p. 1.

[34] W. Scott, in *Proceedings of the International Symposium on Physics of Proton-Antiproton Collision,* edited by Y. Shimizu and K. Takikawa (KEK, National Laboratory for High Energy Physics, Tsukuba, 1985), p. 68; G. Arnison, et al. (UA1 Collaboration), *Phys. Lett.* **177B**, 244 (1986).

[35] G. Arnison, et al. (UA1 Collaboration), *Phys. Lett.* **172B**, 461 (1986).

[36] The curves shown are 1.5× the lowest-order QCD predictions, evaluated with $Q^2 = p_\perp^2$. The systematic errors on the data are ±70%. Theoretical uncertainties are of a similar magnitude, but tend to increase the predicted cross section. These are discussed by Eichten, et al., Ref. 2, and by Ellis and Sexton, Ref. 31.

[37] G. Sterman and S. Weinberg, *Phys. Rev. Lett.* **39**, 1436 (1977).

[38] K.-I. Shizuya and S.-H. H. Tye, *Phys. Rev. Lett.* **41**, 787 (1978); M. B. Einhorn and B. G. Weeks, *Nucl. Phys.* **B146**, 445 (1978).

[39] V. L. Ginzburg and L. D. Landau, *Zh. Eksp. Teor. Fiz.* **20,** 1064 (1950).

[40] J. Bardeen, L. N. Cooper, and J. R. Schrieffer, *Phys. Rev.* **106,** 162 (1962).

[41] Y. Nambu, *Phys. Rev. Lett.* **4**, 380 (1960).

[42] S. Weinberg, *Phys. Rev. D*13, 974 (1976), *ibid.* **19**, 1277 (1979).

[43] L. Susskind, *Phys. Rev. D*20, 2619 (1979).

[44] S. Dimopoulos and L. Susskind, *Nucl. Phys.* **B155**, 237 (1979).

[45] E. Eichten and K. Lane, *Phys. Lett.* **90B**, 125 (1980).

[46] E. Farhi and L. Susskind, *Phys. Rev. D*20, 3404 (1979).

[47] Eichten, et al., Ref. 24.

[48] V. Baluni, *Phys. Rev. D*28, 2223 (1983); *Ann. Phys. (NY)* **165**, 148 (1985).

[49] K. D. Lane, in *Proceedings of the 1982 DPF Summer Study on Elementary Particle Physics and Future Facilities,* edited by R. Donaldson, R. Gustafson, and F. Paige (Fermilab, Batavia, Illinois, 1982), p. 222.

[50] JADE Collaboration, W. Bartel, et al., *Phys. Lett.* **144B**, 211 (1982); TASSO Collaboration, M. Althoff, et al., *Phys. Lett.* **122B**, 95 (1983); MARK-J Collaboration, B. Adeva, et al., *Phys. Lett.* **152B**, 439 (1985).

[51] H. J. Behrend, et al. (CELLO Collaboration), *Phys. Lett.* **193B**, 376 (1987).

[52] C. Albajar, et al. (UA1 Collaboration), CERN-EP/87-190, submitted to *Z. Phys.* C.

[53] *Superconducting Super Collider Conceptual Design,* Central Design Group Report SSC-SR-2020 (March, 1986).

[54] M. M. Block and R. N. Cahn, LBL-23472, to be published in the Proceedings of the Rockefeller University meeting on Elastic Scattering and Diffractive Processes, October, 1987.

[55] A. Bassetto, M. Ciafaloni, G. Marchesini, *Phys. Rep.* **100**, 201 (1983).

[56] A. H. Mueller, *Nucl. Phys.* **B213**, 85 (1983); *ibid.* **B228**, 351 (1983); *ibid.* **B241**, 141 (1984); J. B. Gaffney and A. H. Mueller, *ibid.* **B250**, 109 (1985). For a convenient review, see R. K. Ellis, in *Supercollider Physics,* edited by D. E. Soper (World Scientific, Singapore, 1986), p. 77.

[57] A. H. Mueller and P. Nason, *Nucl. Phys.* **B266**, 265 (1986).

[58] Preliminary results of the UA1 Collaboration for the fraction of gluon jets splitting into $c\bar{c}$ pairs are reported by M. Della Negra, in *6th Topical Workshop on Proton-Antiproton Collider Physics,* edited by K. Eggert, H. Faissner, and E. Radermacher (World Scientific, Singapore, 1987), p. 181.

[59] A systematic development is given in J. Wess and J. Bagger, *Supersymmetry and Supergravity* (Princeton University Press, Princeton, New Jersey, 1983). See also the Lectures at the 1984 Theoretical Advanced Study Institute (Ann Arbor), in *TASI Lectures in Elementary Particle Physics*, edited by David N. Williams (TASI Publications, Ann Arbor, 1984): M. T. Grisaru, p. 232; D. R. T. Jones, p. 284; G. L. Kane, p. 326; P. C. West, p. 365; and the lectures at the 1985 SLAC Summer Institute, contained in *Supersymmetry,* edited by Eileen C. Brennan, SLAC Report No. 296. Other useful references include P. Fayet, in *Proceedings of the 21st International Conference on High Energy Physics*, Paris, 1982, edited by P. Petiau and M. Porneuf [*J. Phys. (Paris) Colloq.* **43**, C3–673 (1982)]; and S. Yamada, in *Proceedings of the 1983 International Symposium on Lepton and Photon Interactions at High Energies*, Ithaca, New York, edited by D. G. Cassel and K. L. Kreinick (Newman Laboratory of Nuclear Studies, Cornell University, Ithaca, 1984), p. 525. The search for supersymmetry in hadron collisions is treated in S. Dawson and A. Savoy–Navarro, in *Proceedings of the 1984 Summer Study on Design and Utilization of the Superconducting Super Collider*, edited by R. Donaldson and Jorge G. Morfín (Fermilab, Batavia, Illinois, 1984), p. 263; S. Dawson, in *Supercollider Physics,* edited by D. E. Soper (World Scientific, Singapore, 1986), p. 171; J. Ellis, in *Superstrings and Supergravity,* Proceedings of the 28th Scottish Universities' Summer School in Physics, edited by A. T. Davies and D. G. Sutherland (SUSSP Publications, Edinburgh, 1986), p. 399; and in the papers of Ref. 23.

[60] S. Coleman and J. Mandula, *Phys. Rev.* **159**, 1251 (1967).

[61] R. Haag, J. Lopuszanski, and M. Sohnius, *Nucl. Phys.* **88**, 257 (1975).

[62] See, for example, S. Weinberg, *Phys. Rev. D***26**, 287 (1982).

[63] Recent limits on the squark and gluino masses are reported in C. Albajar, et al. (UA1 Collaboration), *Phys. Lett.* **198B**, 271 (1987).

Table 1: Branching fractions per generation of Z'.

$u\overline{u}$	24/180
$d\overline{d}$	15/180
e^+e^-	5/180
$h\overline{h}$	51/180
E^+E^-	17/180
$\nu_e\overline{\nu}_e$	1/180
$\nu_E\overline{\nu}_E$	1/180
$N_e\overline{N}_e$	25/180
$N_E\overline{N}_E$	16/180
$n\overline{n}$	25/180

Table 2: Feynman amplitudes for parton-parton scattering, in QCD.

Process	$\lvert\mathcal{M}\rvert^2$	value at $\theta^* = \pi/2$
$q_i q_j \to q_i q_j$	$\frac{4}{9} \cdot \frac{\hat{s}^2 + \hat{u}^2}{\hat{t}^2}$	2.22
$q_i q_i \to q_i q_i$	$\frac{4}{9}\left(\frac{\hat{s}^2 + \hat{u}^2}{\hat{t}^2} + \frac{\hat{s}^2 + \hat{t}^2}{\hat{u}^2}\right) - \frac{8}{27} \cdot \frac{\hat{s}^2}{\hat{t}\hat{u}}$	3.26
$q_i \overline{q}_i \to q_j \overline{q}_j$	$\frac{4}{9} \cdot \frac{\hat{t}^2 + \hat{u}^2}{\hat{s}^2}$	0.22
$q_i \overline{q}_i \to q_i \overline{q}_i$	$\frac{4}{9}\left(\frac{\hat{s}^2 + \hat{u}^2}{\hat{t}^2} + \frac{\hat{u}^2 + \hat{t}^2}{\hat{s}^2}\right) - \frac{8}{27} \cdot \frac{\hat{u}^2}{\hat{t}\hat{s}}$	2.59
$q_i \overline{q}_i \to gg$	$\frac{32}{27} \cdot \frac{\hat{u}^2 + \hat{t}^2}{\hat{u}\hat{t}} - \frac{8}{3} \cdot \frac{\hat{u}^2 + \hat{t}^2}{\hat{s}^2}$	1.04
$gg \to q_i \overline{q}_i$	$\frac{1}{6} \cdot \frac{\hat{u}^2 + \hat{t}^2}{\hat{u}\hat{t}} - \frac{3}{8} \cdot \frac{\hat{u}^2 + \hat{t}^2}{\hat{s}^2}$	0.15
$g q_i \to g q_i$	$-\frac{4}{9} \cdot \frac{\hat{u}^2 + \hat{s}^2}{\hat{u}\hat{s}} + \frac{\hat{u}^2 + \hat{s}^2}{\hat{t}^2}$	6.11
$gg \to gg$	$\frac{9}{2}\left(3 - \frac{\hat{u}\hat{t}}{\hat{s}^2} - \frac{\hat{u}\hat{s}}{\hat{t}^2} - \frac{\hat{s}\hat{t}}{\hat{u}^2}\right)$	30.4

Table 3: Cross sections (in pb) for pair production of electroweak gauge bosons.

Pair	630 GeV	1.8 TeV	40 TeV
	$\bar{p}p$	$\bar{p}p$	pp
W^+W^-	0.43	6.4	214
$W^\pm\gamma$	0.011	0.37	18
$W^\pm Z$	0.051	1.65	73
ZZ	0.034	0.074	33

Table 4: Fundamental Fields of the Standard Model and Their Superpartners

Particle	Spin	Color	Charge
g gluon	1	8	0
$\tilde{g}$ gluino	1/2	8	0
γ photon	1	0	0
$\tilde{\gamma}$ photino	1/2	0	0
$W^{\pm}, Z^0$ intermediate bosons	1	0	$\pm 1, 0$
$\tilde{W}^{\pm}, \tilde{Z}^0$ wino and zino	1/2	0	$\pm 1, 0$
q quark	1/2	3	2/3, -1/3
$\tilde{q}$ squark	0	3	2/3, -1/3
e electron	1/2	0	-1
$\tilde{e}$ selectron	0	0	-1
ν neutrino	1/2	0	0
$\tilde{\nu}$ sneutrino	0	0	0
H^+ H'^0 H^0 H'^- Higgs bosons	0	0	$\pm 1, 0$
$\tilde{H}^+$ $\tilde{H}'^0$ $\tilde{H}^0$ $\tilde{H}'^-$ Higgsinos	1/2	0	$\pm 1, 0$

Table 5: Limits on the Masses of Superpartners

Particle	Limit
$\tilde{\gamma}$	could be as light as a few GeV/c^2, or massless
$\tilde{g}$	$\gtrsim 53$ GeV/c^2
$\tilde{W}$	$\gtrsim$ 25 GeV/c^2 for massless $\tilde{\gamma}$ and $\tilde{\nu}$
$\tilde{Z}$	$>$ 41 GeV/c^2 for massless $\tilde{\gamma}$ and $M(\tilde{e}) = 22$ GeV/c^2
$\tilde{q}$	if stable: $>$ 14 GeV/c^2; if unstable (and photino is massless): $>$ 17.8 GeV/c^2 for $e_{\tilde{q}} = 2/3$; 3 GeV/$c^2 \lesssim M \lesssim$ 7.4 GeV/c^2 or $\gtrsim$ 16 GeV/c^2 for $e_{\tilde{q}} = -1/3$; perhaps $\gtrsim 45$ GeV/c^2
$\tilde{\ell}^{\pm}$	$\gtrsim$ 20 GeV/c^2
$\tilde{e}^{\pm}$	$\gtrsim 50$ GeV/c^2 if photino is massless

Table 6: Hierarchy of Superpartner Production Rates

Final States	Mechanism	Magnitude
$(\tilde{g}, \tilde{q})^2$	QCD	α_s^2
$(\tilde{g}, \tilde{q}) \cdot (\tilde{\gamma}, \tilde{Z}^0, \tilde{H}^0, \tilde{H}'^0, \tilde{W}^\pm, \tilde{H}^\pm)$	electroweak/QCD	$\alpha \cdot \alpha_s$
$\tilde{\ell}\tilde{\nu}, \tilde{\ell}\tilde{\ell}^*, \tilde{\nu}\tilde{\nu}^*$	decay of $W^\pm, Z^0$	α
	virtual $W^\pm, Z^0$	α^2
$(\tilde{\gamma}, \tilde{Z}^0, \tilde{H}^0, \tilde{H}'^0, \tilde{W}^\pm, \tilde{H}^\pm)^2$	electroweak	α^2

Table 7: Expected discovery limits for superpartners from associated production of squarks and gauginos in 40 TeV pp collisions. All superpartner masses are set equal. [After *EHLQ*.]

	Mass limit [GeV/c^2]		
$\int dt\mathcal{L}$ [cm^{-2}]	10^{38}	10^{39}	10^{40}
Superpartner			
Gluino (1000 events)	900	1,600	2,500
Squark ($\tilde{u} + \tilde{d}$) (1000 events)	800	1,450	2,300
Photino (100 events)	350	750	1,350
Zino (1000 events)	250	500	825
Wino (1000 events)	300	550	1,000

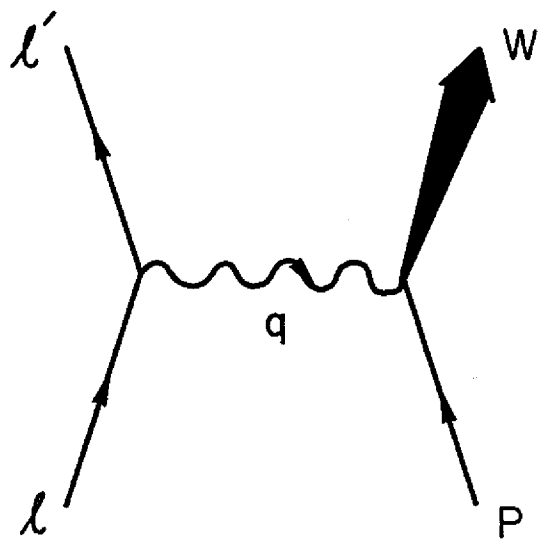

Figure 1: Kinematics of deeply inelastic scattering.

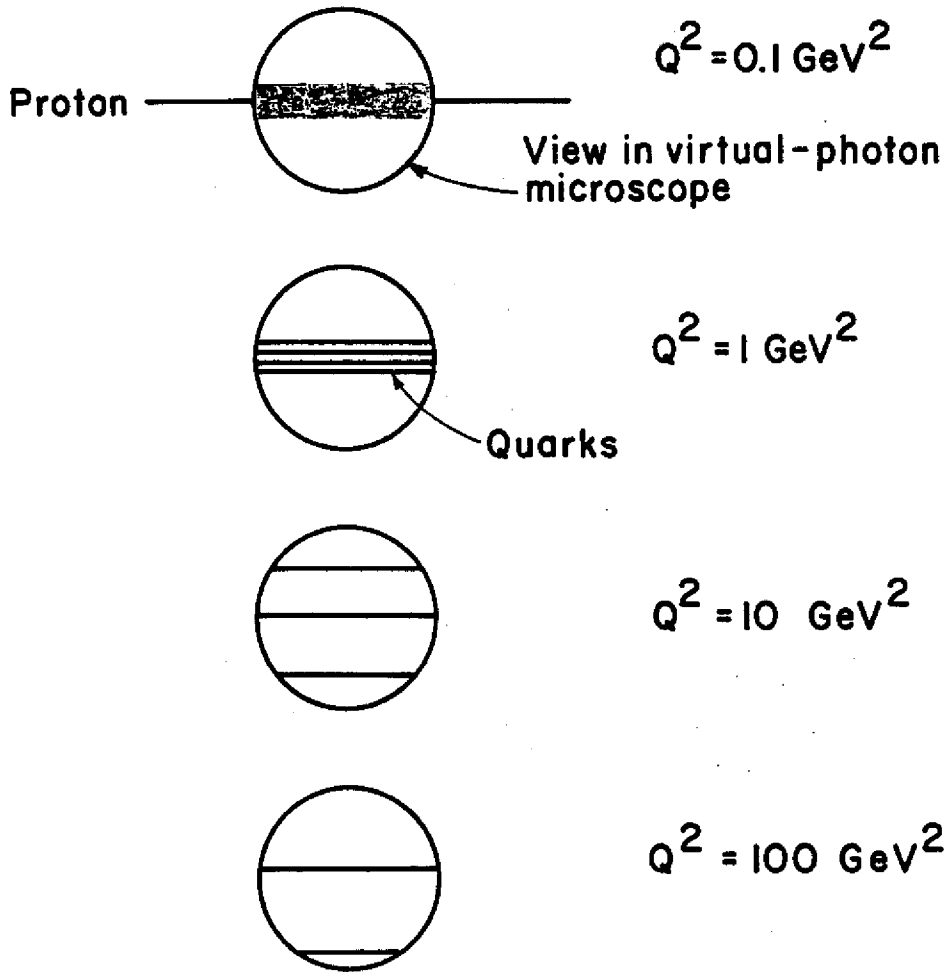

Figure 2: Parton model view of the proton.

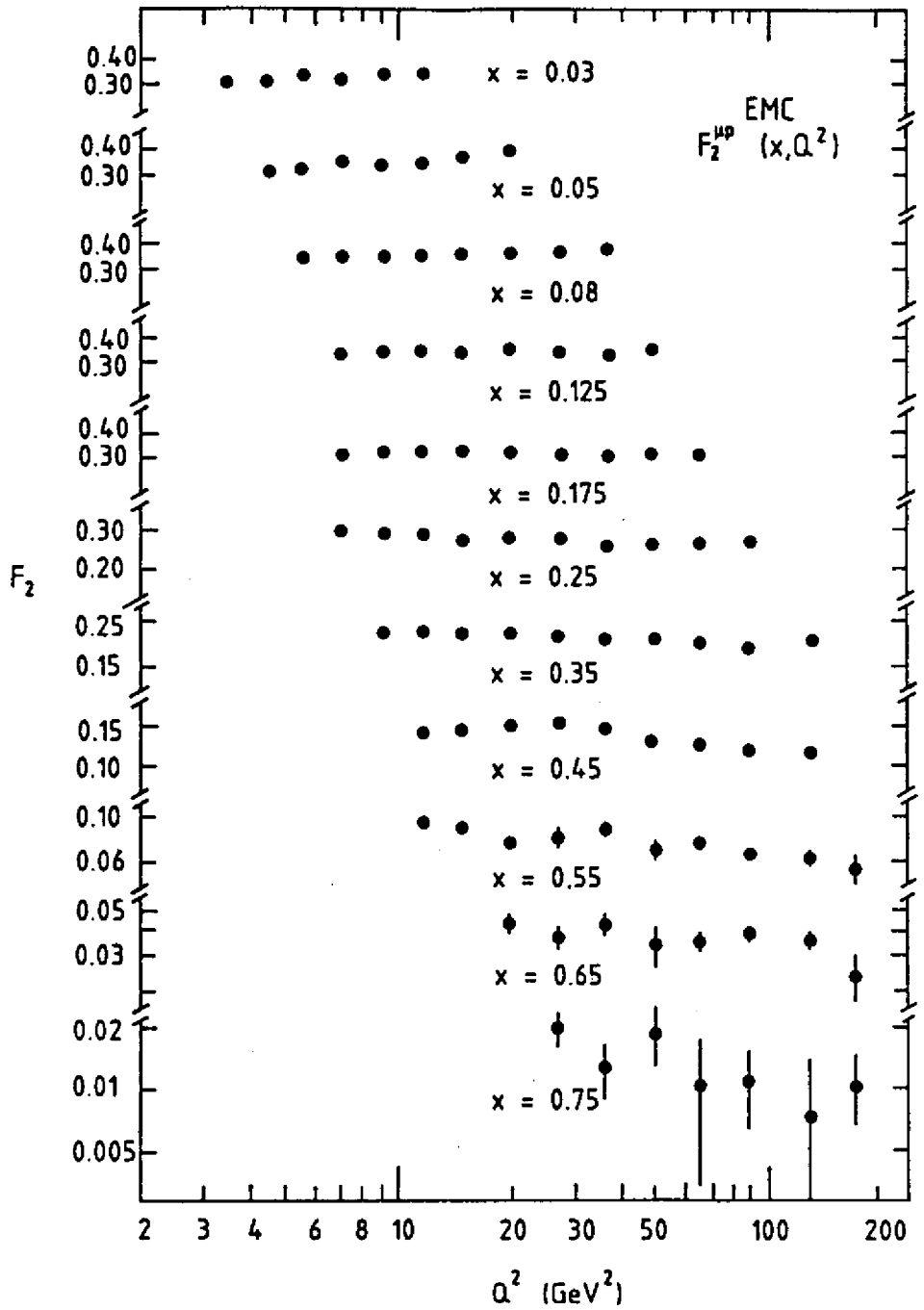

Figure 3: The structure function $F_2^{\mu p}(x)$ measured by the European Muon Collaboration depends only weakly on the momentum transfer Q^2. The data are from Ref. 13.

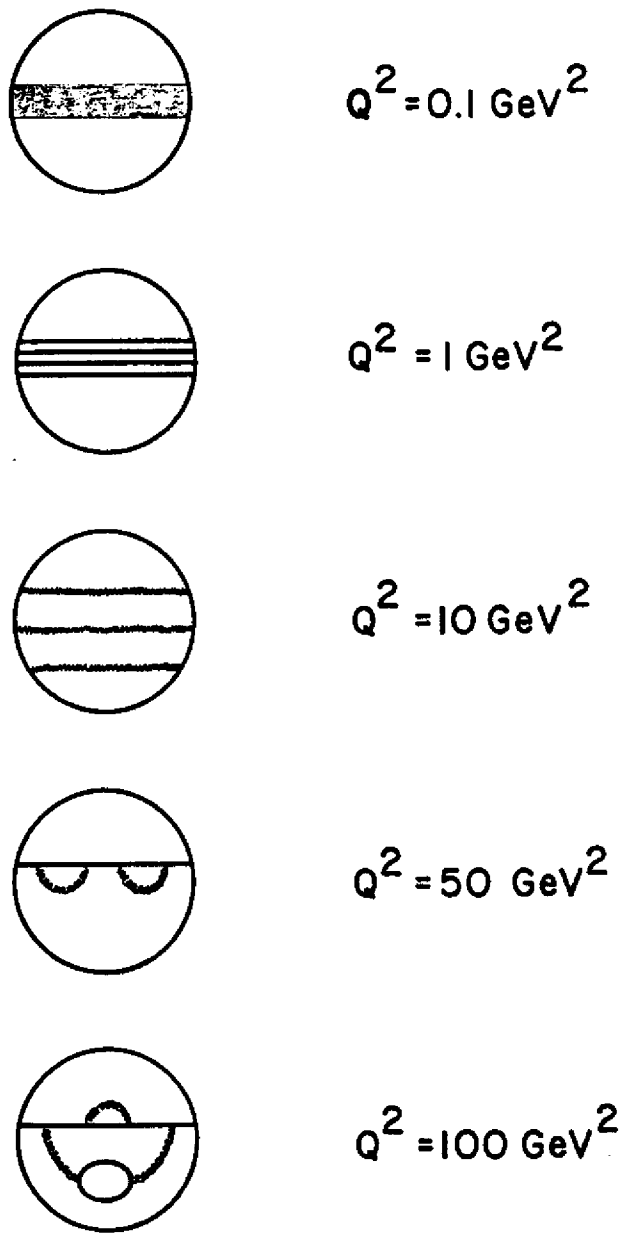

Figure 4: Interacting field theory view of the proton.

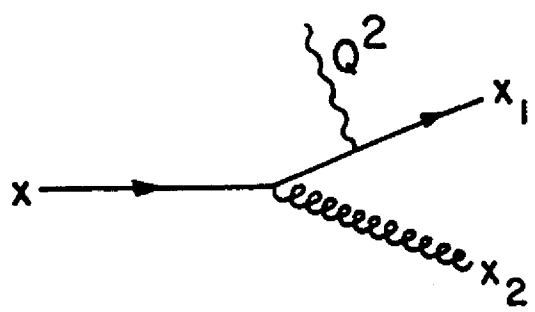

Figure 5: Virtual dissociation of a quark into a quark and a gluon. A high-Q^2 probe may catch the system in mid-fluctuation.

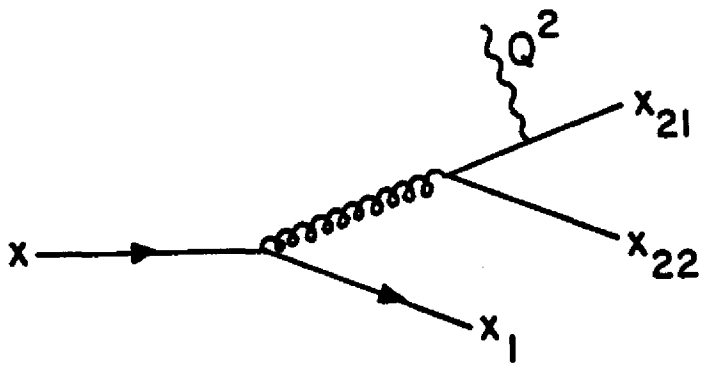

Figure 6: Virtual dissociation of a gluon into a quark and an antiquark, which enhances the population of low-x quarks and antiquarks seen by a probe of high Q^2.

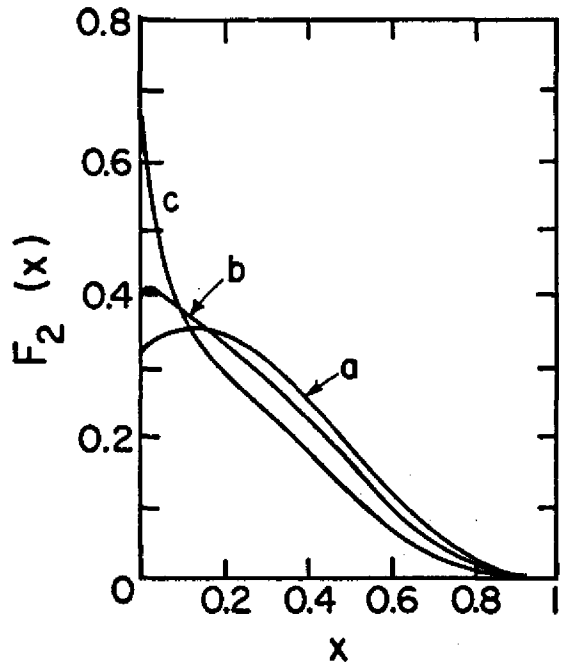

Figure 7: Schematic evolution of the parton structure function in an interacting field theory: (a) low, (b) medium, (c) high Q^2.

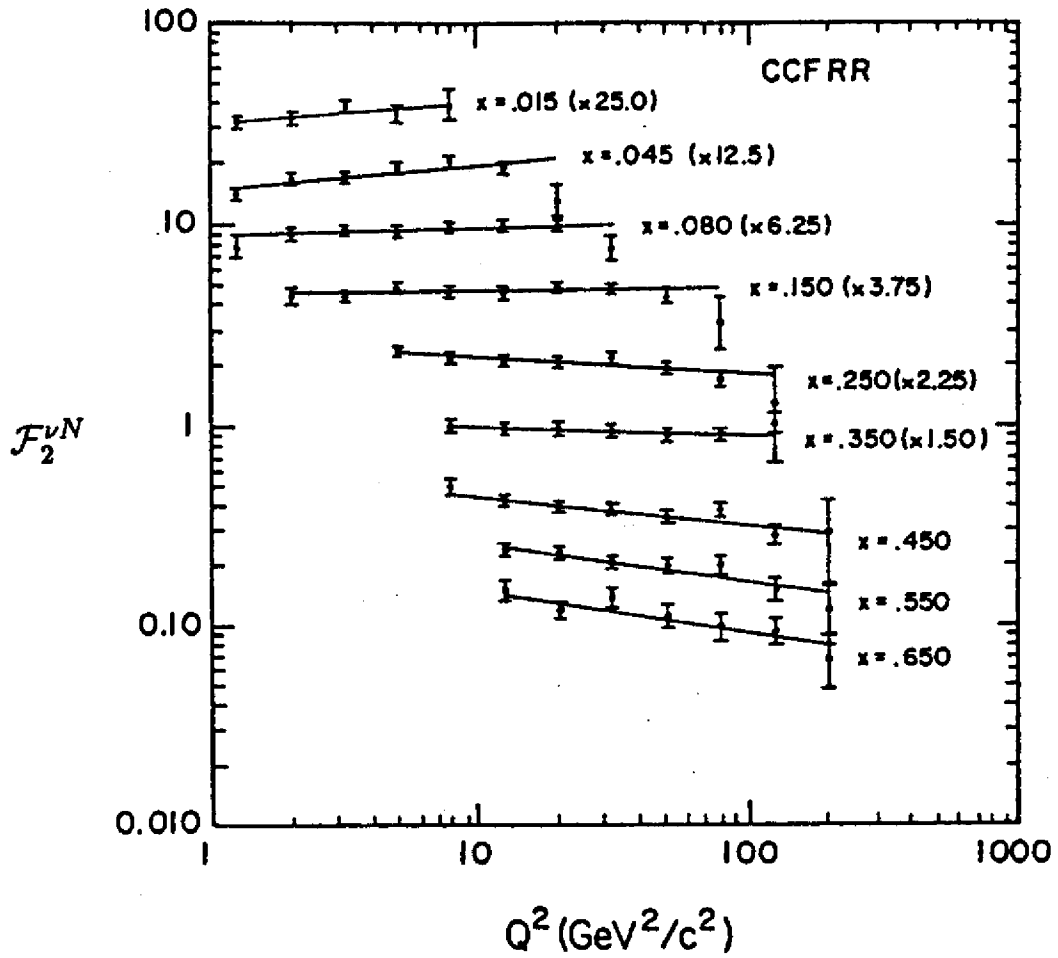

Figure 8: The structure function $\mathcal{F}_2^{\nu N}$ measured by the Chicago Columbia Fermilab Rochester Rockefeller Collaboration [from Ref. 14]. The ratio of longitudinal to transverse cross sections is taken to be given by QCD.

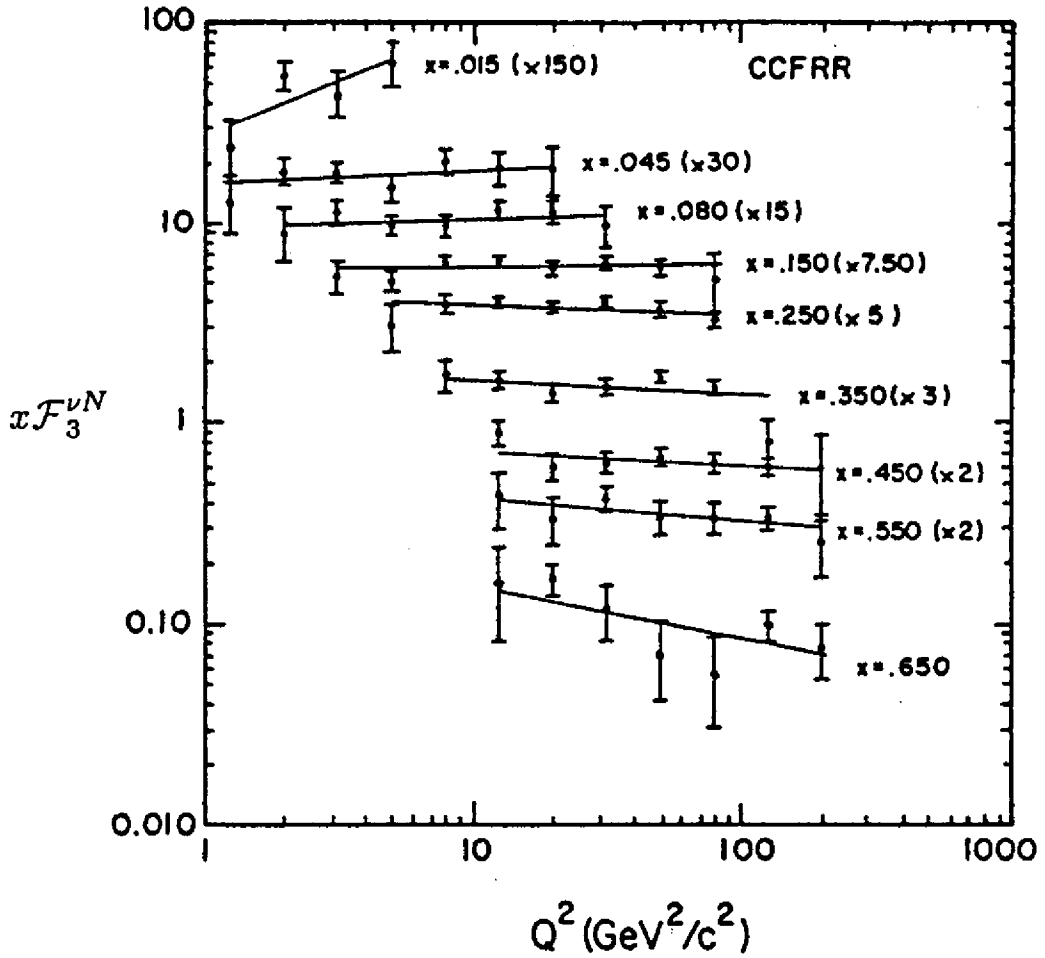

Figure 9: The nonsinglet structure function $x\mathcal{F}_3^{\nu N}$ measured by the Chicago Columbia Fermilab Rochester Rockefeller Collaboration [from Ref. 14]. As in Fig. 8, the ratio of longitudinal to transverse cross sections is taken to be given by QCD.

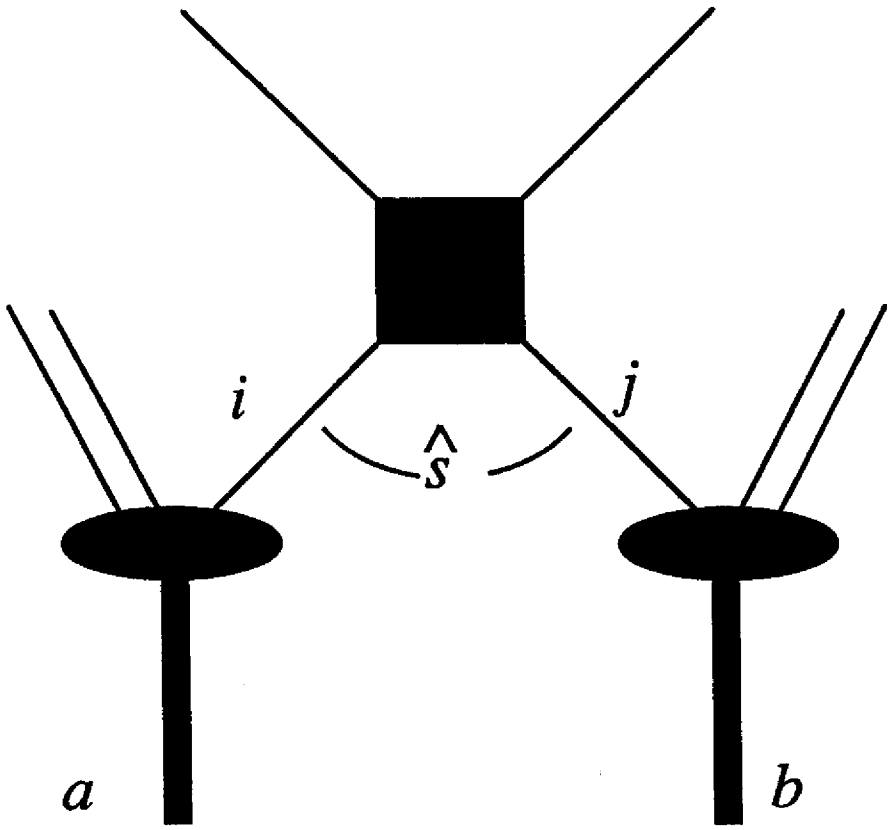

Figure 10: Parton-model representation of a hard-scattering event.

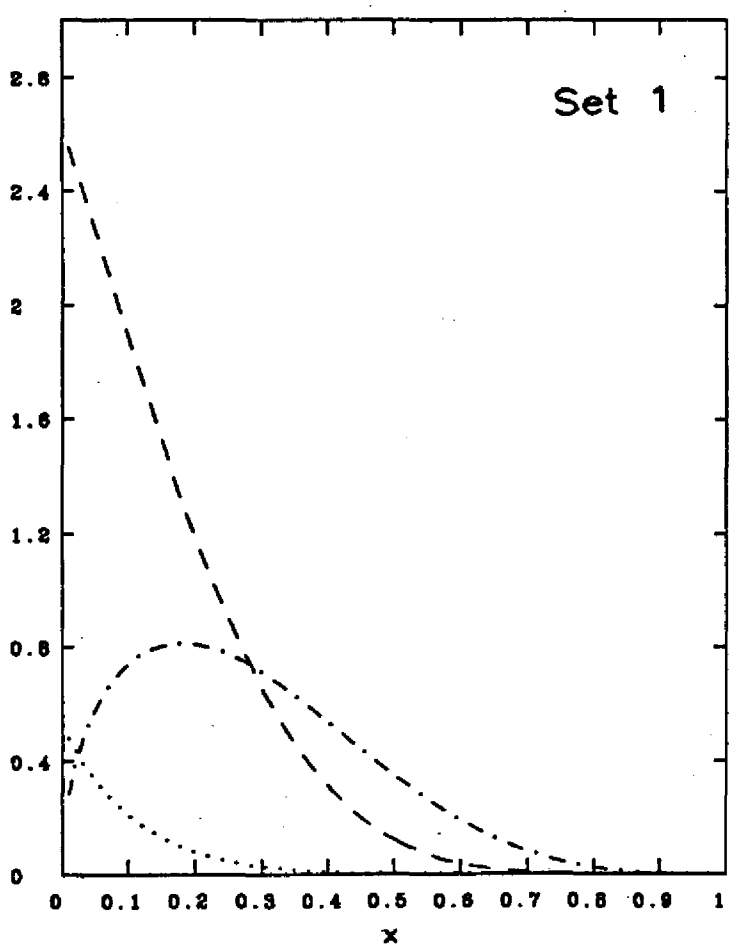

Figure 11: Parton distributions of Set 1 at $Q^2 = 5$ GeV^2: valence quark distribution $x[u_v(x) + d_v(x)]$ (dot-dashed line), $xG(x)$ (dashed line), and $q_\nu(x) \equiv x[u_s(x) + d_s(x) + 2s_s(x)]$ (dotted line) (from *EHLQ*).

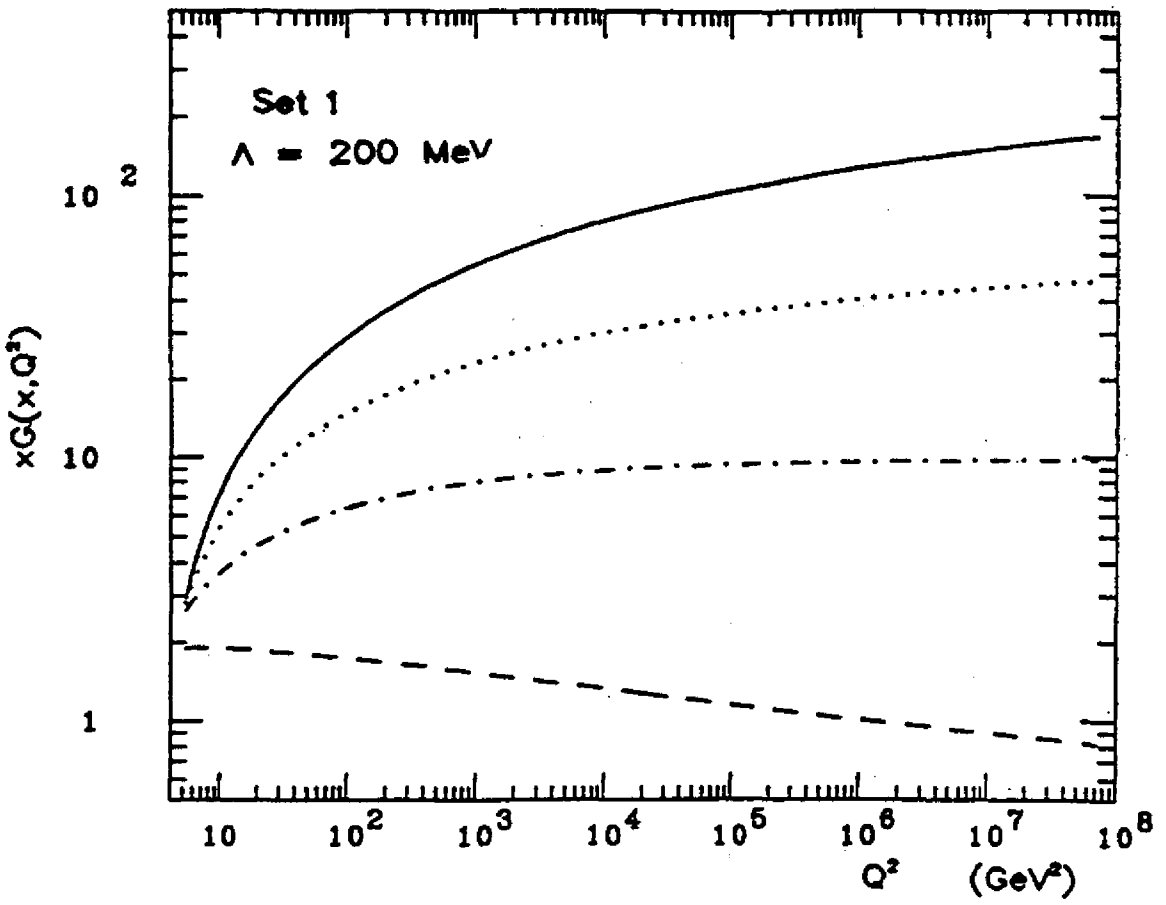

Figure 12: Q^2-evolution of the gluon distribution $xG(x)$ of Set 1: $x = 10^{-4}$ (solid line), 10^{-3} (dotted line), 10^{-2} (dot-dashed line), 0.1 (dashed line) (from *EHLQ*).

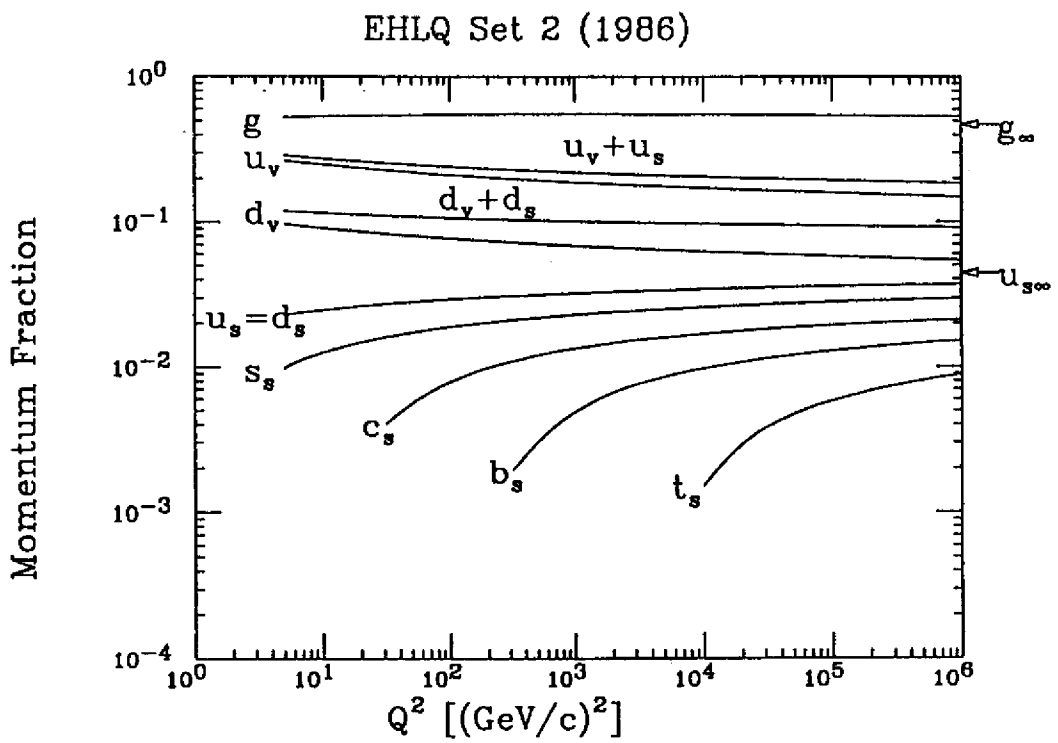

Figure 13: Momentum fractions of parton species in Set 2 of the 1986 *EHLQ* distributions.

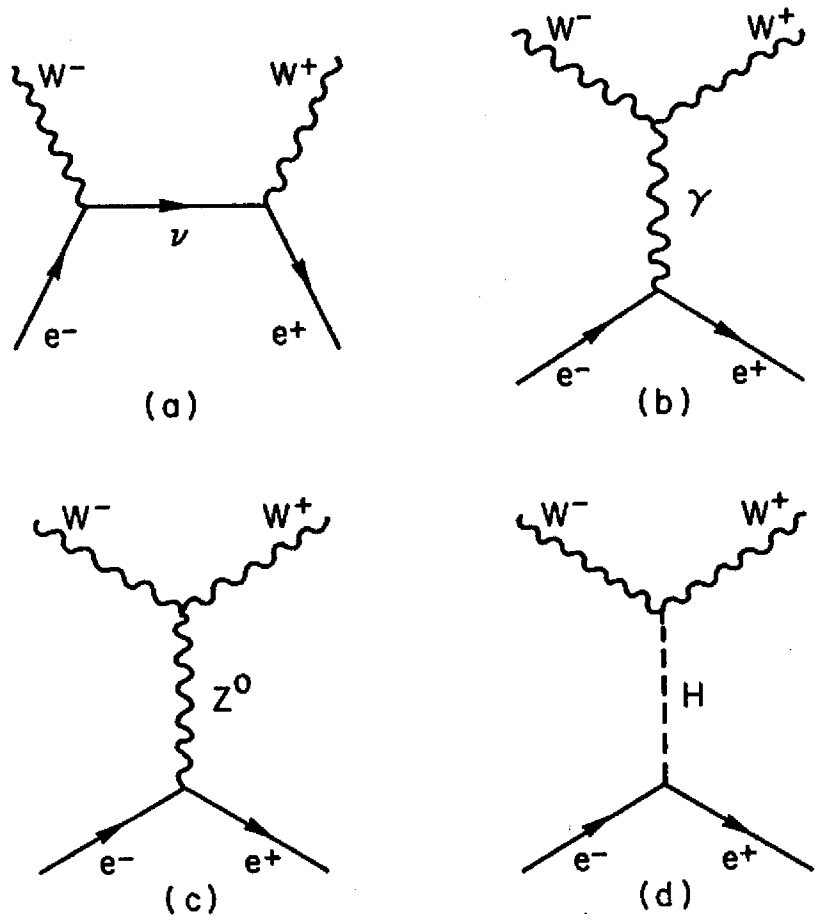

Figure 14: Lowest-order contributions to the reaction $e^+e^- \to W^+W^-$ in the Standard Model.

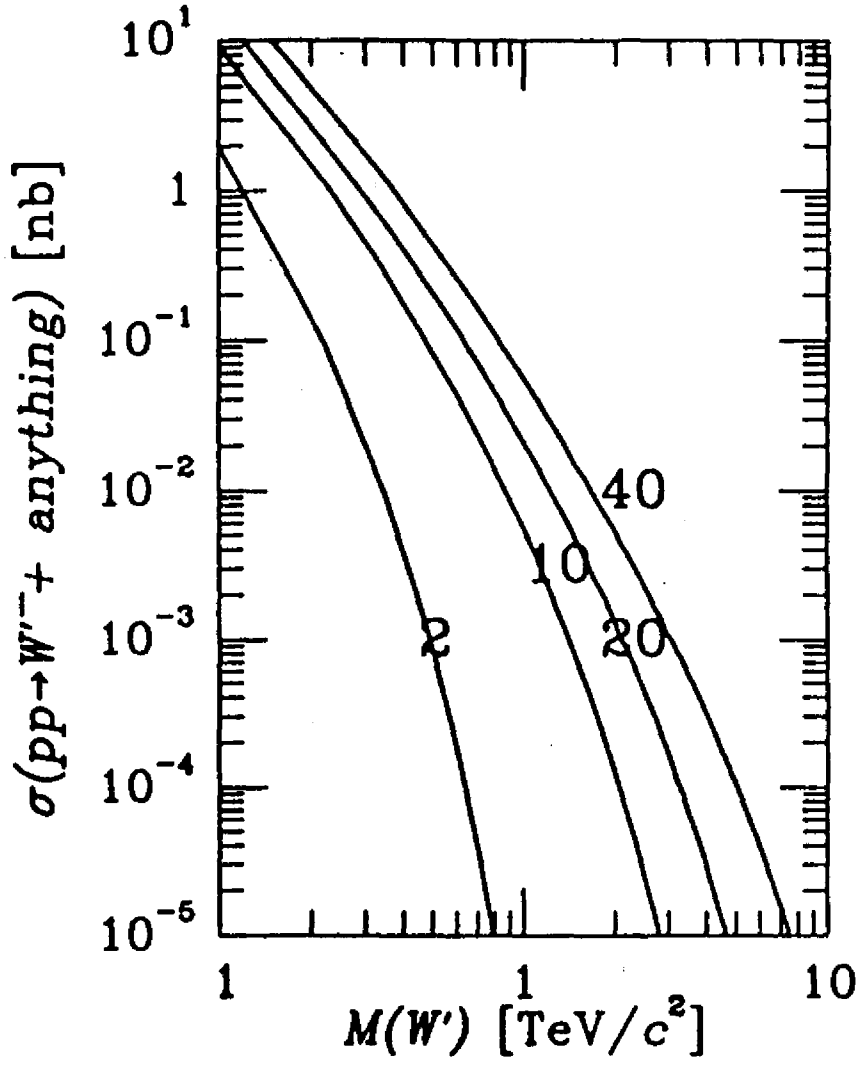

Figure 15: Cross section for the production of a heavy W-boson with rapidity $|y| < 1.5$ in pp collisions at 2, 10, 20, and 40 TeV (after *EHLQ*).

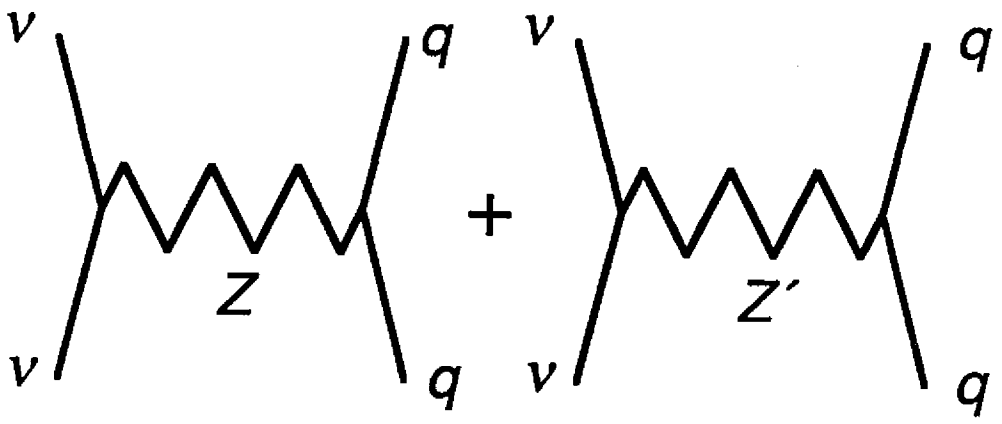

Figure 16: Influence of a second neutral intermediate boson on neutral current interactions.

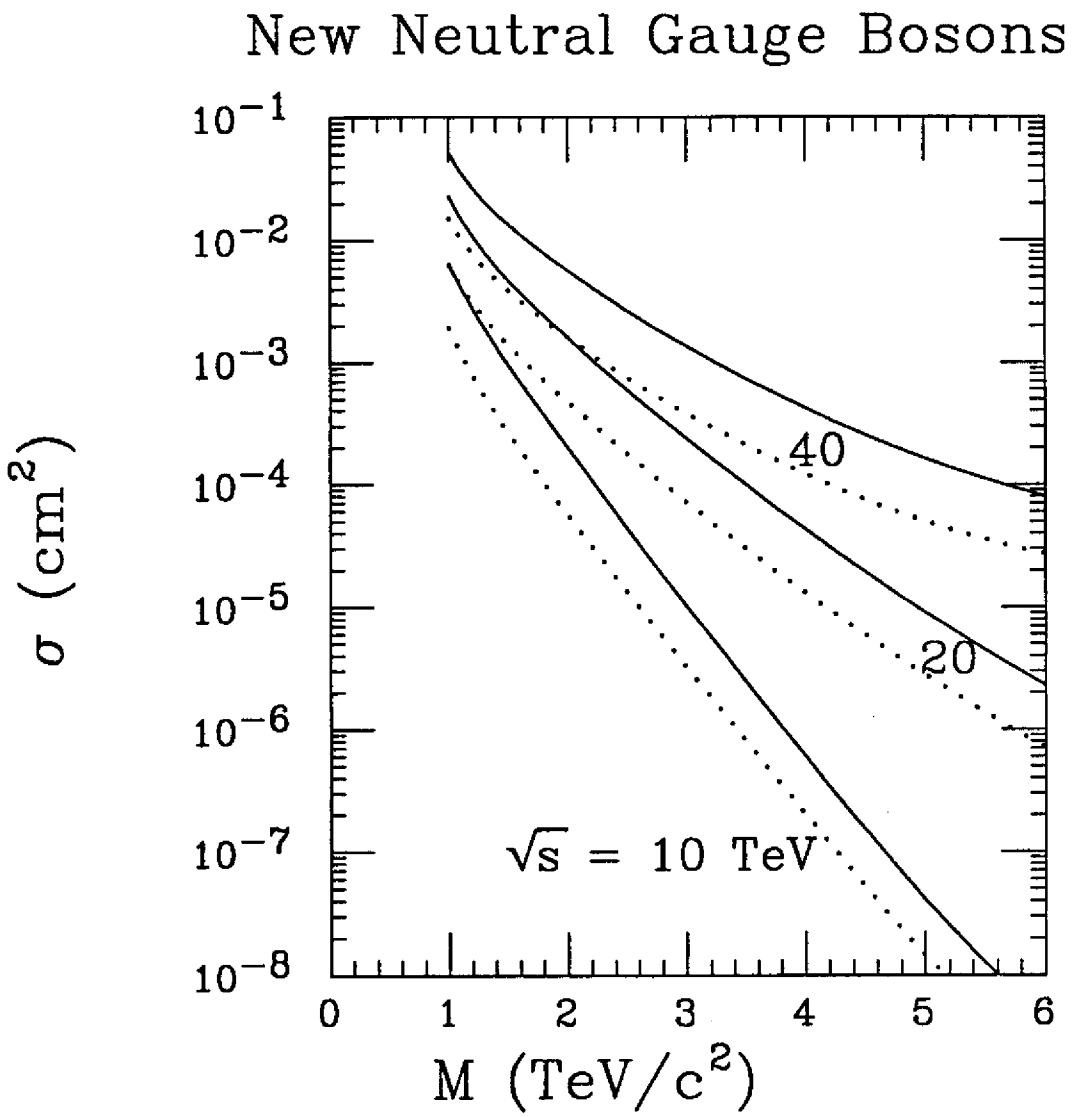

Figure 17: Cross section for the production of a heavy $Z^{0\prime}$-boson with rapidity $|y| < 1.5$ in pp collisions at 2, 10, 20, and 40 TeV. Solid lines: Weinberg-Salam couplings; dotted lines: E_6 couplings.

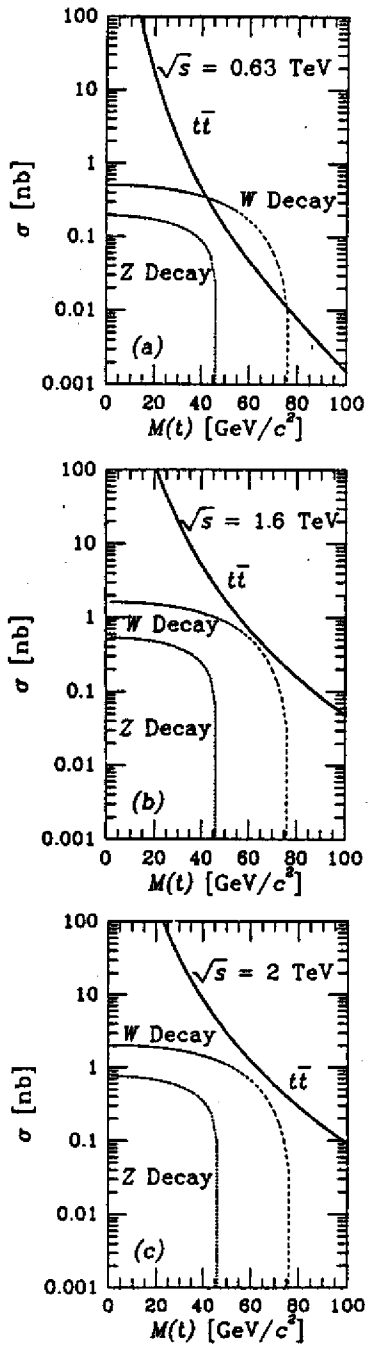

Figure 18: Cross sections for the production of t or $\bar{t}$ quarks in $\bar{p}p$ collisions as a function of the mass of the heavy quark. (a) $\sqrt{s} = 630$ GeV; (b) $\sqrt{s} = 1600$ GeV; (c) $\sqrt{s} = 2000$ GeV.

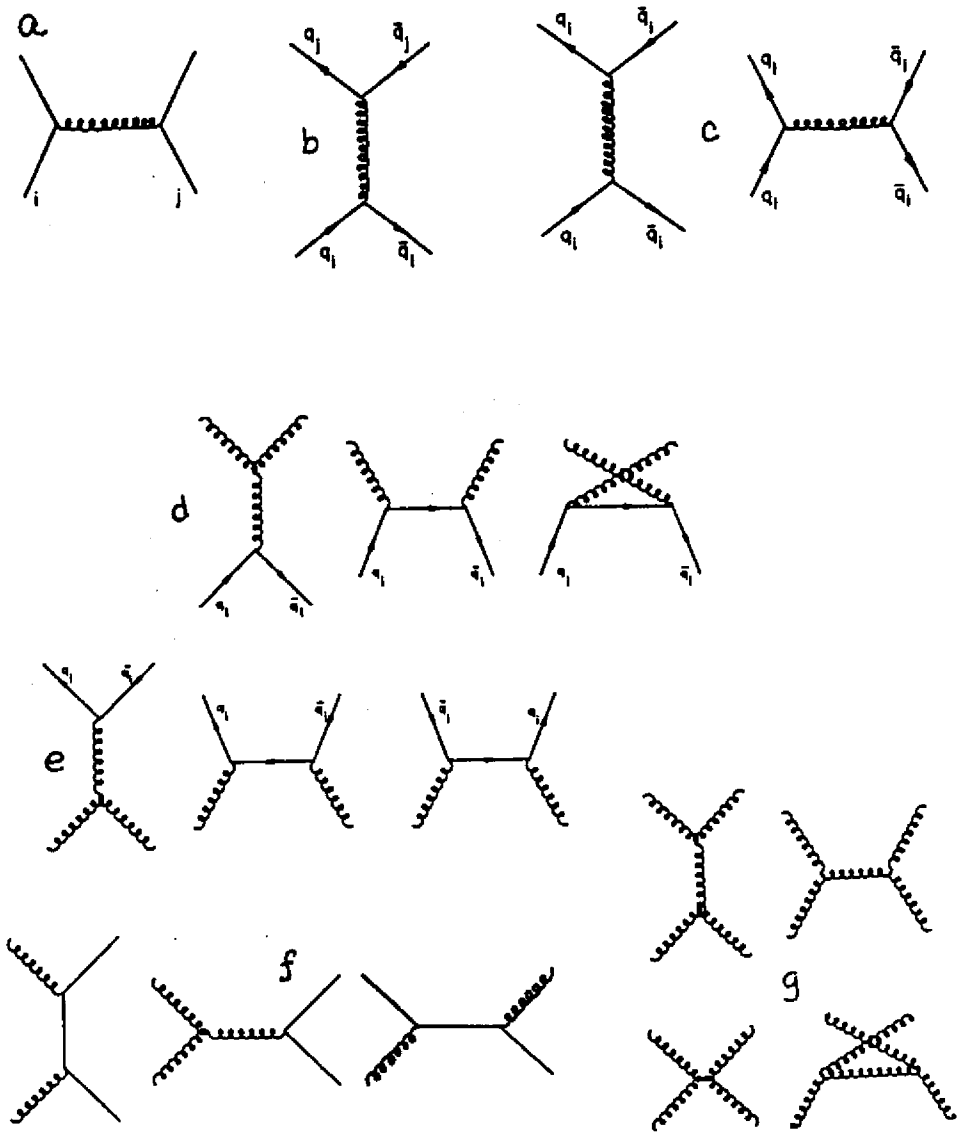

Figure 19: $O(\alpha_s^2)$ contributions to parton-parton scattering in QCD. (a) $q_i q_j \to q_i q_j$ or $q_i \overline{q}_j \to q_i \overline{q}_j, i \neq j$. (b) $q_i \overline{q}_i \to q_j \overline{q}_j, i \neq j$. (c) $q_i \overline{q}_i \to q_i \overline{q}_i$. (d) $q_i \overline{q}_i \to gg$. (e) $gg \to q_i \overline{q}_i$. (f) $gq \to gq$ or $g\overline{q} \to g\overline{q}$. (g) $gg \to gg$.

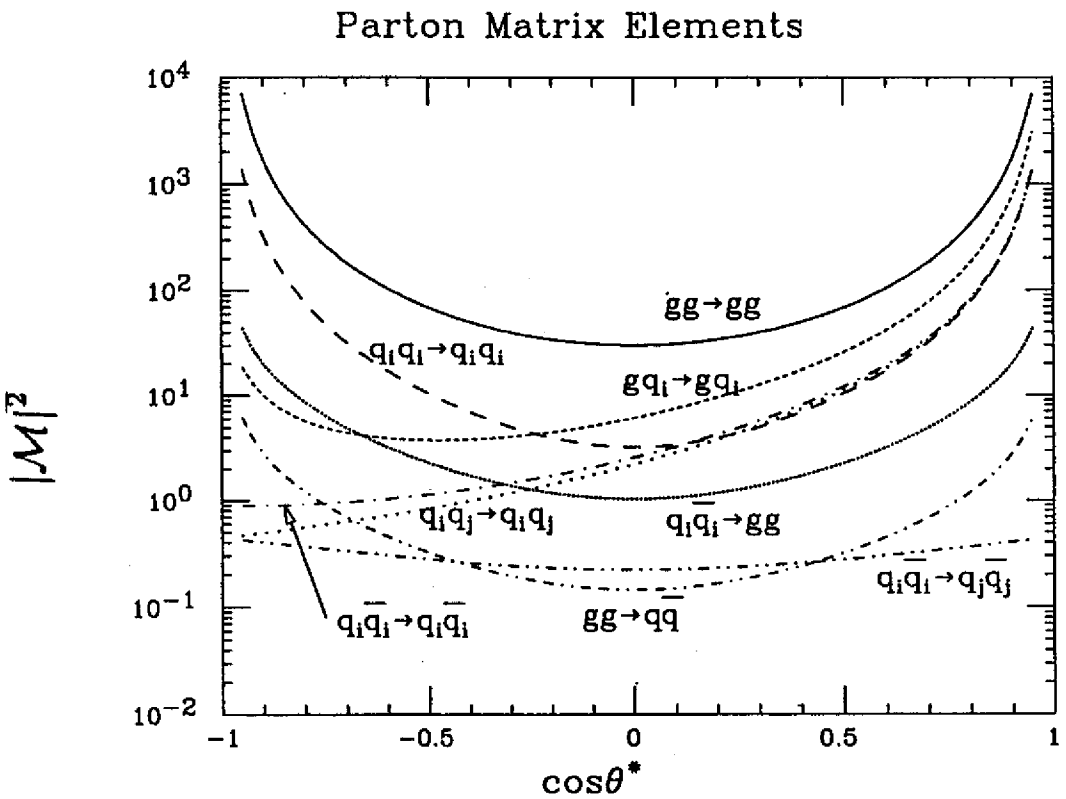

Figure 20: Angular distributions given by the Born terms for parton-parton scattering in QCD (after Ref. 33).

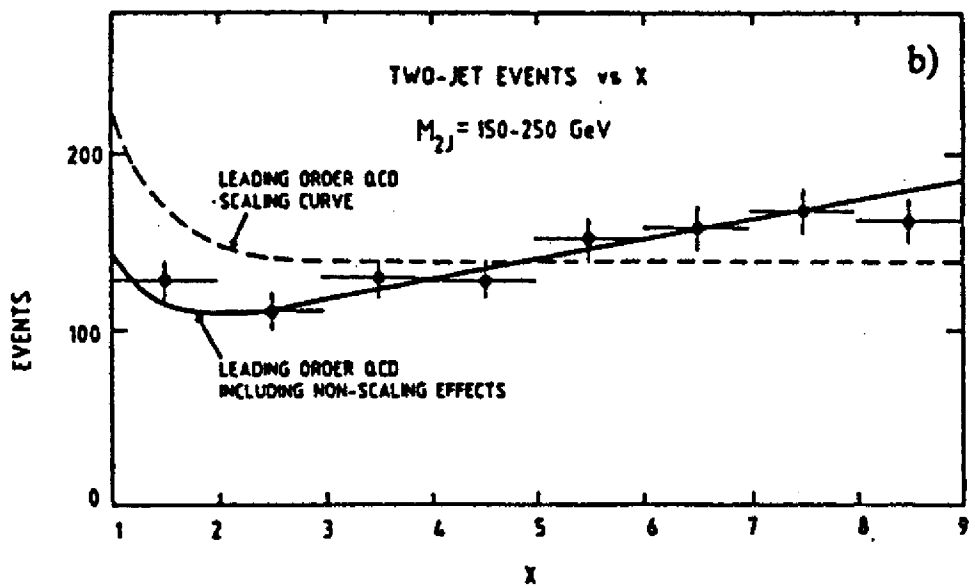

Figure 21: Angular distribution of two jet events observed by the UA1 Collaboration in $\overline{p}p$ collisions at $\sqrt{s} = 540$ GeV, as described in the text. The curve shows the shape predicted by the QCD Born terms convoluted with the *EHLQ* structure functions (Set 1).

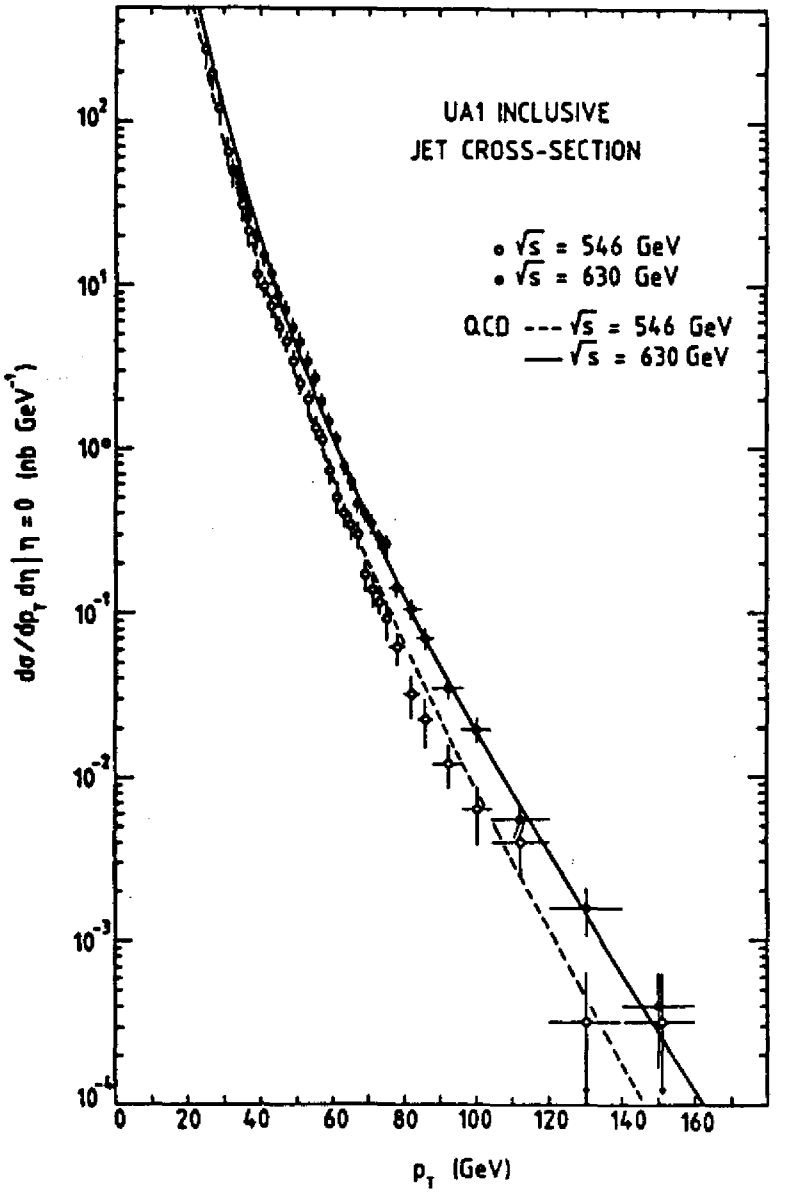

Figure 22: The inclusive jet cross section measured by the UA1 Collaboration for the pseudorapidity interval $|\eta| < 0.7$, as a function of the jet transverse momentum. The open dots correspond to the data at $\sqrt{s} = 546$ GeV and the solid dots to those at $\sqrt{s} = 630$ GeV.

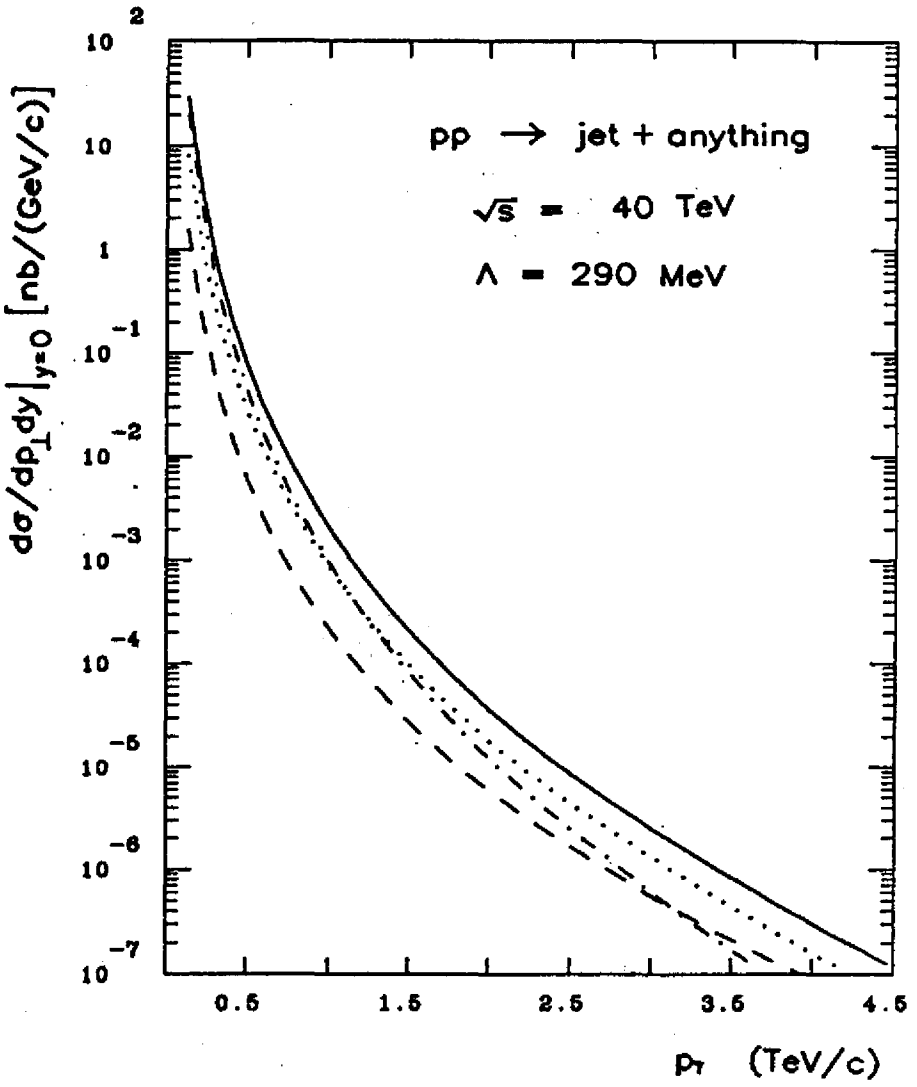

Figure 23: Differential cross section for jet production at $y = 0$ (90° c.m.) in pp collisions at 40 TeV, according to Set 2 of the *EHLQ* parton distributions (from *EHLQ*). Dotted line: gg final state; dot-dashed line: gq final state; dashed line: qq final state; solid line: total.

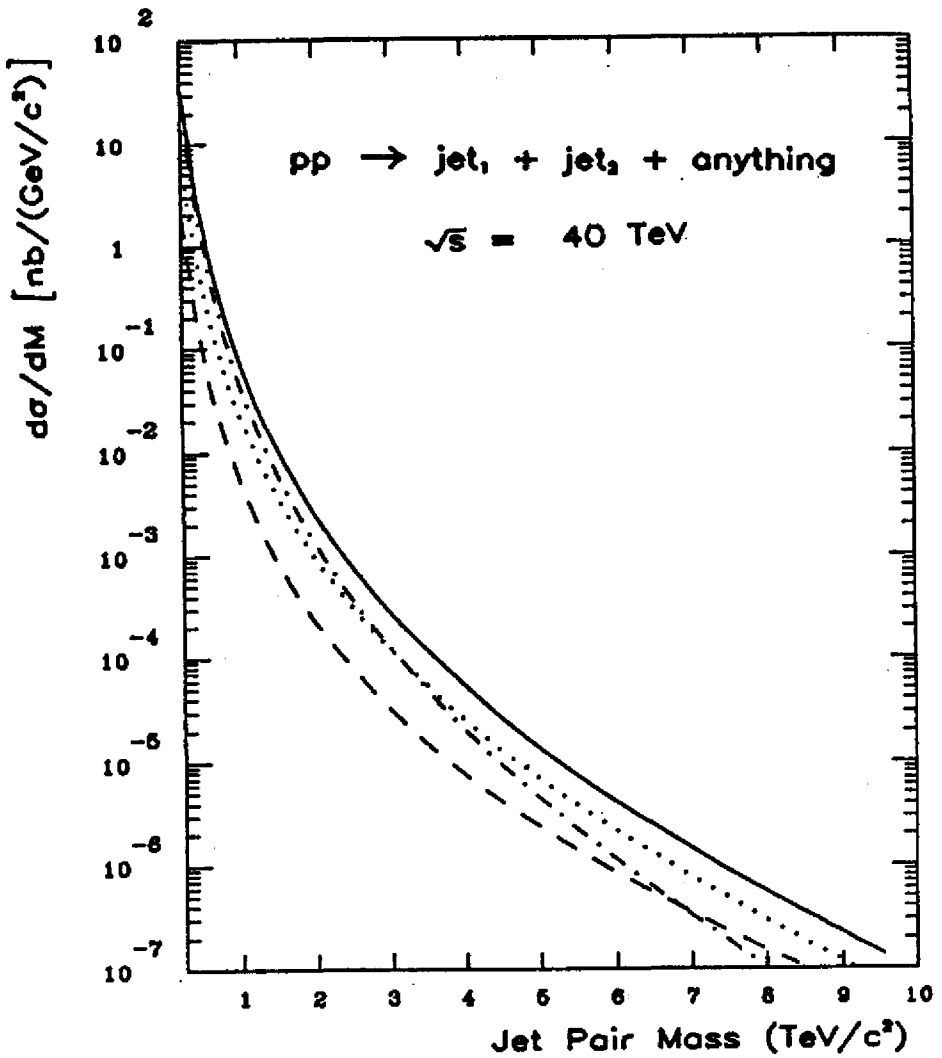

Figure 24: Invariant mass spectrum for two-jet events produced in proton-proton collisions at $\sqrt{s} = 40$ TeV, according to Set 2 of the *EHLQ* parton distributions. Both jets must satisfy $|y_i| < 1.5$. (From *EHLQ*.) Dotted line: gg final state; dot-dashed line: gq final state; dashed line: qq final state; solid line: total.

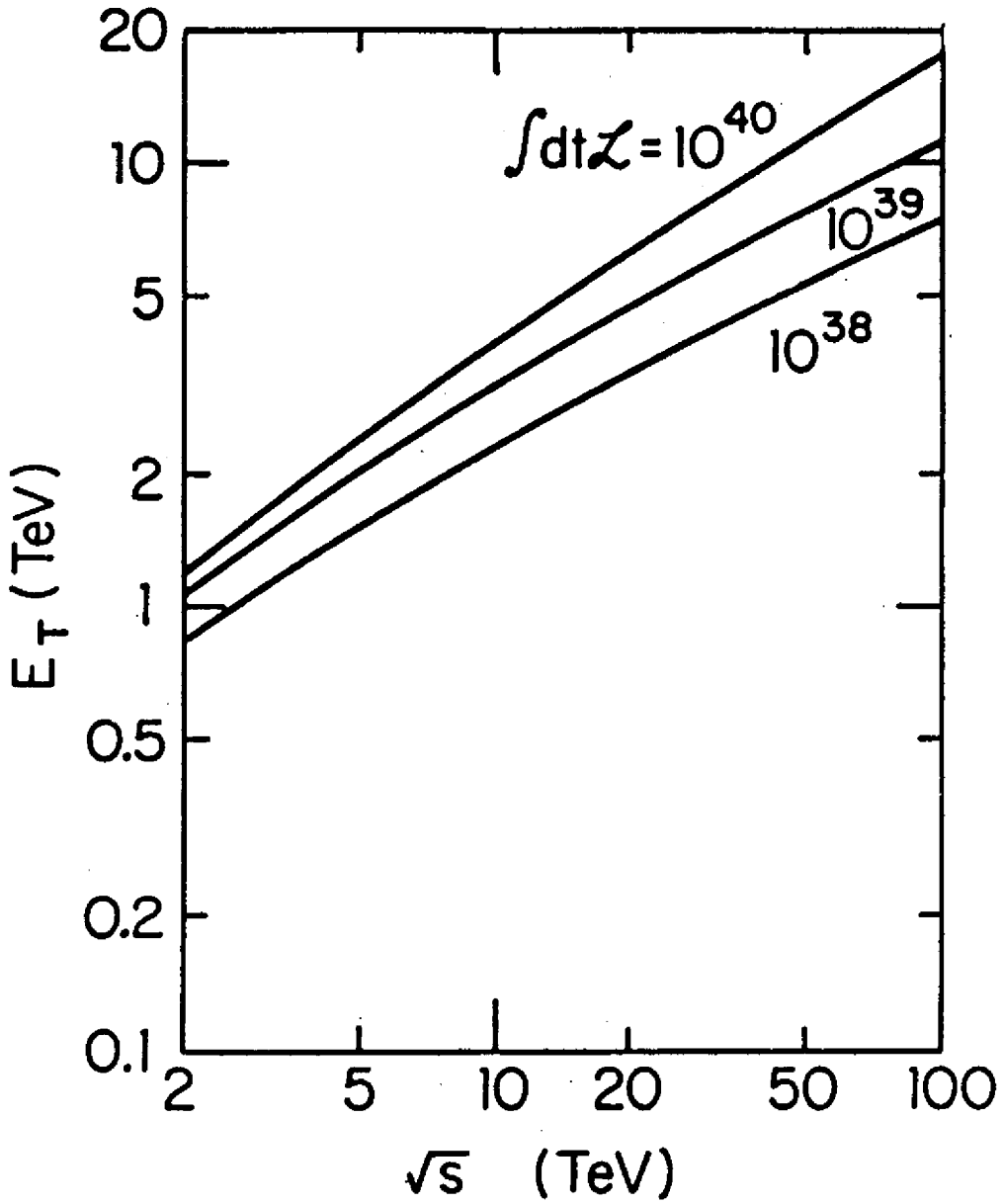

Figure 25: Discovery reach of hadron colliders for the observation of two-jet events, according to Set 2 of the *EHLQ* parton distributions, for integrated luminosities of 10^{38}, 10^{39}, and 10^{40} cm^{-2} (from *EHLQ*).

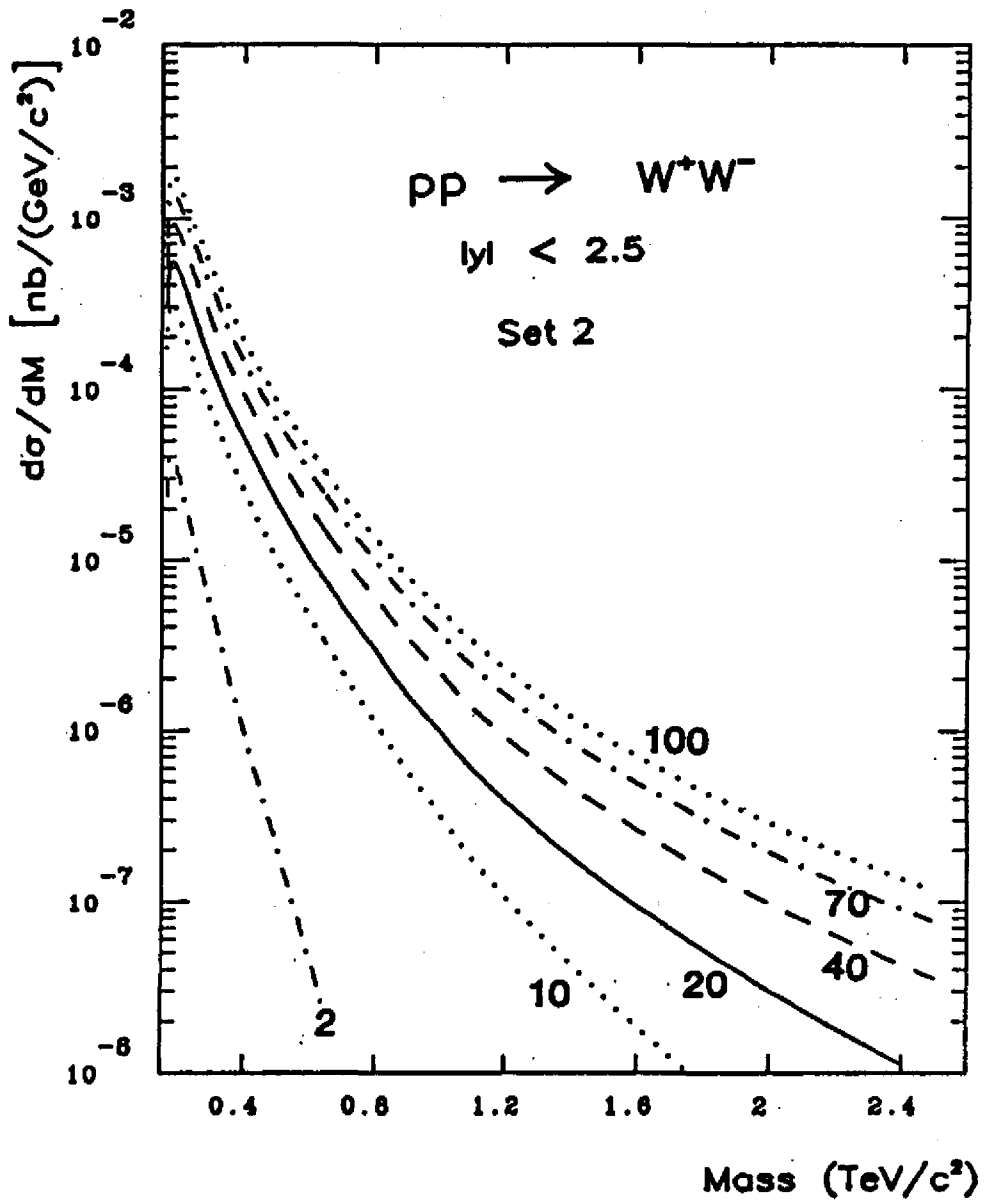

Figure 26: Mass spectrum of W^+W^- pairs produced in pp collisions, according to the Standard Model and Set 2 of the *EHLQ* parton distributions. Both the W^+ and the W^- must satisfy $|y| < 2.5$ (from *EHLQ*).

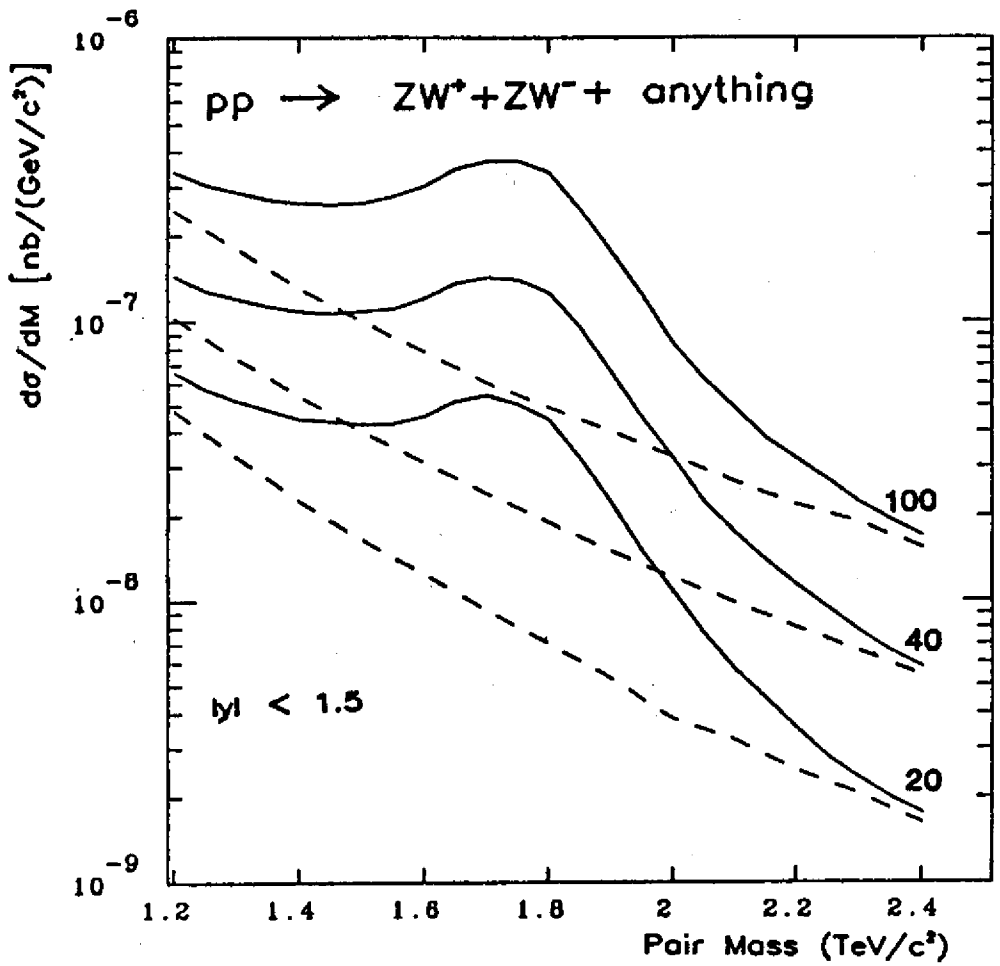

Figure 27: Mass spectrum of $Z^0W^+ + Z^0W^-$ pairs produced in pp collisions, according to Set 2 of the *EHLQ* parton distributions. Both Z^0 and $W^\pm$ must satisfy $|y| < 1.5$. The cross sections are shown with (solid lines) and without (dashed lines) the technirho enhancement (from *EHLQ*).

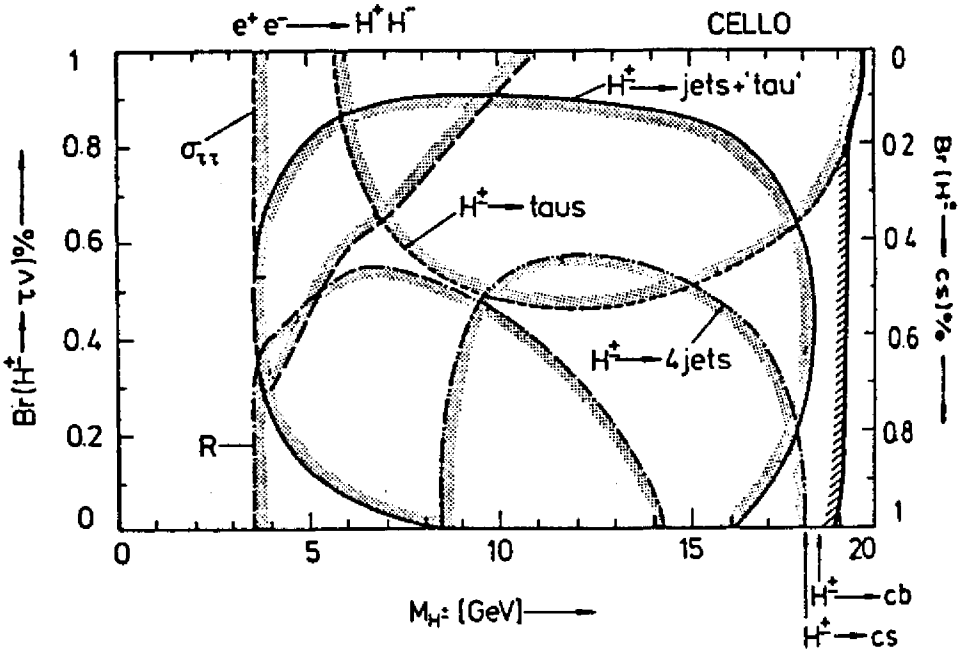

Figure 28: Limits at 95% confidence level on the mass of charged Higgs bosons or technipions as a function of the branching ratio into leptons or hadrons (from Ref. 51). The area on the shaded side of the contour is excluded in each case.

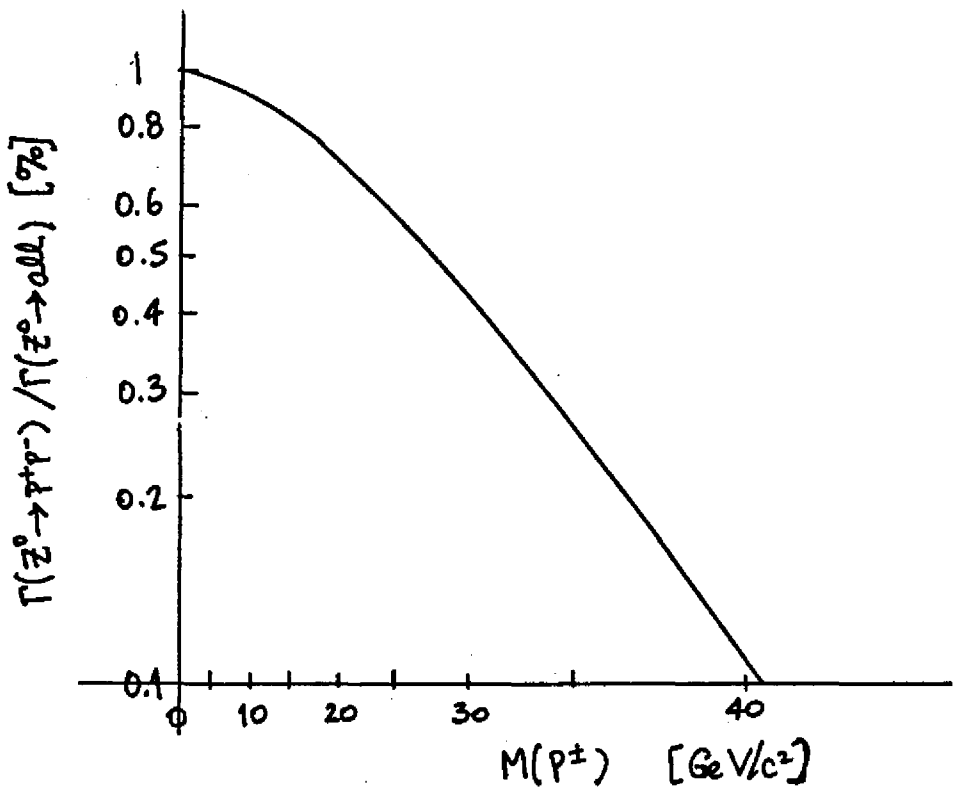

Figure 29: Branching ratio for the decay of Z^0 into charged technipions in the Farhi-Susskind model.

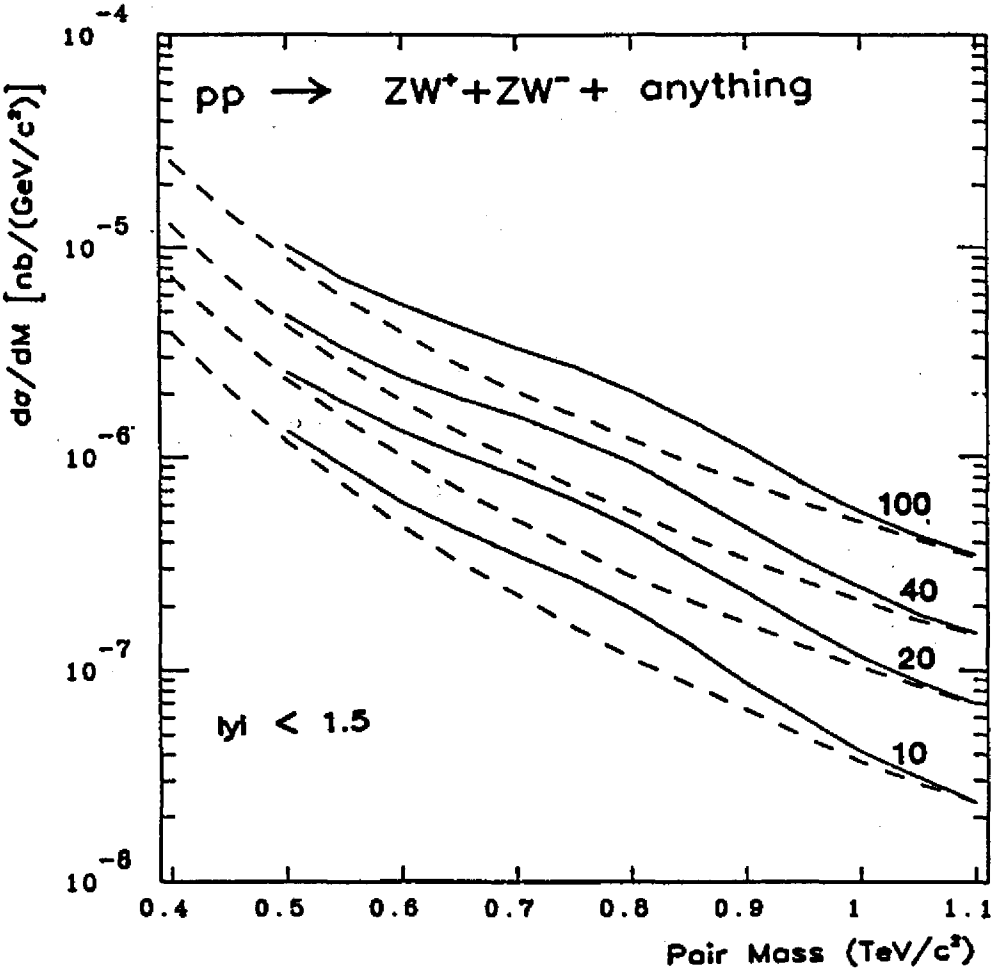

Figure 30: Mass spectrum of $W^{\pm}Z^{0}$ pairs produced in pp collisions, according to the Farhi-Susskind model (from *EHLQ*). Both intermediate bosons must satisfy $|y| < 1.5$. The cross sections are shown with (solid lines) and without (dashed lines) the technirho (specifically, $\rho_2^{\pm}$) enhancement.

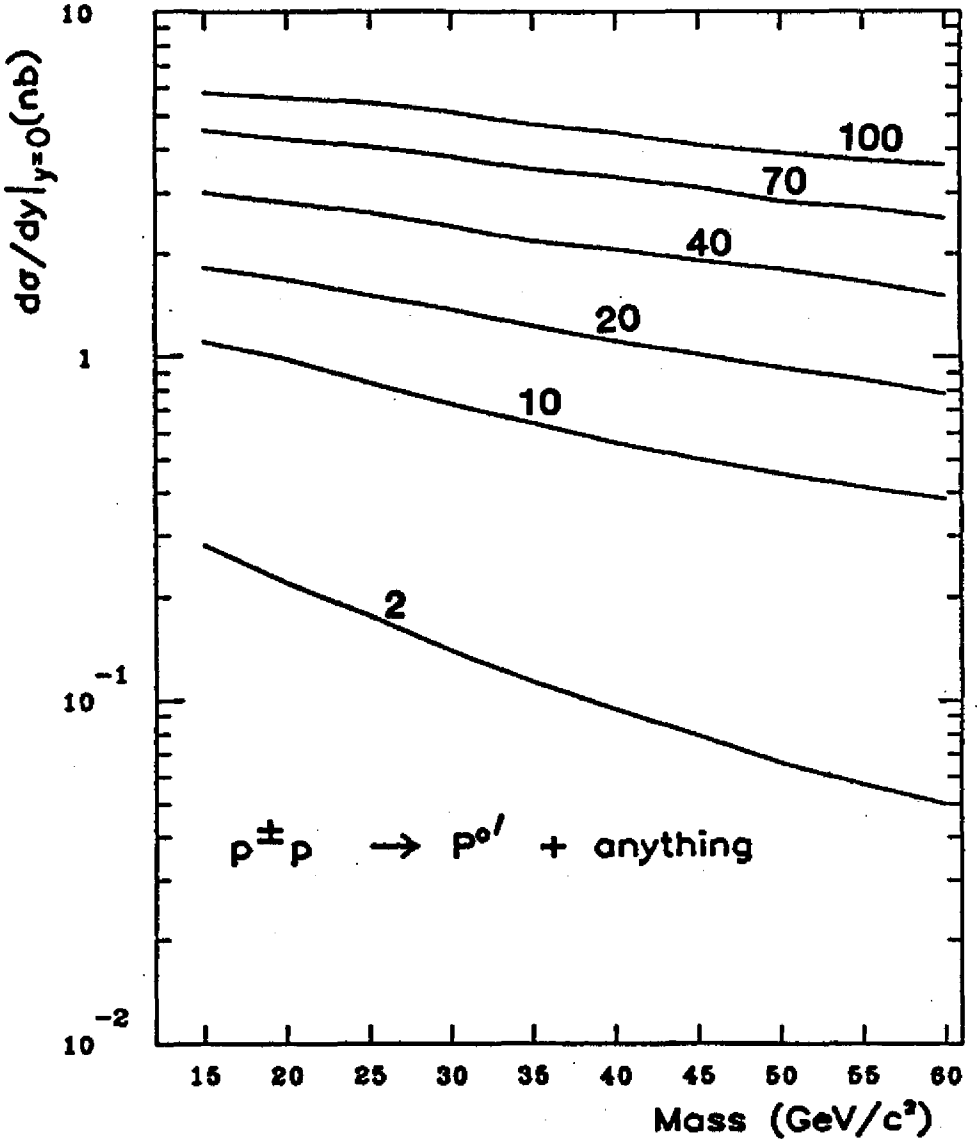

Figure 31: Differential cross section for the production of the color-octet technipion $P_8^{0\prime}$ at $y = 0$ in pp or $\overline{p}p$ collisions at 2, 10, 20, 40, 70, and 100 TeV (from *EHLQ*). The expected mass is approximately 240 GeV/c^2.

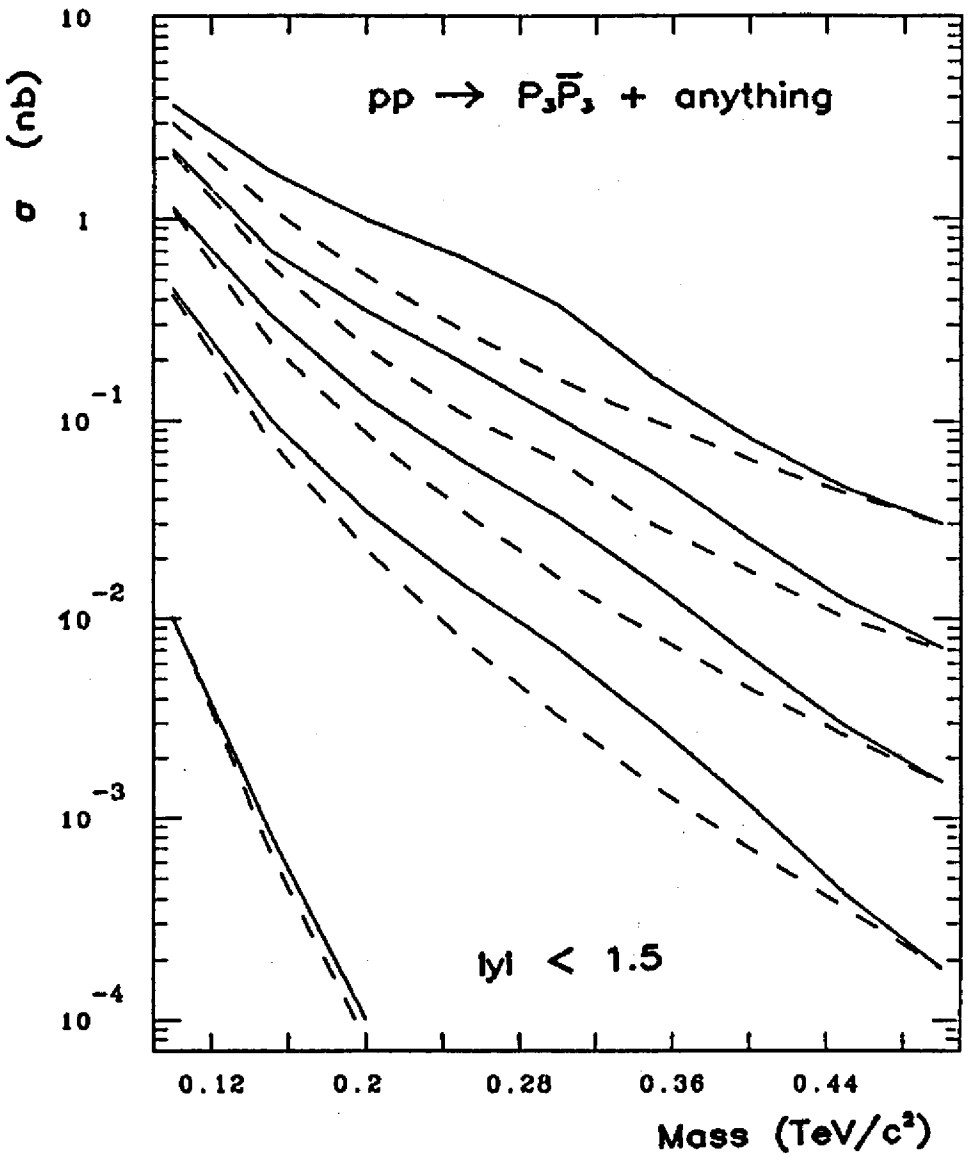

Figure 32: Integrated cross section for the production of $P_3\overline{P}_3$ pairs in pp collisions (from *EHLQ*). Rapidities of the technipions must satisfy $|y| < 1.5$. The cross sections are shown with (solid lines) and without (dashed lines) the technirho enhancement. The expected mass is around 160 GeV/c^2.

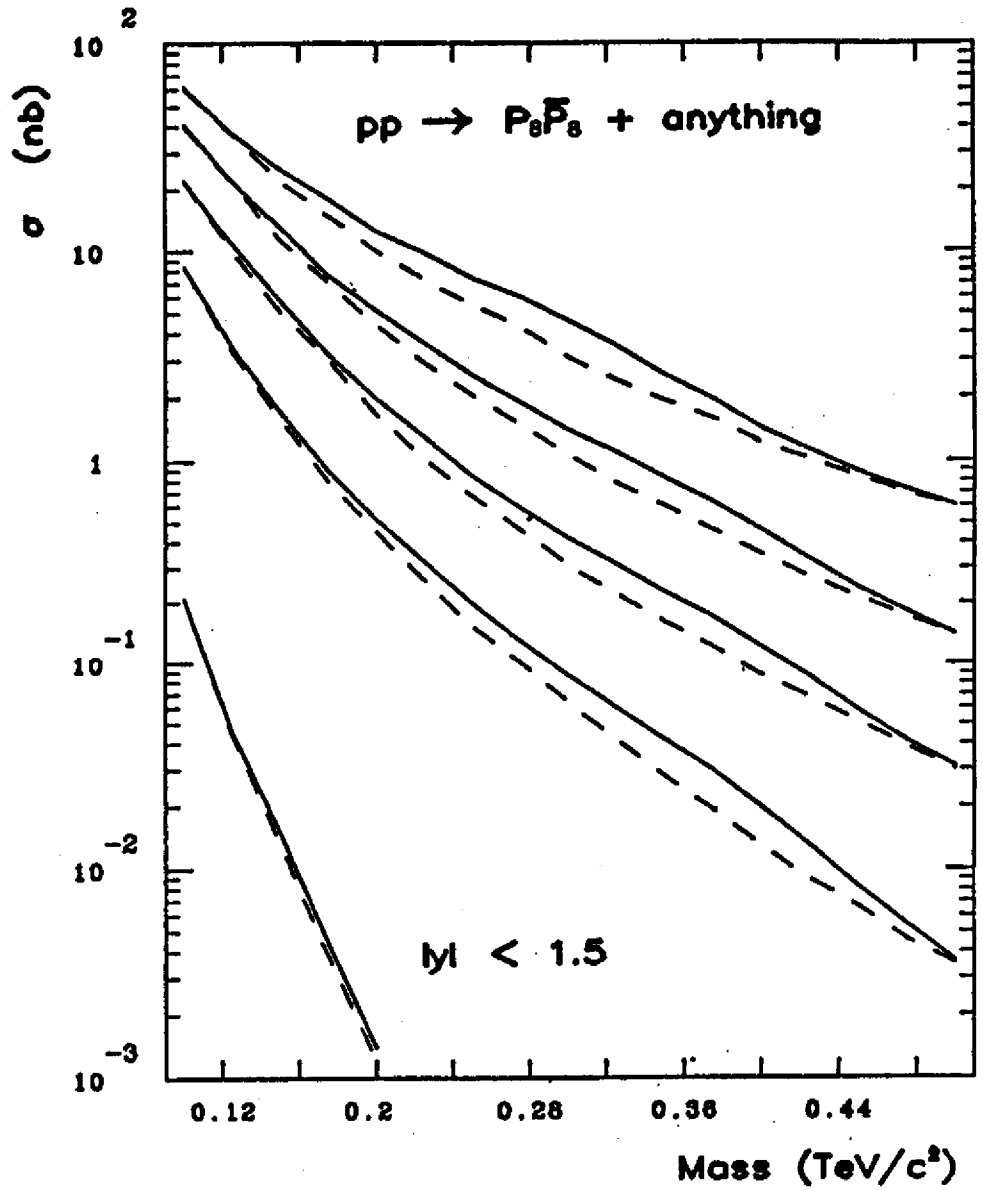

Figure 33: Integrated cross section for the production of $P_8\overline{P}_8$ pairs in pp collisions (from *EHLQ*). Both $P_8^+P_8^-$ and $P_8^0P_8^0 + P_8^{0\prime}P_8^{0\prime}$ charge states (which occur with equal cross sections) are summed. Rapidities of the technipions must satisfy $|y| < 1.5$. The cross sections are shown with (solid lines) and without (dashed lines) the technirho enhancement. The expected mass is around 240 GeV/c^2.

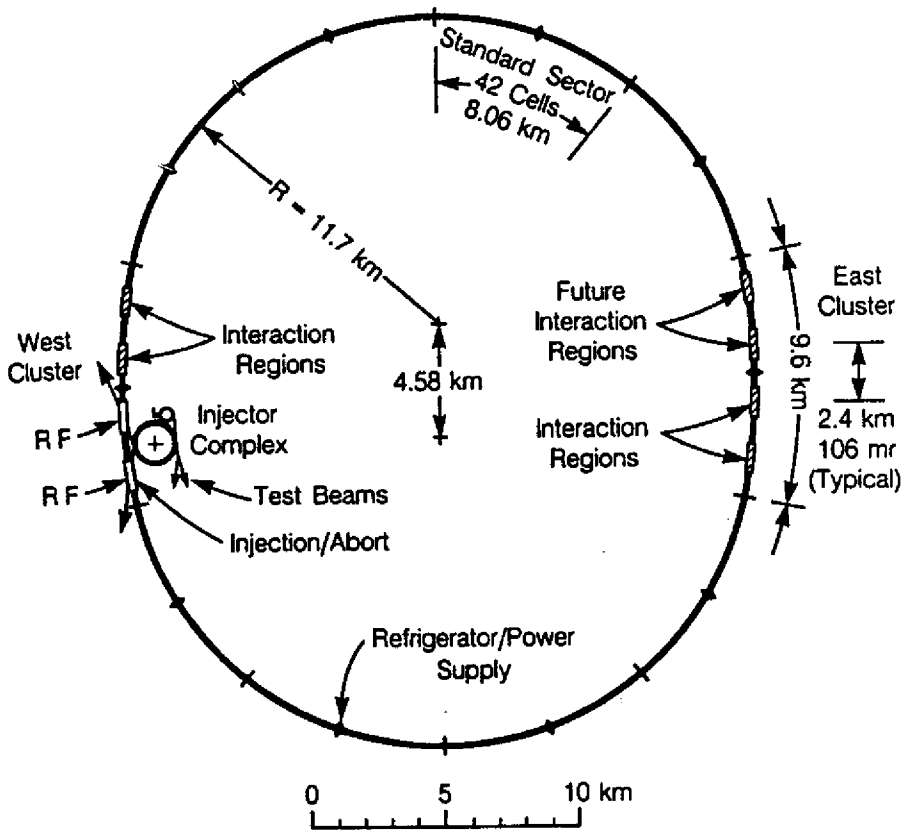

Figure 34: SSC collider ring layout. East and west clusters are joined by arcs of 11.7 km radius. The east cluster consists of four interaction regions separated by 2.4 km. The west cluster has two interaction regions and two utility straight sections (open rectangles) for injection and abort and for acceleration (RF). The cascade of synchrotrons that forms the injector is inside the main ring at the utility straight sections. There are 10 refrigeration and power units around the ring (black diamonds).

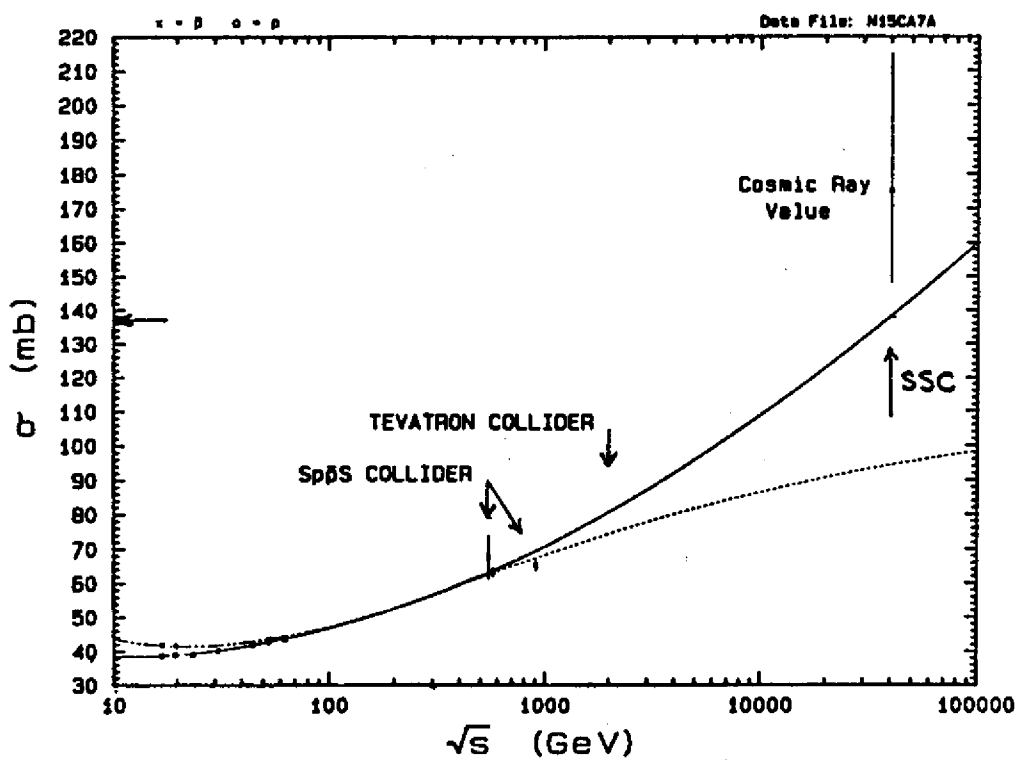

Figure 35: Two high energy extrapolations (solid and dotted lines) of the $p^{\pm}p$ total cross sections. The fit to the low-energy $\overline{p}p$ total cross section is shown separately as the dot-dashed line (from Ref. 54).

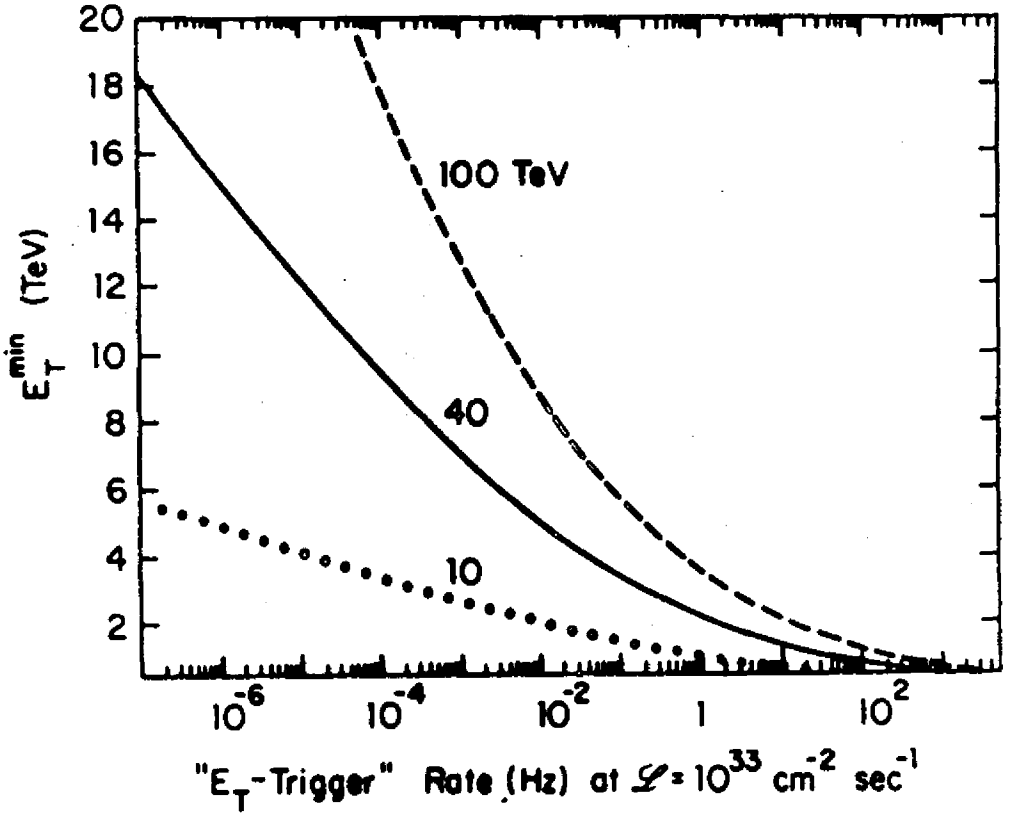

Figure 36: Counting rate for an E_T-trigger in pp collisions at an instantaneous luminosity of $\mathcal{L} = 10^{33}$ cm^{-2}sec^{-1} (after *EHLQ*). The threshold is defined for transverse energy deposited in the central region of rapidity, defined by $|y_i| < 2.5$ for jets 1 and 2.

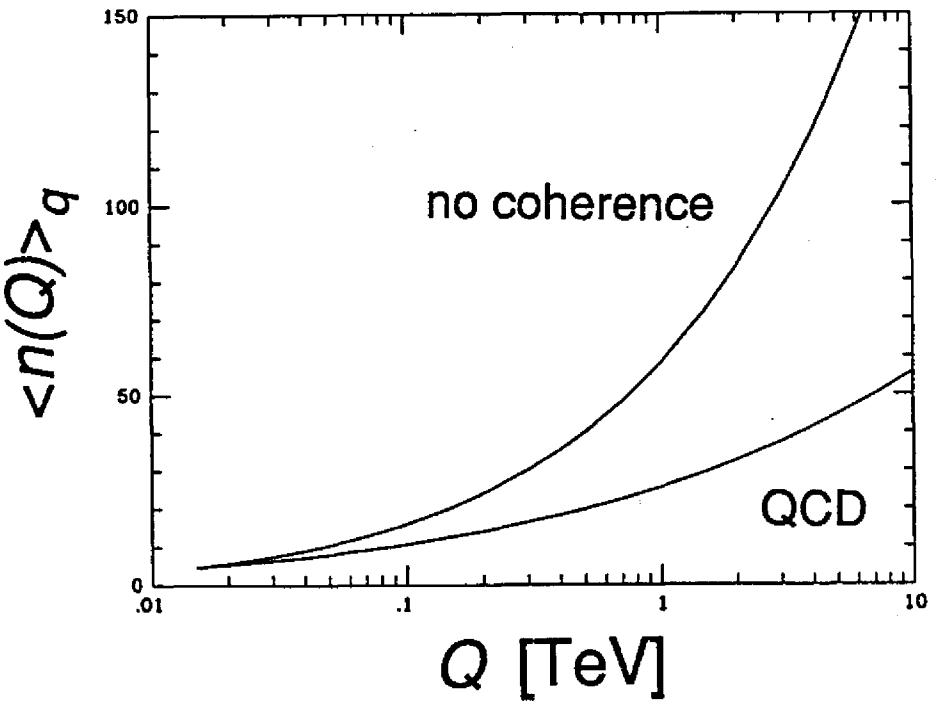

Figure 37: Growth of average multiplicity of hadrons produced in the fragmentation of a quark jet. For a jet produced at a hard interaction scale of 1 TeV, incoherent Monte Carlo programs overestimate the hadron multiplicity by more than a factor of two. (From Ellis, Ref. 56.)

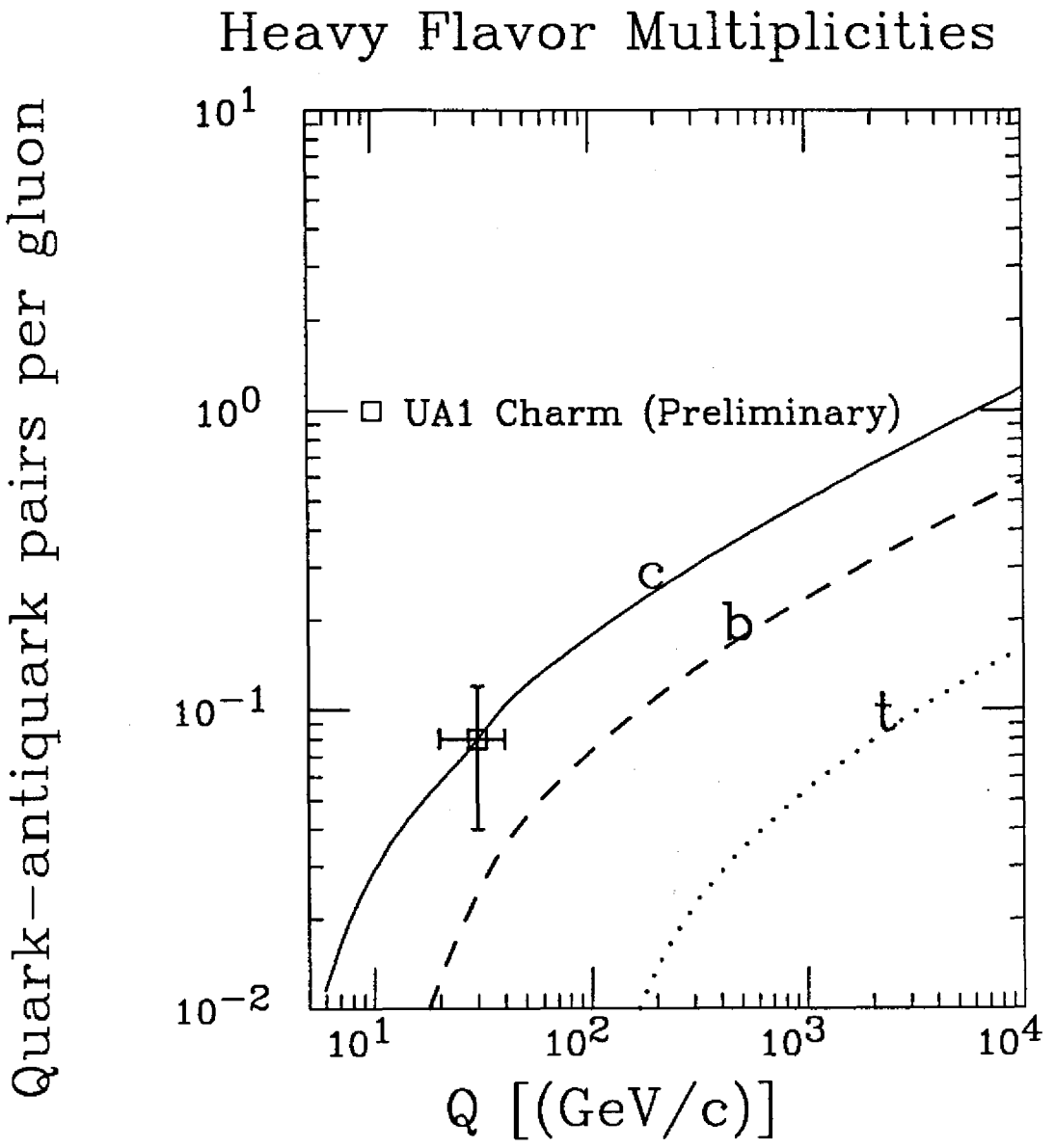

Figure 38: Evolution of gluon jets into heavy flavors, according to QCD perturbation theory, Ref. 57. For the curves shown, $\Lambda = 200$ MeV, and the masses of the charmed, bottom, and top quarks are 1.8 GeV/c^2, 5 GeV/c^2, and 40 GeV/c^2, respectively.

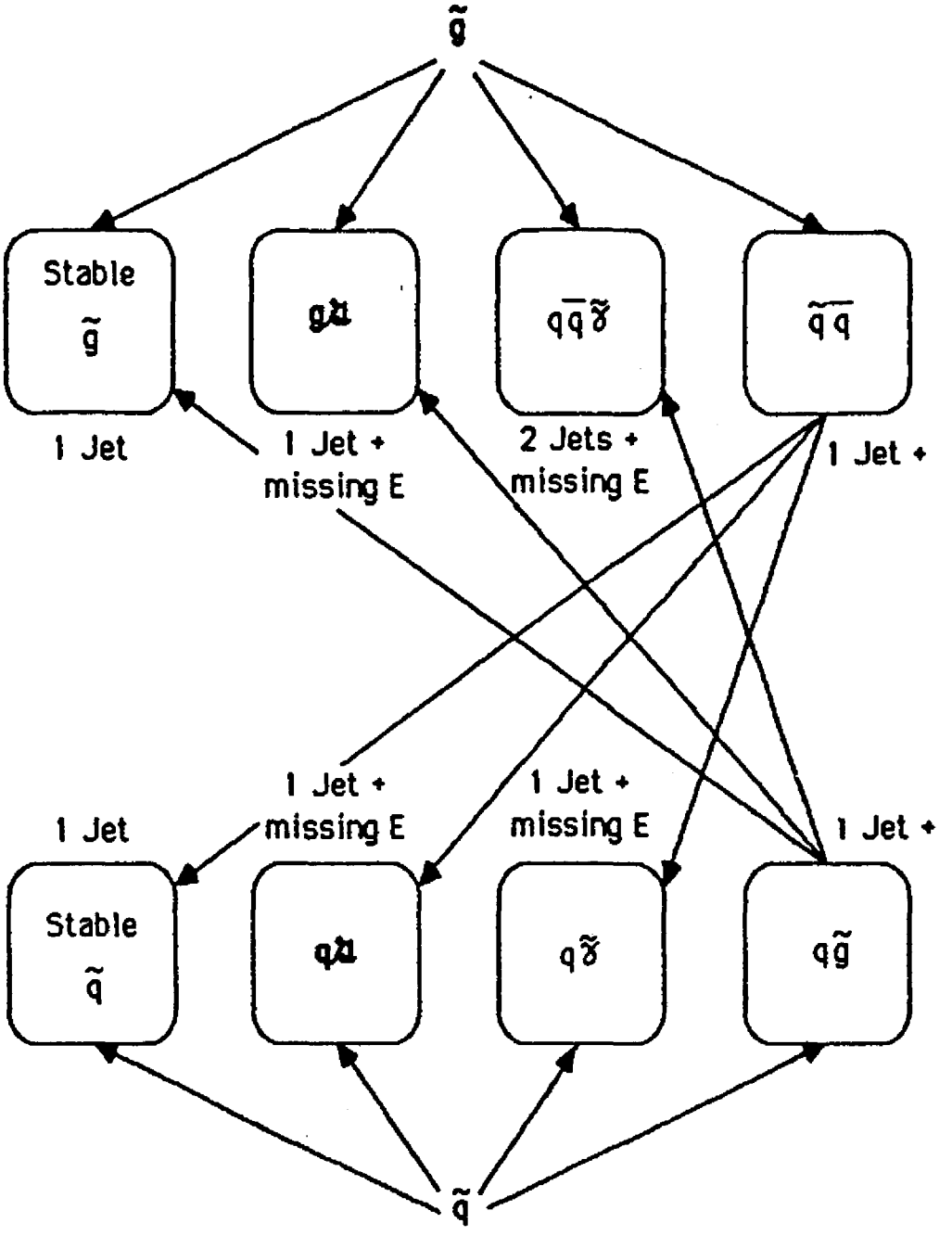

Figure 39: Signatures of the strongly interacting superpartners.

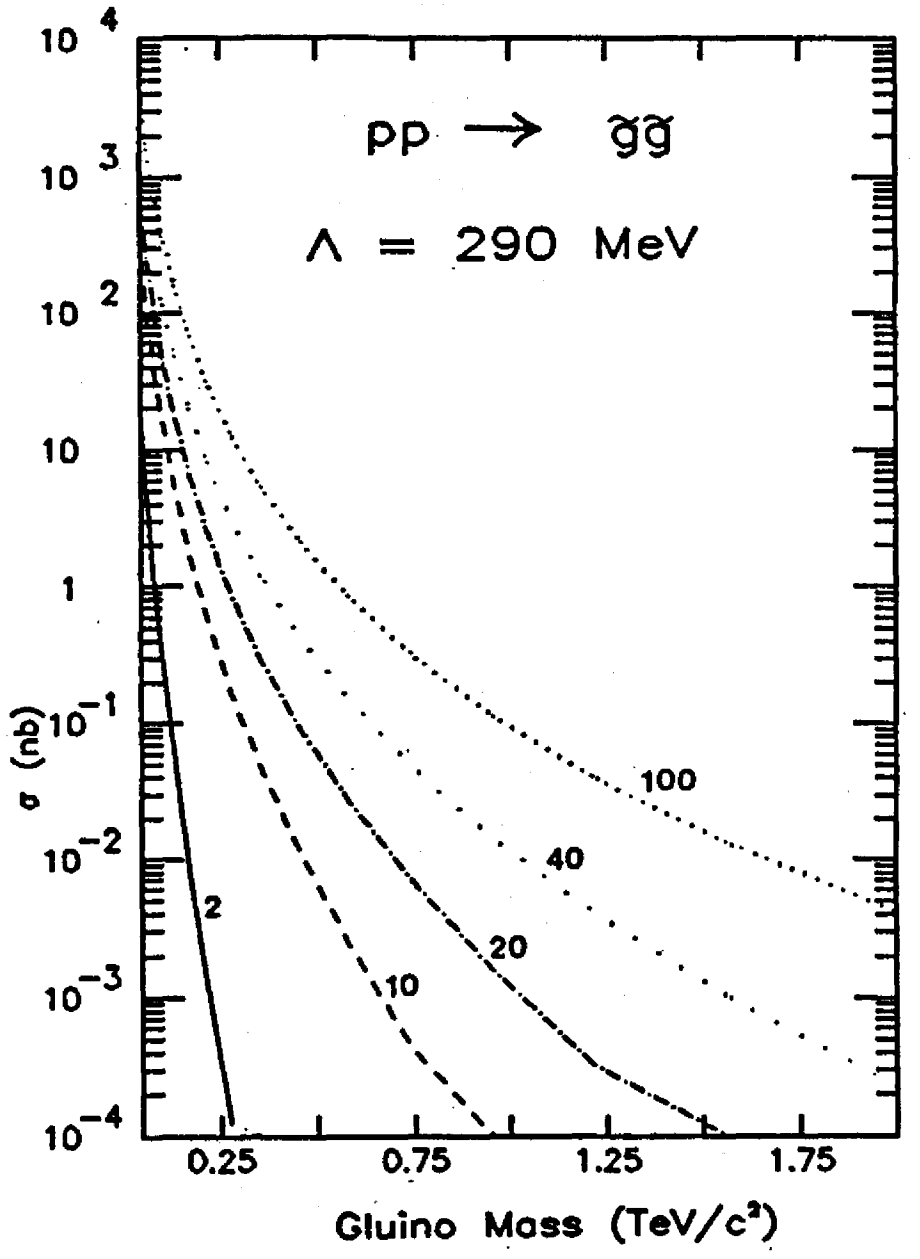

Figure 40: Cross sections for the reaction $pp \to \tilde{g}\tilde{g}$ + anything as a function of gluino mass, for collider energies $\sqrt{s}$ = 2, 10, 20, 40, and 100 TeV, according to the *EHLQ* parton distributions (Set 2). Both gluinos are restricted to the interval $|y_i| < 1.5$. For this illustration, the squark mass is set equal to the gluino mass (from *EHLQ*).

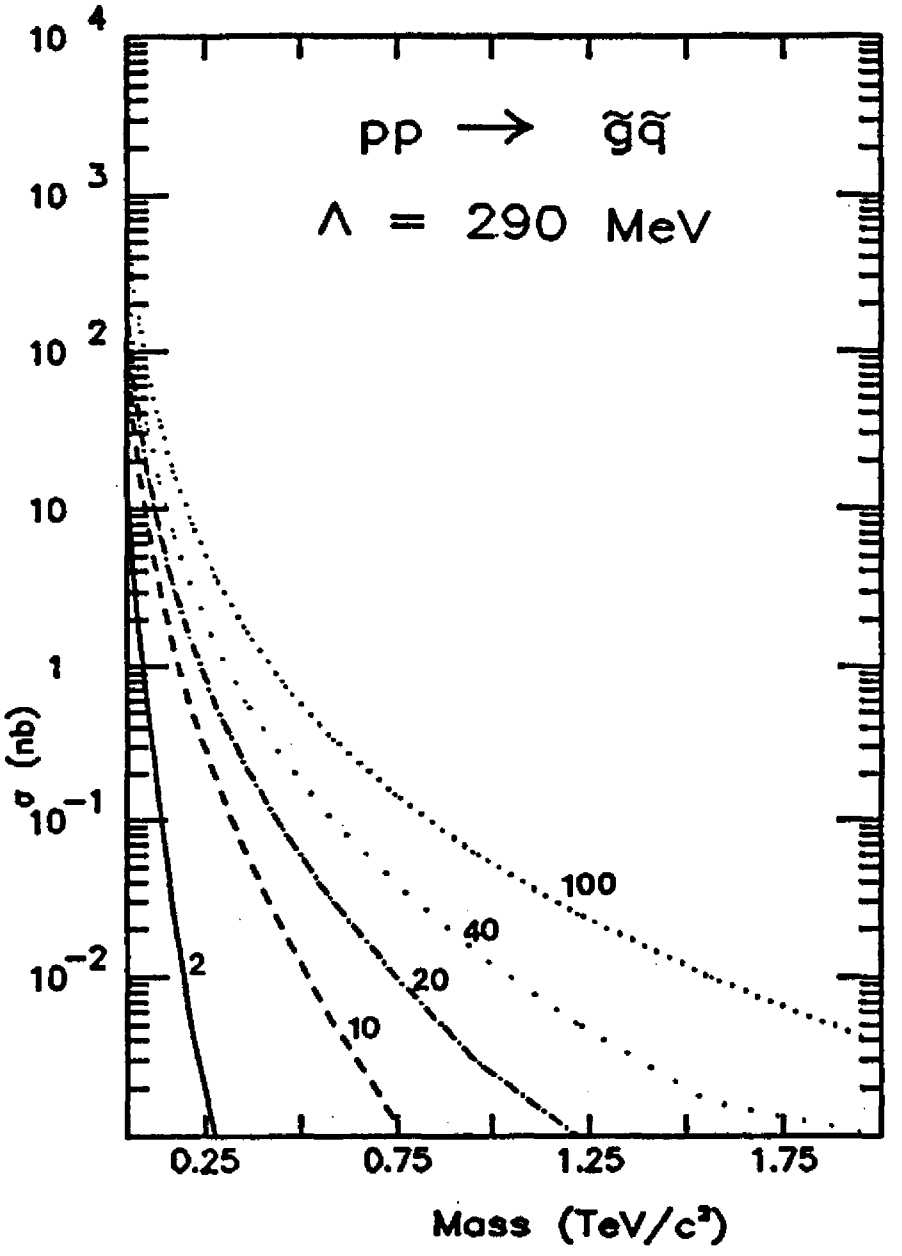

Figure 41: Cross sections for the reaction $pp \to \tilde{g}(\tilde{q}_u$ or $\tilde{q}_d$ or $\tilde{q}_u^*$ or $\tilde{q}_d^*)+$anything as a function of the superparticle mass for collider energies $\sqrt{s}$ = 2, 10, 20, 40, and 100 TeV, according to the *EHLQ* parton distributions (Set 2). We have assumed equal masses for the squarks and gluino and have included the partners of both left-handed and right-handed quarks. Both squark and gluino are restricted to the rapidity interval $|y_i| < 1.5$ (from *EHLQ*).

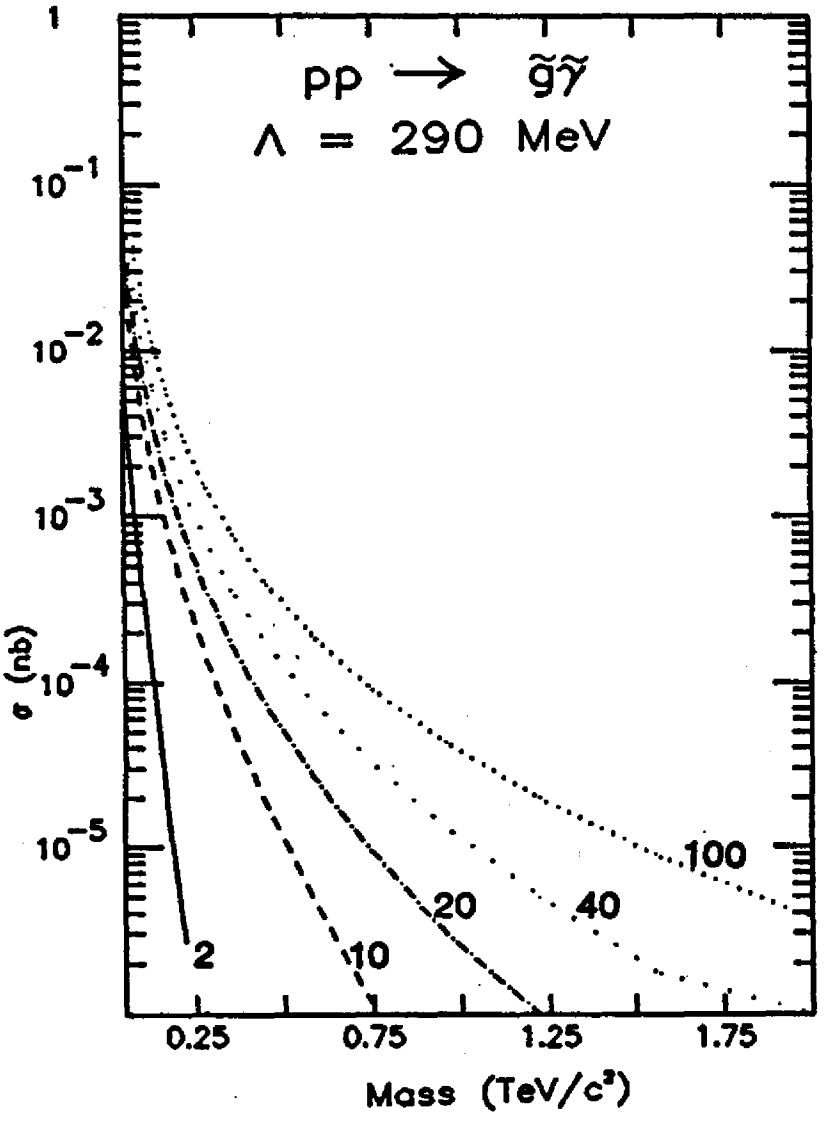

Figure 42: Cross sections for the reaction $pp \to \tilde{g}\tilde{\gamma}$ + anything as a function of the photino mass, for $\sqrt{s} = 2$, 10, 20, 40, and 100 TeV. Both gluino and photino are restricted to the rapidity interval $|y_i| < 1.5$. All squark and gaugino masses are taken to be equal (from *EHLQ*).